HIDRAULICA

HYDRAULICS-PNEUMATICS-TRIBOLOGY-ECOLOGY-SENSORICS-MECHATRONICS

http://hidraulica.fluidas.ro

CONTENTS

HIDRAULICA Magazine is indexed by international databases

EDITORIAL

The Place of Researchers and the Recognition They Enjoy (or Not) in the Romanian Society

The main problem of Romanian researchers is the status they have in society. It's not necessarily about the level of their earnings or the place they occupy in the social hierarchy, it's about the confidence that the results of their work enjoy, and this tells us something about them and about Romanian society at the same time.

The European Union claims to provide funding for projects, but on one condition: projects must be good! And, you see, that's it,

Ph.D.Eng. Gabriela MATACHE
CHIEF EDITOR

Romanian projects are not very good, so the research money coming back to Romania is kind of 'brittle'. A good policy, based on the formula: "Give me money to tell you if you're good!" There are European research projects. These are more rare, but more valuable, and involve investments. With a lot of good chances, and possibly luck, helped by friends in Brussels, one can get such a project (can get stuck with such a project), to implement it in Romania. It is not funded by European money, as it is said, it is financed by the Romanian Government; at the end of work, Brussels comes and makes 'acceptance inspection'; if the work complies with the eligible costs of the project, maybe settlement takes place, but usually it does not comply, it misses something, and in this case settlement takes place only in part, or it does not take place at all.

Scientific research aims to achieve high-quality scientific results; if they are numerous, the better. Organically and naturally, by the nature of their profession, researchers feel the need to publish their results, communicate them in the framework of conferences, debate upon them in workshops, symposia, etc. Well, the management of scientific research does not appreciate the quality, but the number, the amount: how many published papers a researcher has, how many conferences he/she has attended, where, with whom, why ... All this, in the name of an aberrant building of a good image of Romania in the world, referring to an EU directive, allegedly. Obviously, such quantitative criteria can fundamentally distort scientific activity.

The policy of scientific research in Romania ensures that the researcher has a 'pretty good bread on the table', a car, a trip abroad, a home credit, in short, something to shut him/her up, "not to have conflicts". The Romanian scientist should be a little bourgeois, caring about anything but science. Which is not true, but our man is forced to 'swallow' and consent. As a result, the decision-maker asks: "So, why increase the research budget in Romania? To feed some people who have low perspectives?"

Under these circumstances, in which the Romanian society places the researcher under the level of politicians, journalists and priests in the hierarchy of those who strive for the truth, their migration to communities where they enjoy credibility and appreciation is part of a natural search for normality, and we should not be surprised by it.

Vector Estimation of Centrifugal Force and CAD Techniques for Protection Mechanism at Over-Speed of the Low-Power Wind Turbine Rotor

Assoc. Prof. PhD. Eng. **Teodor MILOȘ**[1], Prof. Em. PhD. Eng. **Mircea BĂRGLĂZAN**[2], Lecturer PhD. Eng. **Rodica BĂDĂRĂU**[3]

[1] Politehnica University of Timisoara, teodor.milos@upt.ro

[2] mircea.barglazan@upt.ro

[3] rodica.badarau@upt.ro

Abstract: Rotor over-speed protection for small power wind turbine requires a possible cheap and reliable mechanical system. This is because any electric or electronic device depends on the electrical power source which by an electrical damage becomes unavailable. Between these protection devices centrifugal mechanism is priced at acceptable cost, but contains some subtleties of interpretation of the mode of operation. In this paper, it is explained step by step the original solution of this mechanism put in place for a 5 kW wind turbine. After triggering the centrifugal mechanism, the rotor blades are rotated to the flag position producing aerodynamic braking of the rotor. The speed is reduced to 20 ... 30 rpm, after which the action of the centrifugal mechanism is greatly reduced (centrifugal force decreases) so that the force in the compressed spring plus the aerodynamic torque of the blades relative to the axis of the blade spindle causes the return to the initial working position. Adjusting ballast weight of centrifugal mechanism and the reliable automatically operation of the whole system should be tested repetitively on an endurance stand.

Keywords: Vector, centrifugal force, wind turbine, centrifugal mechanism, over-speed protection

1. Introduction

The centrifugal over-speed mechanism acts on the rotor blades and is activated by centrifugal force that occurs due to the rotor rotation movement. It has an apparently complex structure because only one component of the centrifugal force has an active role in triggering it, so that in order to understand its operation and utility, the nominal operating data of the turbine are taken into account.

The nominal generator speed is 120 rpm, and can increase up to a maximum of 150 rpm. The turbine is coupled directly to the electric generator ("direct drive"), namely it does not contain a gearbox or speed amplifier. The rotor speed must be in the rotation domain of the electric generator.

The rotor blades can be rotated up to 45°. The pitch angle, β_s, must be maintained at the rated position and at speeds higher than the rated speed it should increase by about 45°, which means that the blades tend to be near to the flag position, in the wind direction and as a result aerodynamic braking occurs.

The problem to be solved is to automatically change the pitch angle when the rotor speed tends to exceed the limit of 120 rpm. There are two torques which acts on the blade rotating around its axis: an aerodynamic torque given by the force of the air in the direction perpendicular to the blade and a torque of a centrifugal force component of the counterweights. The centrifugal mechanism must contain an elastic element (spring) to ensure that the blades are brought back to the initial position as soon as the speed has fallen below the threshold limit. This pre-tensioned spring acts on the blade by means of a crank mechanism, producing a torque balance between the above mentioned torques.

In addition to the technical and economic aspects, it is also necessary to take into account the rotor safety, for which an automatic mechanical system is more reliable than an electric or electronic one. Occasionally, wind speeds over 30 m/s were recorded in the area.

Putting and maintaining in the wind direction is ensured by the tail of the aggregate.
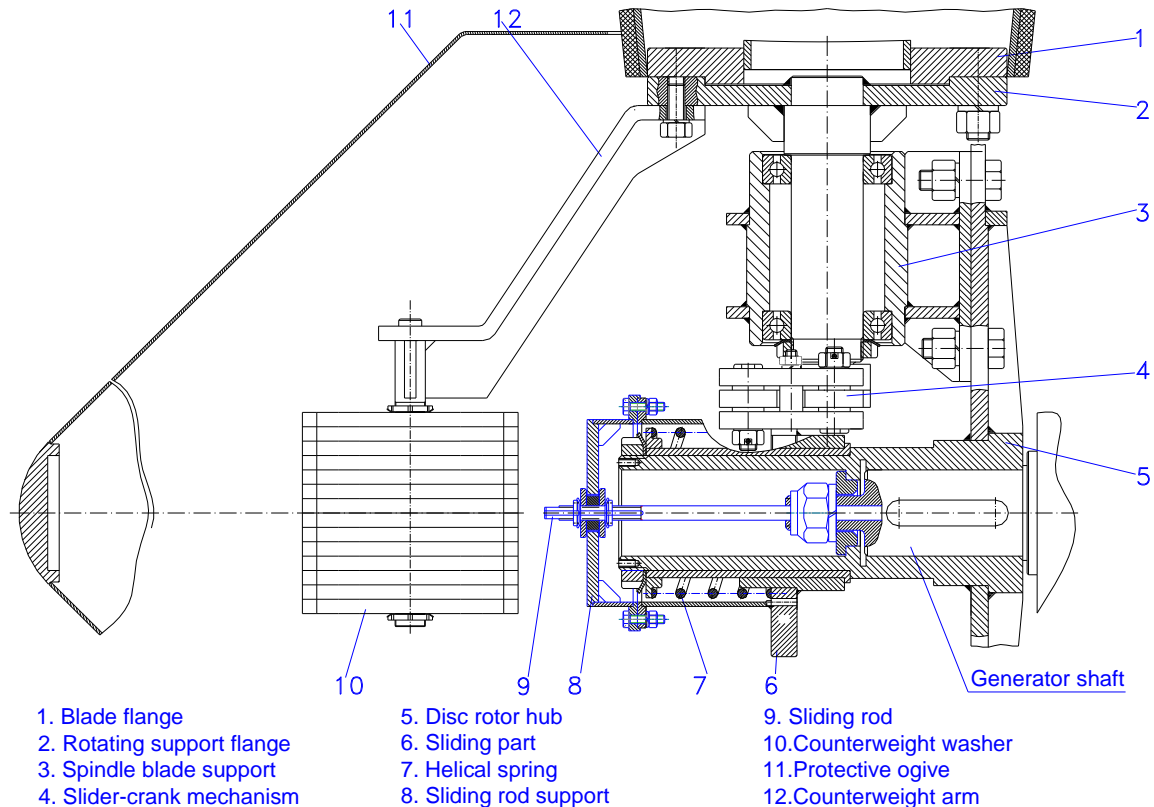
Fig. 1. Centrifugal protection mechanism for over-speed

1. Blade flange
2. Rotating support flange
3. Spindle blade support
4. Slider-crank mechanism
5. Disc rotor hub
6. Sliding part
7. Helical spring
8. Sliding rod support
9. Sliding rod
10. Counterweight washer
11. Protective ogive
12. Counterweight arm

2. Vector estimation of centrifugal force

Politehnica University of Timisoara, in the framework of a multidisciplinary research program (mechanical, electrical, automation), has produced and put into operation a wind power unit of 5 kW. For protection against over-speed of the rotor, in the case of excessively high winds, a centrifugal mechanism was explored and designed, which is triggered automatically when the maximum permitted engine speed is exceeded, causing the blades to turn to the flag position followed by aerodynamic braking.

The centrifugal over-speed mechanism (Fig. 1) operates alternately in the sense that in a few seconds after triggering the rotor blades are placed in the flag position and aerodynamic braking occurs. The turbine speed decreases and the spring (7) of the mechanism returns the blades to the optimum working position, after which, if the wind persists at speeds above the permissible working limit, the rotor is operating again in load or if it is thrown away from the load, then even more, returns the rotor blades to the flag position.

The decisive part of the centrifugal mechanism is the counterweight. Attached to the rotating motion flange, it develops a centrifugal force whose tangential component with respect to the axis of the blade causes the blade to rotate towards the flag position. The geometric form obtained (Fig. 3) finally resulted from the following constraints:

- Position of the center of gravity in relation to the axis of the blade shall be at approximately maximum 300 mm, from gauge conditions;
- Contain correction elements (knobs) in order to adjust the spinning speed of the centrifugal mechanism by changing the rotating mass;
- Counterweight does not touch the rotor hub on the stroke domain, rotating between 0° and 45°.

The centrifugal force that occurs due to the rotation movement acts at the counterweight gravity center. If the entire subassembly of the counterweight is represented in 3D in the AutoCAD-Inventor design environment, then accessing the iProperties feature gives the coordinates of the center of gravity, mass, etc. The coordinates of the center of gravity are given in relation to the

reference system chosen to construct the subassembly in 3D and are denoted by X_g, Y_g, Z_g. A Cartesian reference system is selected in which the rotation axis is reference system axis. According to the drawing, there are two perpendicular rotation axes located in the same vertical plane: the axis of rotation of the rotor, OX, and the axis of the blade rotation, OZ. The third axis, OY, will be perpendicular to the plane (XOZ) at point O and in the sense that the OX rotated clockwise to OY will give the OZ oriented vertically upward.
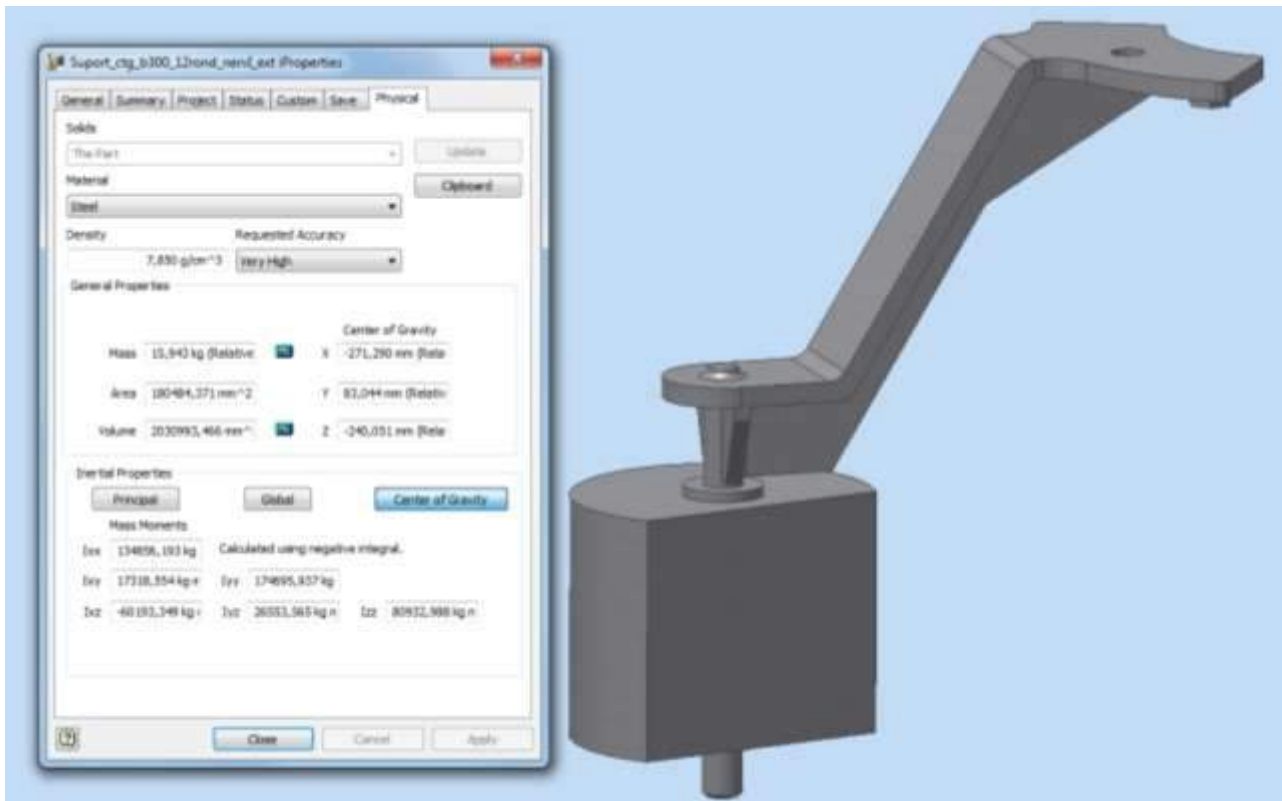
Fig. 2. The 3D representation of counterweight and the data plate displayed by the 3D design environment

As one can see in Fig. 2, the counterweight consists of an arm which is fixed on the blade flange and a rod to the other end, and on the rod a semi-cylindrical massive part is inserted. Because the entire system functionality is done by stand tests and in-situ, it is necessary that the weight of the counterweight to be adjustable. That's why the semi-cylindrical part was split into 10 mm thick washers.

The maximum number of washers initially provided was 14. Following the calculations and preliminary tests, an optimum of 12 washers was reached.

The projection of counterweight and center of gravity in the XOY plane is like in Fig. 3. The vector radius of the center of gravity, $\vec{r}$, projected in the plane (XOY) is denoted by R_{XY}.

$$R_{XY} = \sqrt{X_g^2 + Y_g^2} \qquad (1)$$

The angle of this projection to the OX axis is denoted by α and is a calculation parameter for the centrifugal force and its torque. If taken as the reference plane for the angle α, the plane (XOZ), then the starting point α of the counterweight gravity center is α_{min} and will be calculated with the relation (2) (it is taken in absolute value because some coordinates can be negative).

$$\alpha_{min} = arctg\left(\frac{|Y_g|}{|X_g|}\right) \qquad (2)$$
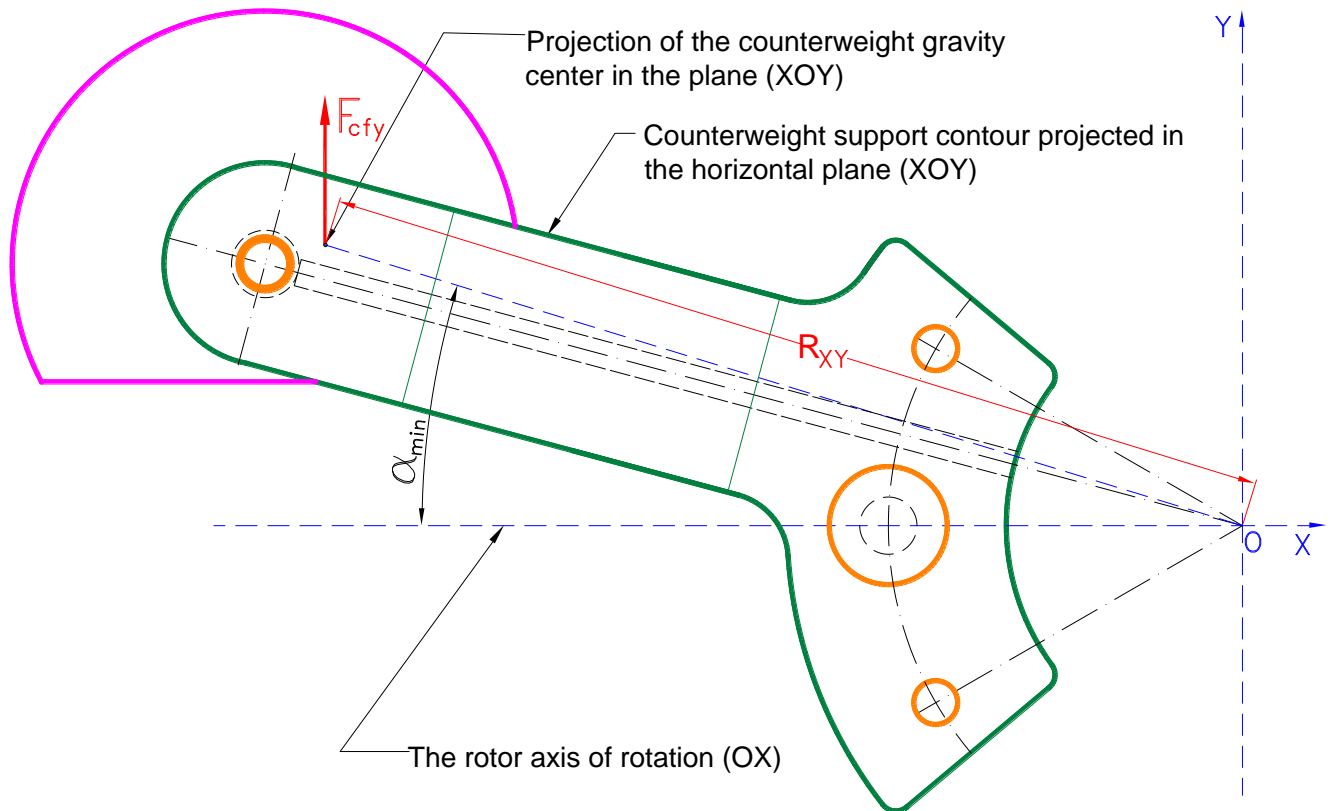
Fig. 3. Projection of counterweight in a plan (XOY)

According to theoretical mechanics and vector calculations the centrifugal force is determined with the relation (3):

$$\overrightarrow{F_{cf}} = m_{cg}[\vec{\omega} \times (\vec{\omega} \times \vec{r})] \tag{3}$$

Where **m_{cg}** is the mass of the counterweight, $\vec{\omega}$ is the angular velocity of the rotor and $\vec{r}$ is the radius of the generic gravity center. The unity axes vectors of the reference system are $\vec{\imath}, \vec{\jmath}, \vec{k}$. In this reference system $\vec{\omega}$ has a component only on the OX axis.

$$\vec{\omega} = \omega\vec{\imath} \tag{4}$$

The vector radius of the center of gravity is expressed with the relation:

$$\vec{r} = r_x\vec{\imath} + r_y\vec{\jmath} + r_z\vec{k} \tag{5}$$

Developing the double vector product (3), we obtain:

$$\vec{\omega} \times \vec{r} = \begin{bmatrix} \vec{\imath} & \vec{\jmath} & \vec{k} \\ \omega & 0 & 0 \\ r_x & r_y & r_z \end{bmatrix} = -\omega r_z\vec{\jmath} + \omega r_y\vec{k} \tag{6}$$

$$\vec{\omega} \times (\vec{\omega} \times \vec{r}) = \begin{bmatrix} \vec{\imath} & \vec{\jmath} & \vec{k} \\ \omega & 0 & 0 \\ 0 & -\omega r_z & \omega r_y \end{bmatrix} = -\omega^2 r_y\vec{\jmath} - \omega^2 r_z\vec{k} = -\omega^2(r_y\vec{\jmath} + r_z\vec{k}) \tag{7}$$

It is observed that the centrifugal force has components only on the OY and OZ axes as expected. Rotation of the blade has effect only on the OY axis component. This vector-expressed component has the expression:

$$\overrightarrow{F_{cfy}} = -m_{cg}\omega^2 r_y\vec{\jmath} \tag{8}$$

Scalar form is important for calculations. According to Fig. 3 and the notations above, the generic coordinate r_y is the projection R_{XY} on the OY axis and thus:

$$F_{cfy} = m_{cg}\omega^2 R_{XY} sin(\alpha_{min} + \alpha) \tag{9}$$

The torque, $\overrightarrow{M_{cf}}$, made by the centrifugal force is determined, as vector, with the relation:

$$\overrightarrow{M_{cf}} = \overrightarrow{F_{cf}} \times \vec{r} = \begin{bmatrix} \vec{\imath} & \vec{\jmath} & \vec{k} \\ 0 & -m\omega^2 r_y & -m\omega^2 r_z \\ r_x & r_y & r_z \end{bmatrix} \tag{10}$$

Developing the matrix in (10) results:

$$\overrightarrow{M_{cf}} = -m\omega^2 \left[(r_y r_z - r_y r_z)\vec{\imath} + r_x r_z \vec{\jmath} - r_x r_y \vec{k} \right] = -m\omega^2 (r_x r_z \vec{\jmath} - r_x r_y \vec{k}) \tag{11}$$

For the intended system is important the component of the OZ axis, which causes the rotation of the blade:

$$\overrightarrow{M_{cfz}} = m\omega^2 r_x r_y \vec{k} \tag{12}$$

The scalar form of the active torque, M_{cfz}, using peculiar notations for each blade rotation, becomes:

$$M_{cfz} = m_{cg}\omega^2 R_{XY} sin(\alpha_{min} + \alpha)R_{XY} cos(\alpha_{min} + \alpha) =$$
$$= m_{cg}\omega^2 R_{XY}^2 sin(\alpha_{min} + \alpha)cos(\alpha_{min} + \alpha) \tag{13}$$

In calculations and graphical representations is used the rotational speed, n [rpm], instead of the angular velocity, ω, where:

$$\omega(n) = \frac{\pi n}{30} \tag{14}$$

With the customizations introduced above the relationship (13) becomes:

$$M_{cfz}(n, \alpha) = m_{cg}[\omega(n)]^2 R_{XY} sin(\alpha_{min} + \alpha)R_{XY} cos(\alpha_{min} + \alpha) =$$
$$= m_{cg}[\omega(n)]^2 R_{XY}^2 sin(\alpha_{min} + \alpha)cos(\alpha_{min} + \alpha) \tag{15}$$

3. Slider- crank mechanism

The counterweights attached to each blade cannot be left to act independently because the rotor rotates with the blade rotation axis into vertical plane, on each blade will act a variable weight force dependent from the rotor angle of rotation. That is why the three rotor blades with the counterweights on them must be connected together by a crank shaft mechanism with a sliding piece along the rotor axis of rotation. On each blade there is a slider-crank mechanism coupled with the sliding piece through a cylindrical joint. This mechanism is schematically represented in three significant positions (Fig. 4). The handle of the mechanism is rigidly connected to the rotor blade spindle at point O (Fig. 4). In turn, the sliding piece is driven by a pre-compressed helicoidally spring to return the blades to the working position after the rotor speed drops below the permissible limit, following aerodynamic braking. Through this mechanism the three blades are connected simultaneously and will rotate identically depending on the dynamic equilibrium of this mechanical system. The force in the pre-compressed helical spring acts on the rod through the Fb component. At point A of crank articulation, this component breaks down in two perpendicular directions (Fig. 5). The tangential component, F_m, determines the rotation torque on the blade spindle, heaving the force arm "l_m".
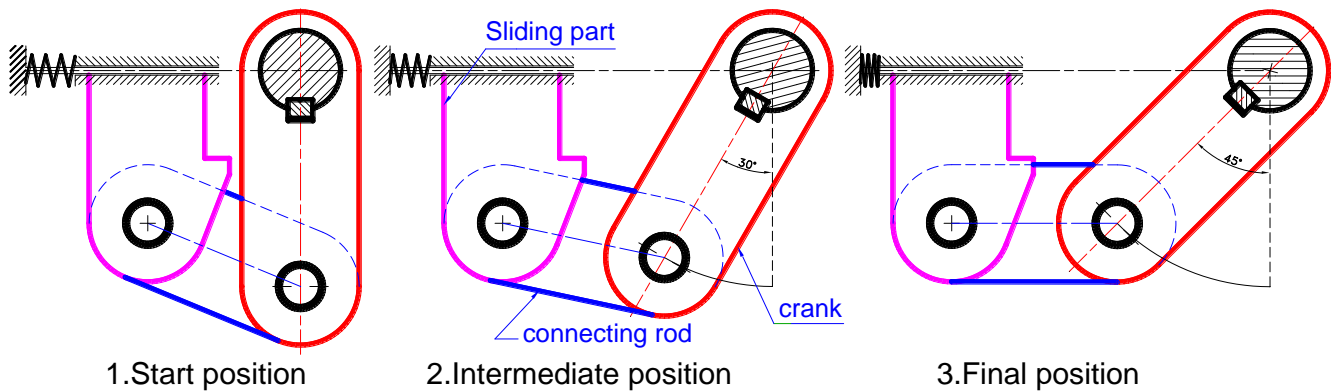
Fig. 4. Three successive positions of the slider-crank mechanism
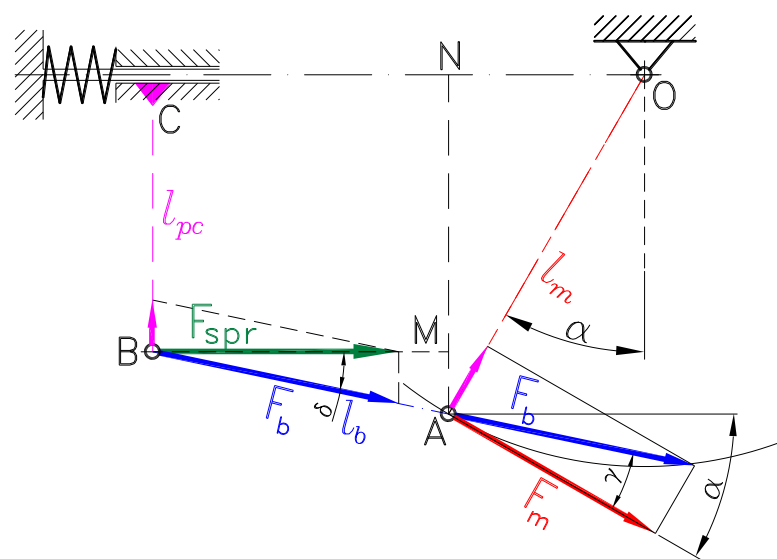
Fig. 5. The decomposition of forces in the slider-crank mechanism

The force given by the spring is evenly distributed over the three slider-crank mechanism (if there are 3 blades). This force acts directly on the sliding part, respectively in the joint B of the connecting rod (slider). On the connecting rod acts only one component of the force of the spring, respectively F_b. The spring force F_{spr} is decomposed in two non-orthogonal directions, showed in Fig. 5. If note δ the angle between the force F_b and F_{spr} results:

$$F_b = \frac{F_{spr}}{3\cos(\delta)} \tag{16}$$

where:

$$\cos(\delta) = \frac{BM}{l_b} \tag{17}$$

The force F_b acts on the crank in the joint A where it breaks into two orthogonal components. The component F_m determines torque against the crank with arm "l_m" and observing the relationship between the angles $\gamma + \delta = \alpha$ results:

$$F_m = F_b \cos(\gamma) = F_b \cos(\alpha - \delta) \tag{18}$$

From the geometric configuration results BM and δ:

$$BM = \sqrt{l_b^2 - AM^2} = \sqrt{l_b^2 - \left(l_m \cos(\alpha) - l_{pc}\right)^2} \tag{19}$$

$$\delta = arccos\left(\frac{BM}{l_b}\right) \tag{20}$$

Combining (16) and (18) results:

$$F_m = \frac{F_{spr}\cos(\alpha-\delta)}{3\cos(\delta)} \tag{21}$$

The torque of spring elastic force is determined with the scalar relation:

$$M_{spr}(\alpha) = F_m l_m = \frac{l_m F_{spr}\cos(\alpha-\delta)}{3\cos(\delta)} \tag{22}$$

4. The dynamics of the centrifugal protection mechanism at over-speed

The forces and torques to be calculated in function of two independent variables and the coordinates of the counterweight gravity center obtained from the 3D representation of the counterweight for the initial position of the whole assembly. These are:

- Turbine rotor speed n, for which a variation range of 50 ... 150 rpm
- The current angular position α of counterweight relative to the initial position, α_{min} and final (to flag), where $\alpha_{max} = \alpha_{min} + 45°$
- The first constant calculation is the mass of counterweight, m_{cg}
- The second calculation constant is the active crank length, l_m
- The following three constants are the coordinates of the counterweight gravity center: X_g, Y_g, Z_g

The forces and torques occurring in the operation of this automatic mechanical system are determined by the rotor speed, n, and the current angular position α of the counterweight from the initial position, α_{min}.

Assuming that the turbine is optimally charged depending on the rotational speed and wind velocity, the torque of aerodynamic forces is calculated in relation to the axis of the blade shaft in 6 ... 10 working points. By interpolating these calculated values, the curve of the aerodynamic torque is obtained according to the rotational speed, (Fig. 6).
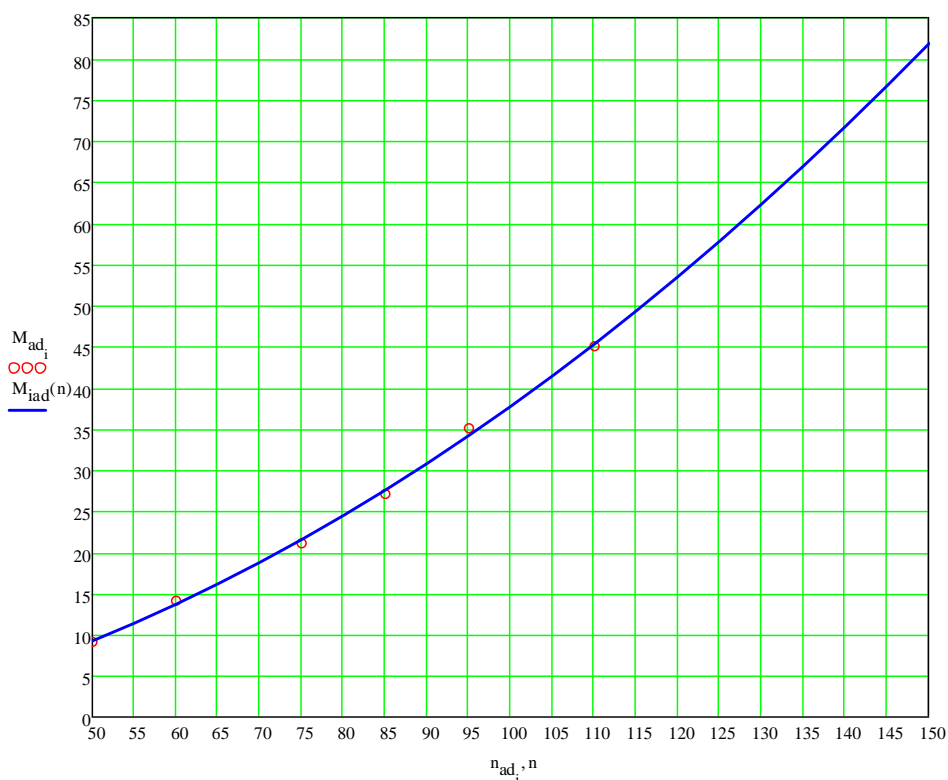
Fig. 6. The aerodynamic torque, M_{ad}, curve versus rotational speed, n

Dynamic balance with respect to the blade axis of rotation occurs between three torques: the torque of centrifugal force, M_{cfz}, the torque of aerodynamic forces relative to the axis of the blade spindle, Mad, and torque on the crank arm of the pre-compressed spring force, M_{spr}. Taking into account the sign of these torques, the relationship follows:

$$M_{spr}(\alpha) + M_{ad}(n) = M_{cfz}(\alpha, n) \tag{23}$$

By replacing the torques determined above, the relation (23) becomes:

$$\frac{l_m F_{spr}\cos(\alpha-\delta)}{3\cos(\delta)} + M_{ad}(n) = m_{cg}[\omega(n)]^2 R_{XY}^2 sin(\alpha_{min}+\alpha)cos(\alpha_{min}+\alpha) \tag{24}$$

The relationship (24) deduces the spring pre-compressed force which to be performed to maintain the balance within the optimum turbine speed range. When exceeding the maximum permissible rotational speed for the turbine, the dynamic balance is broken and counterweights turn the blades to the flag position followed by the aerodynamic braking of the rotor. The values obtained for $F_{spr}(\alpha, n)$ are very useful in spring dimensioning and enabling the mechanism to be triggered at the admissible limit speed.

$$F_{spr}(\alpha, n) = \frac{3\left(m_{cg}[\omega(n)]^2 R_{XY}^2 sin(\alpha_{min}+\alpha)cos(\alpha_{min}+\alpha) - M_{ad}(n)\right)\cos(\delta)}{l_m\cos(\alpha-\delta)} \tag{25}$$

5. Conclusions

All the components of this automated mechanical system can be calculated with sufficient accuracy, except for the aerodynamic torque. The friction forces were not taken into account because their size order is negligible relative to the other forces and torques which in turn are influenced by the tolerance fields of the component parts. The deduced relationships allow numerical simulation of this mechanism, modifying functional parameters, dimensions, etc. through which an optimal variant can be reached. As an automated mechanical system that needs to intervene promptly and safely, it is necessary to test it on a test bench in a repetitive manner. The approval of the system can be done only after at least one year of operation on a site with an aero-energy potential, so that all situations of climatic events can be traveled: high wind gusts, rain, snow, chill, extreme temperatures (negatives and positives), long periods of rest, etc.

References

[1] R. Bădărău, T. Miloș, "Protection Centrifugal Mechanism of the Wind Turbine Rotor of Overspeed", A XV-a Conferinţă internaţională – multidisciplinară, "Profesorul Dorin Pavel - fondatorul hidroenergeticii româneşti" – Sebeş, 2015, Vol. 28/2015, ISSN 2067-7138, pp. 297-304;
[2] R. Bădărău, T. Miloș, "Cinematica mecanismului centrifugal de protecţie la supraturare a rotorului de turbină eoliană de putere mică", A XVI-a Conferinţă internaţională – multidisciplinară, "Profesorul Dorin Pavel - fondatorul hidroenergeticii româneşti" – Sebeş, 2016, Vol. 30/2016, ISSN 2067-7138, pp. 29-36;
[3] R. Bădărău, T. Miloș, "Dinamica mecanismului centrifugal de protecţie la supraturare a rotorului de turbină eoliană de putere mica", A XVI-a Conferinţă internaţională – multidisciplinară, "Profesorul Dorin Pavel - fondatorul hidroenergeticii româneşti" – Sebeş, 2016, Vol. 30/2016, ISSN 2067-7138, pp. 37-46;
[4] P. Gipe, "Wind turbine basics", Chelsea Green Publishing Company, Vermont, USA, 2009;
[5] *** "Microgrid Integrated Small Power Renewable Energy Hybrid Systems", Grant UEFISCDI-PCCA 36/2012., Parteneriat UEFISCDI 2012-2016, Raport ştiinţific 2015, 2016;
[6] *** "Improvement of the Structures and Efficiency of Small Horizontal Axis Wind Generators with Non-Regulated Blades", EEA-Grant RO-0018/2009;
[7] R. Bădărău, "Contribuţii la studiul turbomaşinilor axiale neîntubate", Teză de doctorat, Editura Politehnica, Timişoara, ISBN: 978-606-554-372-0, 2011.

Dynamics of Hydraulic Cylinders.
Classical Mathematical Models and Simulations

Prof. PhD Eng. **Anca BUCUREȘTEANU**[1]

[1] University POLITEHNICA of Bucharest; ancabucuresteanu@gmail.com

Abstract: This paper presents mathematical models in dynamic mode for the study of hydraulic cylinders. It analyses the influence of the distributor type used for cylinder actuation but also the necessary correlation of pump flow, cylinder features and adjustment of pressure valve. The paper has a practical character because some unwanted dynamic aspects, such as, for example, the jerky start can be avoided since the designing phase of an installation.

Keywords: Cylinders dynamics, stabilization of pressure and speed, adjustment of pressure valve

1. Introduction. Hypotheses for calculation

At first consider the calculation diagram in Figure 1.

Fig. 1. The calculation diagram

Hydraulic pump HP supplies cylinder C through the electro-hydraulic distributor DCV. Surface chamber S_1 will be supplied by path A while the oil goes freely from surface chamber S_2 to tank T. The cylinder operates against force F and its rod moves with current speed v. The initial volume of oil from the left chamber of cylinder is V_0. As long as the distributor is not actuated (E-), the pump discharges freely on path P-A-T. When distributor (E+) is actuated, the connection P-B-A is performed (at cylinder). Pressure valve MV ensures the adjustment of the maximum pressure admitted at value p_{MV} [1]. The instantaneous pressure will be read on pressure gauge M. Depending on pressure, it is considered that through pressure valve MV can pass a quantity of oil ΔQ that can start from 0 and can reach value Q, where Q is pump flow, assumed constant. The instantaneous size X can have values included in interval [0, c] where c is the maximum stroke of cylinder rod.

We shall consider that the pump is initially turned on, then distributor DCV is actuated; this one switches instantaneously. These hypotheses on how the actuation is performed are shown in Figure 2.

Fig. 2. The hypotheses on how the actuation is performed

If pressure valve does not open, then all the flow of the pump reaches the cylinder. If pressure valve opens, in cylinder C arrives only flow Q_1 [1].

2. Mathematical- theoretical models

For such a system, the specialized literature [1] takes into consideration the mathematical model below:

$$Q = S \cdot v + \frac{V_0}{E_o} \cdot \frac{dp}{dt} \tag{1}$$

$$M \cdot \frac{dv}{dt} + b \cdot v + F = p \cdot S \tag{2}$$

In the relations (1) and (2) there were also noted: M - mass of powered mobile assembly; E_0 - modulus of oil elasticity; p - instantaneous pressure; t – time; b - cylinder damping factor.
PHASE 1. In the first phase, the cylinder rod does not move ($v = 0$), the pump sends fluid until reaching the value corresponding to resistance force F, covering the compressibility effects too. In these conditions we can consider:

$$v = 0 \tag{3}$$

$$Q = \frac{V_0}{E_o} \cdot \frac{dp}{dt} \tag{4}$$

$$dp = \frac{E_o \cdot Q}{V_0} \cdot dt \tag{5}$$

$$\int_{0}^{\frac{F}{S}} dp = \frac{E_0 \cdot Q}{V_0} \cdot \int_{0}^{t_1} dt \tag{6}$$

From relation (5) we can determine the time needed to this phase:

$$t_1 = \frac{F}{S} \cdot \frac{V_0}{E_O \cdot Q} \tag{7}$$

After time t_1, the pressure $p = F/S$ is reached, and speed is $v = 0$.
PHASE 2. From this moment on, the mathematical model becomes:

$$v \neq 0 \tag{8}$$

$$Q = S \cdot v + \frac{V_0 + x \cdot S}{E_O} \cdot \frac{dp}{dt} \tag{9}$$

$$M \cdot \frac{dv}{dt} + b \cdot v + F = p \cdot S \tag{10}$$

The volume of oil in section chamber S_1 is variable over time, depending on position. It is recommended to replace the value $V_0 + xS$ with an average volume V_M:

$$Q = S \cdot v + \frac{V_M}{E_O} \cdot \frac{dp}{dt} \tag{11}$$

From relations (10) and (11) we obtain the differential equation below:

$$\frac{d^2v}{dt^2} + \frac{b}{M} \cdot \frac{dv}{dt} + \frac{S^2 \cdot E_O}{M \cdot V_M} \cdot v = \frac{S \cdot E_O}{M \cdot V_M} \cdot Q \tag{12}$$

In this equation, the following notations will be made:

$$A = \frac{b}{M} \tag{13}$$

$$B = \frac{S^2 \cdot E_O}{M \cdot V_M} = \omega_0^2 \tag{14}$$

$$C = \frac{S \cdot E_O}{M \cdot V_M} \cdot Q = \omega_0^2 \cdot \frac{Q}{S} \tag{15}$$

With these notations, the equation (12) becomes:

$$\frac{d^2v}{dt^2} + A \cdot \frac{dv}{dt} + B \cdot v = C \tag{16}$$

In order to solve it, consider the attached equation [2]:

$$k^2 + A \cdot k + B = 0 \tag{17}$$

Depending on the values of expression $A^2 - 4B$, the following solutions will be obtained:
1. $A^2 - 4 \cdot B > 0$

$$v = \frac{\dfrac{C}{B}}{k_1 - k_2} \cdot \left(k_2 \cdot e^{k_1 \cdot t} - k_1 \cdot e^{k_2 \cdot t}\right) + \frac{C}{B} \tag{18}$$

Where k_1 and k_2 are the solutions of equation (17).
2. $A^2 - 4 \cdot B = 0$

$$v = \frac{-C}{B} \cdot e^{k \cdot t} + \frac{C}{B} \cdot k \cdot e^{k \cdot t} \cdot t + \frac{C}{B} \tag{19}$$

In the relation (19), k is the double solution of equation (17).
3. $A^2 - 4 \cdot B < 0$

$$v = e^{\alpha \cdot t} \cdot \left(\frac{-C}{B} \cdot \cos \beta \cdot t + \frac{\alpha}{\beta} \cdot \frac{C}{B} \cdot \sin \beta \cdot t\right) + \frac{C}{B} \tag{20}$$

In the relation above, it is considered that the complex conjugate roots ($i^2 = -1$) of equation (17) are:

$$k_{1,2} = \alpha \pm i \cdot \beta \tag{21}$$

Out of these three cases, the case 3 [3] has practical applicability. Therefore we shall continue to refer only to this one. Analyzing the equation (17) it can be noticed that $\alpha = -A/2 < 0$ always. If $\alpha = 0$, namely no account is taken of cylinder damping, then $\beta = \omega_0$.
From the relations above we can determine the evolution of pressure in this second phase:

$$p = \frac{F}{S} + \frac{M \cdot Q}{S^2} \cdot e^{\alpha \cdot t} \cdot \frac{\alpha^2 + \beta^2}{\beta} \cdot \sin \beta \cdot t \tag{22}$$

We can consider that the maximum value of pressure p from the relation above is:

$$p_{MAX} = \frac{F}{S} + \frac{M \cdot Q}{S^2} \cdot \frac{\alpha^2 + \beta^2}{\beta} \tag{23}$$

For determining the duration of this second phase (t_2) there are two distinct cases:
a. Maximum pressure resulted from relation (22) is higher than the pressure adjusted at pressure valve MV. This one will open and will limit the pressure in the system. In this situation there is the relation:

$$p_{MAX} > p_{MV} \tag{24}$$

In this case the duration of the phase in which the speed increases and the pressure is limited is:

$$t_2 = \frac{1}{\beta} \cdot Arc\sin \frac{\left(p_{MV} - \dfrac{F}{S}\right) \cdot S^2}{M \cdot Q \cdot e^{\alpha \cdot t_{MAX}}} \cdot \frac{1}{\beta} \approx \frac{1}{\omega_0} \cdot Arc\sin \frac{\left(p_{MV} - \dfrac{F}{S}\right)}{M \cdot Q \cdot \omega_0} \tag{25}$$

Figure 3 shows pressure evolution in this case.
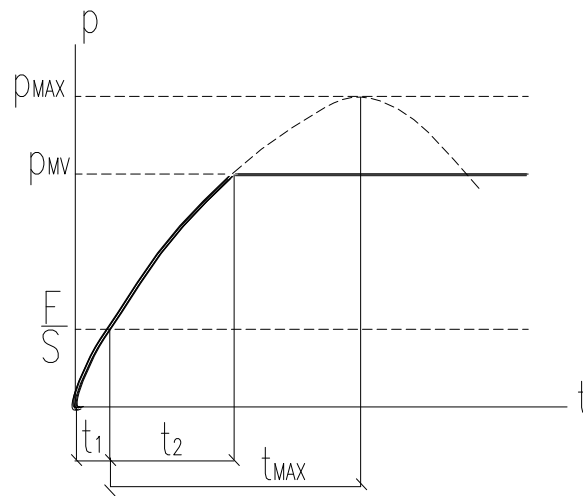
Fig. 3. Pressure evolution in case "a"

In Figure 3 it was noted with t_{MAX} the time for reaching maximum pressure for the first time, if pressure valve would not open. Valve opening has a damping effect.
b. If the valve does not open and the pressure develops according to relation (22), the pressure characteristic in time is shown in Figure 4.
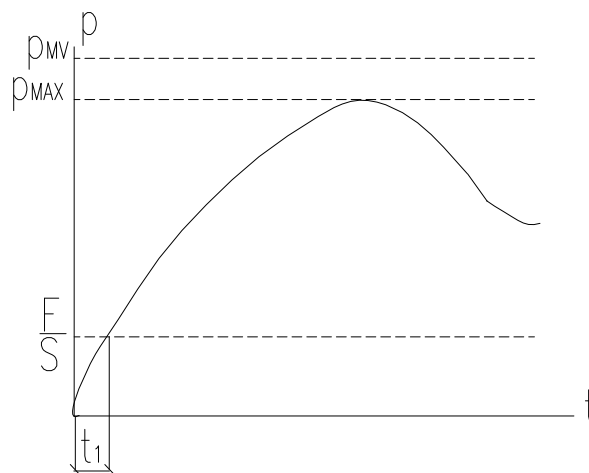
Fig. 4. Pressure evolution in case "b"

This case is undesirable in reality, the pressure oscillations resulting in jerky movements of the cylinder rod.
PHASE 3. Movement continues until reaching maximum speed. This time, a part of pump flow can be discharged through the pressure valve. The system pressure is constant and equal to the value set to pressure valve MV.
The mathematical model is:

$$M \cdot \frac{dv}{dt} + b \cdot v + F = p_{MV} \cdot S \qquad (26)$$

After solving the differential equation, we get the expression of speed in this phase:
If *b* differs from 0:

$$v = C_1 \cdot e^{-\frac{b}{M} \cdot t} + \frac{p_{VM} \cdot S - F}{b} \tag{27}$$

Constant C_1 is determined by stipulating the condition that speed at $t = 0$ is equal to speed v_2 from the end of the previous phase.
If $b = 0$:

$$v = v_2 + \frac{p_{MV} \cdot S - F}{M} \cdot t \tag{28}$$

At the end of this phase, the speed reaches the values resulted from using the entire flow, namely:

$$v_3 = \frac{Q}{S} \tag{29}$$

The duration of this phase is determined with the relation:

$$t_3 = \frac{\dfrac{Q}{S} - v_2}{p_{MV} \cdot S - F} \cdot M \tag{30}$$

PHASE 4. Starting from this moment the movement is performed with speed v_3, at pressure $p = F/S$ until reaching travel end.
The relations above help to determine speeds, pressures and strokes performed in each one of the four phases [3].

3. Simulation of hydraulic cylinders operation [4, 5]

Currently, the specialized programs of simulation of the hydraulic systems [6] in dynamic mode are a real help in design activity. It is recommended to take into account the instructions above in the case of some real units.
For example, consider the case of the cylinder actuated as in Figure 1. Value $p = F/S$ is 71.3 bar, and the second term of the sum in the relation (23) is 33 bar. In these conditions it is required a correct adjustment at pressure valve at 72 bar and a second one at a higher pressure of 120 bar.
For the first case, we obtain the pressure and speed characteristics in Figure 5.
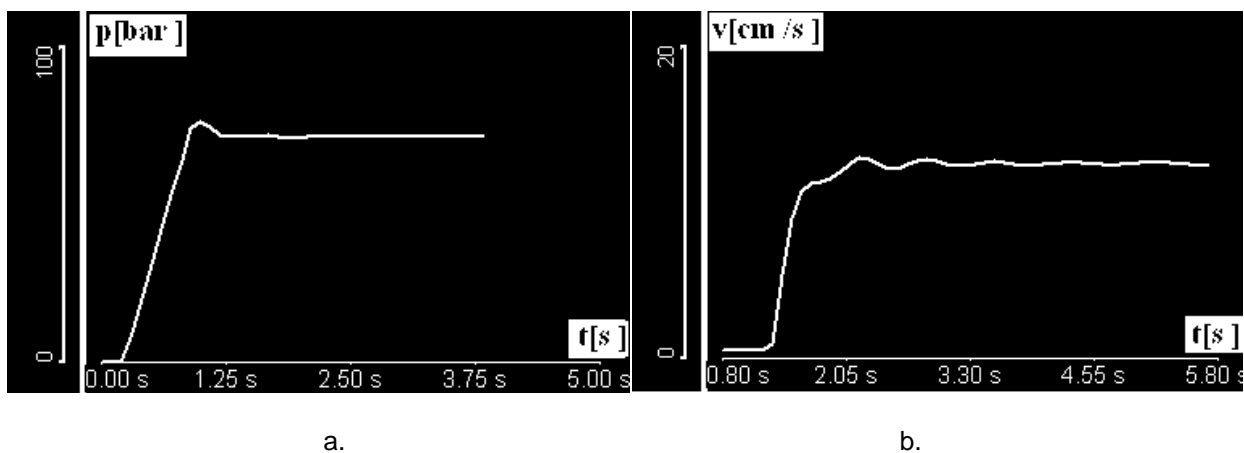
Fig. 5. The pressure (a) and speed (b) characteristics for the pressure valve MV adjusted at 72 bar

If pressure valve MV is adjusted at 120 bar, we obtain the characteristics in Figure 6.
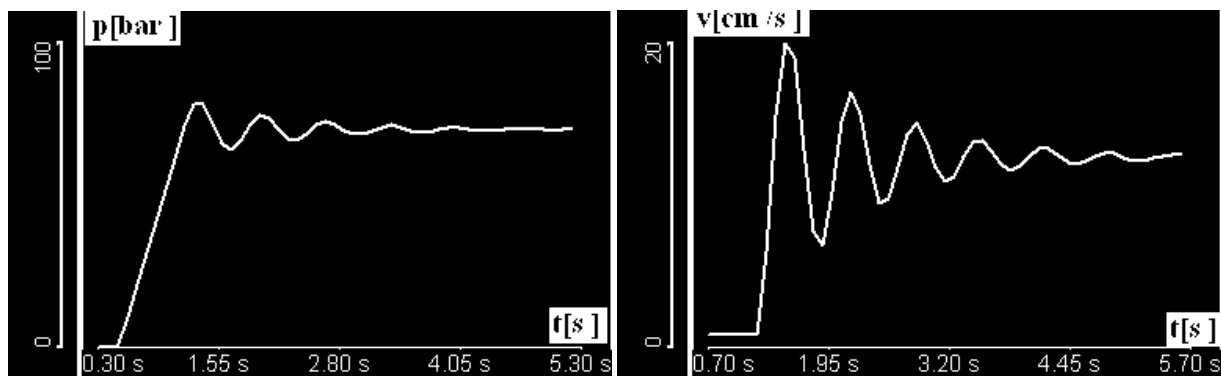
a.   b.

Fig. 6. The pressure (a) and speed (b) characteristics for the pressure valve MV adjusted at 120 bar

From the comparison of these two cases, it can be noticed that a pressure well adjusted at pressure valve MV influences rod speed and stabilizes its movement obviously.
The influence of damping can be increased by throttling the oil output from section chamber S_2 [6].

4. Conclusions

Smooth operation of a hydraulic cylinder is also conditioned by the correct correlation of source flow with the maximum pressure adjusted at this one. It is recommended that calculations of verification or sizing of the hydraulic cylinders are made in the preliminary phase of designing, not forgetting to determine the own beats ω_0. After determining them, even approximately, you can avoid faulty pressure settings. An exaggerated increase of the pressure adjusted at pressure valve MV does not lead to the elimination of jerking motion, and it may even amplify it. A pressure valve can reduce the oscillations of the entire system.

References

[1] D. Prodan, "Machine-Tools Hydraulics" („Hidraulica Maşinilor Unelte"), Printech Publishing House, Bucharest, 2004;
[2] B. Demidovitch, "Collection of Exercises and Problems of Mathematical Analysis" ("Recueil d'Exercices et de Problemes d'Analyse Mathematique"), MIR Publishing House, Moscow, 1974;
[3] F. Esnault, P. Beneteau, "Hydrostatics 1. Power Transmission" ("Hydrostatique 1. Transmission de Puissance"), Ellipses Publishing House, Paris, 1997;
[4] *** Software package: Automation Studio by Famic Technologies Inc.;
[5] *** Catalogues and leaflets ATOS, BOSCH REXROTH, PARKER;
[6] D. Prodan, "Machine-Tools. Modelling and Simulation of Hydrostatic Elements and Systems" („Maşini-unelte. Modelarea şi simularea elementelor şi sistemelor hidrostatice"), Printech Publishing House, Bucharest, 2006.

Genetic Programming Applied for Shaping a Design Hydrograph from the Historical Flows' Pattern

Dr. **Maritza Liliana ARGANIS JUÁREZ**[1,2], M. A. **Juan José BAÑOS MARTÍNEZ**[3], M. I. **Margarita PRECIADO JIMÉNEZ**[4], Ing. **Cecilia GONZÁLEZ CORREA**[1]

[1] Instituto de Ingeniería, Universidad Nacional Autónoma de México; MArganisJ@iingen.unam.mx

[2] Facultad de Ingeniería, Universidad Nacional Autónoma de México; MArganisJ@iingen.unam.mx, cgonzalezco@iingen.unam.mx

[3] Facultad de contaduría y administración, Universidad Nacional Autónoma de México; preciado@tlaloc.imta.mx

[4] Instituto Mexicano de Tecnología del Agua; juanjosebm@yahoo.com.mx

Abstract: *A method based on applying genetic programming (GP) in the ascending and the descending branch of a parameterized hydrograph is proposed in order to get a design hydrograph. Parameterization is done by considering peak flow, the peak time and the approximate time base estimated from the behavior of the annual maximum historical floods envelope and historical annual maximum floods envelope measured in the study site in the study site. With GP, was obtained the hydrograph's behavior before and after the peak flow for the historical data. Additionally, was made comparison of the GP results with a polynomial interpolation of Lagrange. Afterwards a design hydrograph was obtained, for "El Infiernillo" dam, considering the peak design flow, calculated with the Instituto de Ingeniería (IINGEN) Method. The volumes approached with GP was different from that reported by the IINGEN Method, but this difference could be corrected applying a factor to the hydrograph ordinates, with exception of the peak flow to keep the volume. Hydrograph shape obtained using GP and the IINGEN method were similar, with smoothed shapes in hydrograph obtained with GP, but ensuring similar shapes than the historical floods, even the volume, peak and base time.*

Keywords: *Average daily inflows, Base time, Design flood, "El Infiernillo" Dam, Genetic programming, Lagrange polynomial interpolation*

1. Introduction

There are different procedures to obtain the peak flow design, depending on the basin size, the measured data (if it comes to rainfall or runoff), and the basin physiographic information. The determining the behavior of design flow throughout the flood duration (time base) has been the subject of study by different authors: Pegram and Deacon (Pegram & Deacon 1992) worked by Hiemstra and Francis, they using the Pearson hydrographs type (Hiemstra & Francis 1979; Jiménez 2000). IINGEN Method based on alternating blocks and an analysis of annual maximum mean daily flow for a duration equal to the time base of the desired design flood (Domínguez et al. 2012) order spectral to get the shape of the hydrograph (Fuentes et al. 2015) historical increase envelope normalized method using a factor (Arganis et al. 2013), Hermitian hydrographs (Ramírez et al. 2000; Domínguez et al. 2012) among others. Many of these procedures are based in the case of floods that have a one peak, but sometimes provide different forms from those historically measured.

Moreover, the genetic programming (GP) is a random algorithm and it has tools of evolutionary computation for obtaining mathematical models from data of a dependent variable and n independent variables available and there have been several applications of it in problems of hydraulic and hydrological engineering, particularly in the rain runoff processes (Savic et al. 1999; Whigham et al. 2001; Goldberg & Holland 1988; Dorado et al. 2003; Rabuñal et al. 2007; Nourani et al. 2012; Danandeh et al. 2013; Meshgi et al. 2015).

Another deterministic algorithm that is useful to adjust tabular data functions is the Lagrange polynomial interpolation (Luthe et al, 1994; Chapra 2000) and it is applied in this work too to make some comparisons between results.

In this journal genetic programming (GP) was applied to parameterized data of annual maximum historical floods envelope of "El Infiernillo" Dam; located at Michoacán State in México; parameterization was performed on the values of time and flow taking into account the peak time (assumed in the center of all historical floods), the time base (was 15 days of duration) and peak flow of the historic floods (simultaneity assumed by matching the peaks in each year). Applying genetic programming with the simplest operators of addition, subtraction and multiplication polynomial forms were obtained for the ascending and descending branches of historical parameterized envelope. The factors obtained for each array are multiplied by the design peak flow and thus the flood is constructed. The procedure was repeated generating Lagrange polynomials. The results were compared with the flood previously calculated with the IINGEN Method. Similar hydrographs were obtained with all methods; only the volume obtained with the method GP was slightly higher than the IINGEN method, this was achieved by estimating an adjustment fix factor applied to the hydrograph ordinates. The procedure is simple and can be applied in different basins for validation purposes. This procedure is relevant because there are few international studies related to give the design hydrograph shape by considering both variables: volume and peak flow. Having this information another important hydraulic studies such as two dimension flow simulations in order to know flood plain can be performed.

So many countries, even Mexico, don't count with references that stand out procedures to give the estimation of the design hydrograph shape inasmuch as they only make simplification to regular geometric shapes (triangles, for example).

2. Methods

2.1 Study area and data descriptions

 "El Infiernillo" dam was built from 1960 on the Balsas River in Michoacán State, Mexico; is part of the dams system allocated along this river together with "La Villita" and "El Caracol" see Figure 1. The dam has a surface reservoir of 108 000 000 m2 and its spillway was designed for an outflow of 38 800 m3/s. Hydroelectric power generation began in October 1964, during 1965 were installed four units of the first stage and by mid-1975 came into operation the two turbines of the second stage. At the end of September 1967 occurred an extraordinary growing in the Balsas River, with entrance flow of 25 200 m3/s due to Hurricane Beulah and total volume of 7 500 million of m3, which was regularized at a maximum outflow of 7 500 m3/s; it was necessary to operate partially open radial gates to reduce the discharge of pouring the indicated value in order to protect another localized dam downstream (Jose Ma. Morelos) that was in construction (Domínguez et al. 2014).

The sum of four hydrometric stations: Los Pinzanes, Panches, La Pastoria and Caimanera were considered as input date. For the years 1965 to 1994, these data were multiplied by a factor of 1.3, such factor was obtained with the comparison between the sum and data reported in the common period for "El Infiernillo" dam. For the period of years 1998 to 2013 the daily average flow of total inflows reported by the "Comisión Federal de Electricidad (CFE) for the operation dam were used (Domínguez et al. 2014; Gómez 2015).
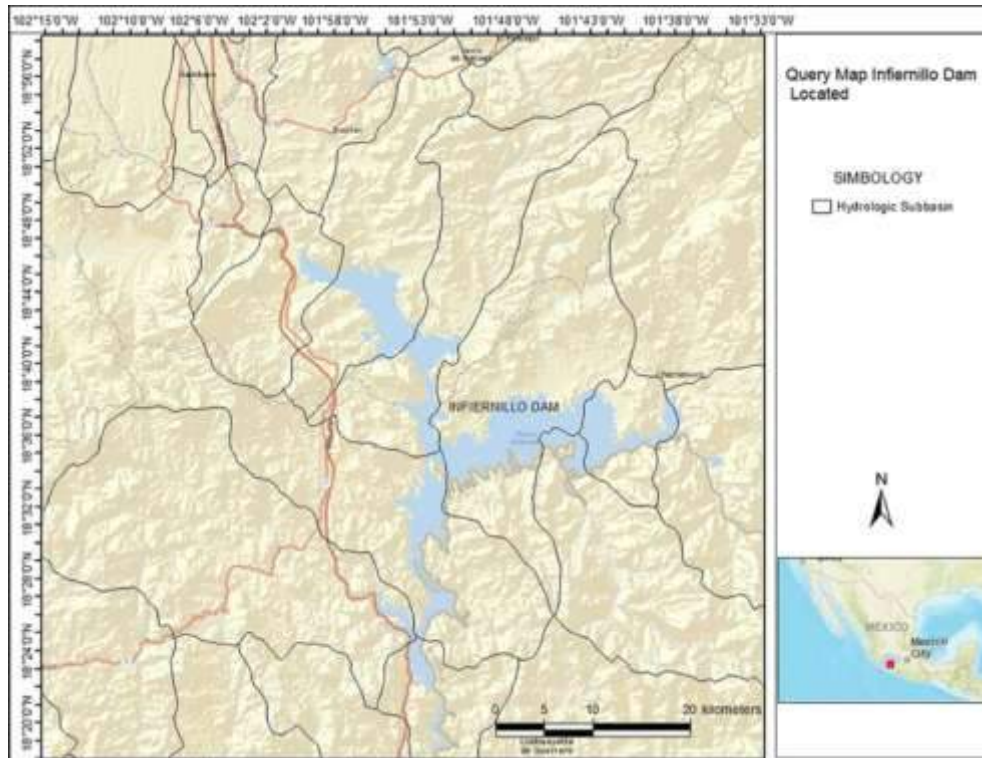
Fig. 1. "El Infiernillo" dam Michoacán, México

The Table 1 represent the daily average flow of total inflows reported as annual maximum flow, this comes from measured average daily inflows of the analyzed reservoir (records of Mexico's hydrometric stations are obtained from, first, the National Databank Surface Water (BANDAS) of the Water National Commission (CONAGUA 2016) and, second, the daily average flow of total inflows reported by the "Comisión Federal de Electricidad" (CFE).

Table 1: Annual maximum flood data. (CONAGUA 2016) and (CFE)

t, year	Q, cubic metre per second	t, year	Q, cubic metre per second
1965	4254.61	1991	5928.7
1965	4254.61	1991	5928.7
1966	2550.66	1992	2713.76
1967	14109.1	1993	2152.94
1968	2681.26	1994	2550.06
1969	5940.1	1995	5069.59
1970	3671.7	1996	3674.3
1971	5603	1997	1754.57
1972	2905.35	1998	5513.89
1973	7142.7	1999	3019.68
1974	2897.5	2000	3572.92
1975	4740.2	2001	4063.66
1976	9720.6	2002	3510.42
1977	3162.5	2003	5949.07
1978	3230	2004	8118.06
1979	2264.75	2005	3740.74

t, year	Q, cubic metre per second	t, year	Q, cubic metre per second
1980	2591.29	2006	3147.41
1981	4203.2	2007	2827.88
1982	1088.11	2008	3519.05
1983	2059.3	2009	2106.23
1984	7408.7	2010	3737.44
1988	2344.28	2011	5242.71
1989	1816.77	2012	2282.33
1990	2688.33	2013	15207.138

2.2 Study Annual maximum floods parameterized envelope curve

To construct the annual maximum historical floods envelope is required the measured average daily inflows of the analyzed reservoir (for Mexico's hydrometric stations, these records are obtained from the National Databank Surface Water (BANDAS) of the Water National Commission (CONAGUA) (CONAGUA 2016), with the hydrometric key and knowing the study area (hydrological region) see the Figure 2 and the Table 2, these data should be complemented with the information available of reservoir operation.

Fig. 2. "El Infiernillo" BANDAS interface (CONAGUA) query maps (CONAGUA 206)

Table 2: Annual maximum flood data. (CONAGUA 2016) and (CFE)

Code	Name	Flow	Basin	State
18481	La Caimanera	Balsas river	Balsas river	Michoacan
18487	Los Pinzones	Tacambaro river	Balsas river	Michoacan
18494	Los Panches	Tepalcatepec canal	Balsas river	Michoacan
18495	La Pastoria	El Marques river	Tepalcatepec river	Michoacan

After reviewing the data reported, the maximum annual flow is selected for each year and a certain number of days before and after the maximum flow, is set to define the time base and the maximum annual flood hydrograph's ascending and descending branches.

To have the worst behavior the peak flow of each annual flood are set matching them in peak time. In this study a time base of 15 days was considered for the historical floods and peak flow was placed on day eight.

For each day the maximum ordinate of all years is obtained, getting the annual maximum historical floods envelope.

The parametres are set for the time in the ascending branch considering the relation of time by the peak time (t/t_p) and the relationship of flow and peak flow (Q/Q_p); for the descending branch behavior was considered like the Hermitian hydrographs way, that is with $(t-t_p)/(t_p-t_b)$ and (Q/Q_p).

2.3 Genetic programming (GP)

Genetic programming (GP) (Koza 1992) takes place in a few years following the emergence of genetic algorithms (Goldberg 1989) in order to build computer programs and mathematical models with evolutionary random algorithms used as optimization methods. The genetic programming algorithm includes the establishment of the independent variables and the dependent variable in the problem, operators and constant vector to be considered for the construction of the models to be tested must also be defined. It should provide a probability of exchange or cross (crossing) of the best individuals (set of selected operations) and a probability of mutation must be given. A number of generations (iterations) is proposed to finish the optimization process. An example of the cross operator between two individuals is presented in Figure 3 were part of their nodes are exchanged each other, resulting in two new individuals.

In this study objective function consisted in minimizing the mean square error between the measured (Q/Q_p) data and the calculated with the models tested by the GP algorithm.

The problem starts with the random generation of an initial population of n individuals (each individual corresponds to a mathematical model consisting of different operators, variables and constants), individuals are then evaluated in the objective function and the best ones are selected (selection can be performed by obtaining a relative frequency of the result obtained by each individual in the objective function divided by the average value given by all tested individuals), individuals with higher relative frequency can be used more than once to be exchanged or crossover, and mutation may also create new individuals and the individuals with lower performance are eliminated and no enter to the exchange process and or mutation; so that the new population is again size n. The new individuals are again tested on their performance, selected and the best creates new individuals who pass to the next generation, this process is repeated until the number of generations or iterations is reached and the best individual in the last generation, will be the one with higher performance and represents the optimal mathematical model found.
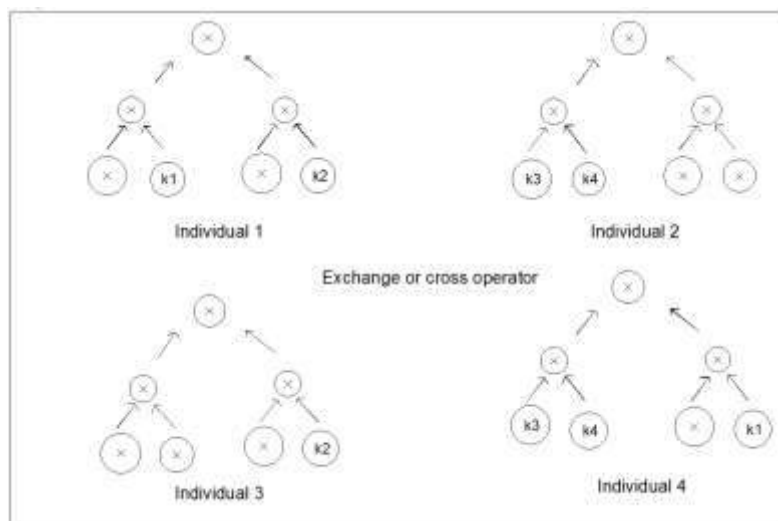
Fig. 3. Example exchange or cross (crossing) operator in GP

In this study the set of arithmetic operators *TS = [+,-,*]* was considered, a vector of constants obtained randomly, independent parameterized variable *(t/t_p)* in the upward branch and *t'= (t-t_p)/(t_b-t_p)* in the descending branch and a parameterized dependent variable (Q/Q_p) was considered too. Populations of 300 individuals (models) of 25 nodes (consisting of operators, variables and

constants), a crosses a probability of zero point nine and mutation probability of zero point five, were considered; finally, 10 000 generations to complete the process were considered.

The GP programming used in this study was developed at the "Instituto de Investigaciones en Matemáticas Aplicadas y en Sistemas" (IIMAS, UNAM).

2.4 Lagrange polynomial interpolation

Lagrange interpolation allows a polynomial of degree *n* passing through *n + 1* points; the polynomial is of the form (Luthe *et al.* 1994), as show in formula (1) .
Parentheses on the far right margin of the page, as formula (1):

$$P(x) = a_1 x^N + a_2 x^{N-1} + ... + a_N x + a_{N+1} \tag{1}$$

the coefficients $a_1, a_2,...,a_N$ are obtained by ensuring that the polynomial passes through each of the points $(x_1,y_1),(x_2,y_2),...,(x_{N+1},y_{N+1})$. It is a simple method to be applied, but its disadvantage is that to interpolate or extrapolate the result data corresponds to the image of the polynomial and may not correspond with the expected behavior of the analyzed function.

In this work it was used the code in Matlab polynomial interpolation of Lagrange presented in the website "Renewable energy of the University School of Industrial Engineering of Eibar (Energías renovables de la Escuela Universitaria de Ingeniería Técnica Industrial de Eibar)" (University of the Vasco Country 2016).

2.5 Mean square error and nonlinear determination coefficient

The mean square error (*MSE*), it is given by formula (2) and the nonlinear determination coefficient (R^2) for the formula (3), were applied in order to verify the goodness of the GP and Lagrange results.

$$MSE = \frac{1}{n}\sum_{i=1}^{n}\left(\frac{Q}{Q_p} - \frac{\overline{Q}}{\overline{Q}_p}\right)^2 \tag{2}$$

Where *n* is the number of data, $\frac{Q}{Q_p}$ and $\frac{\overline{Q}}{\overline{Q}_p}$ are, respectively, the measured and calculated parameterized flow data, and with the formula (3) is calculated the nonlinear determination and correlation coefficient

$$R^2 = \frac{\mathrm{var}\left(e^{\frac{Q}{Q_p}}\right) - \mathrm{var}\left(e^{\frac{\overline{Q}}{\overline{Q}_p}}\right)}{\mathrm{var}\left(e^{\frac{Q}{Q_p}}\right)} \tag{3}$$

Where R^2 is the non linear determination and correlation coefficient; *var* is the variance operator; Q/Q_p is de parameterized flow and e^{Q/Q_p} is the error in the parameterized flow obtained with the tested model .

3. Results and discussion

From the historical record of maximum annual floods a time base of 15 days was selected. The annual maximum historical floods envelope was obtained by setting the peak flow for each flood in the same peak and the maximum of all flow was calculated for each day, see the first column of the Table 3. The parameterized time and flow of the envelope are shown in Table 3, columns three, four and five.

Table 3: Annual Parameterized envelope annual maximum flood

t, days	Q, metre cubic per second	t / t_p, dimensionless	$(t-t_p) / (t_b-t_p)$, dimensionless	Q / Q_p, dimensionless
1	2808.44	0.125		0.1847
2	3857.35	0.250		0.2537
3	3738.70	0.375		0.2459
4	3861.90	0.500		0.2540
5	6191.80	0.625		0.4072
6	6939.20	0.750		0.4563
7	6984.70	0.875		0.4593
8	15207.14	1.000		1.0000
9	14117.44		0.1429	0.9283
10	11470.92		0.2857	0.7543
11	5920.39		0.4286	0.3893
12	4382.91		0.5714	0.2882
13	3994.80		0.7143	0.2627
14	3942.83		0.8571	0.2593
15	4163.04		1.0000	0.2738

3.1 Annual maximum floods parameterized envelope curve with genetic programming

Ascending branch equation

Parameterized data envelope ascending branch were selected and genetic programming algorithm was applied giving the polynomial model, as formula (4):

$$\frac{Q}{Q_p} = 0.3014794 * \left(\frac{t}{t_p} \right)^3 + 0.166641861 * \left(\frac{t}{t_p} \right)^2 + 0.24158976_{N+1} \tag{4}$$

the coefficients $a_1, a_2, ..., a_N$ are obtained by ensuring

Descending branch equation

Moreover, descending branch data were considered and Equation (5) was obtained with genetic programming, as formula (5):

$$\frac{Q}{Q_p} = t'^3 - 0.4786217 * t'^2 - 1.287393114 * t' + 1.057715508 \tag{5}$$

the formula (5) is applicable in interval $t_p < t < t_b$; where, $t' = (t-t_p)/(t_b-t_p)$.

For t_p, the peak flow is ensured with the formula (6):

$$\frac{Q}{Q_p} = 1 \tag{6}$$

the formula (6) is valid at $t = t_p$.

Lagrange polynomials

Ascending branch equation peak flow for ascending branch data were selected up (eight points) and it was used a program implemented in Matlab to obtain the coefficients of the polynomial of Lagrange (grade seven) for the ascending branch, see the formula (7):

$$\frac{Q}{Q_p} = -652.0 * \left(\frac{t}{t_p}\right)^7 + 2682.70 * \left(\frac{t}{t_p}\right)^6 - 445.40 \left(\frac{t}{t_p}\right)^5 + 3810.10 * \left(\frac{t}{t_p}\right)^4 -$$

$$-1803.00 * \left(\frac{t}{t_p}\right)^3 + 464.90 * \left(\frac{t}{t_p}\right)^2 - 59.40 * \left(\frac{t}{t_p}\right) + 3.10 \tag{7}$$

the formula (5) is applicable in interval $t_1 < t < t_p$;

Descending branch equation

Subsequently descending branch data (seven points) and the Matlab program was applied to obtain the Lagrange polynomial coefficients (grade six) for the descending branch, see the formula (8):

$$\frac{Q}{Q_p} = -141.1084t'^6 + 532.2911 * t'^5 - 801.8006 * t'^4 + 609.3198t'^3 -$$

$$-239.849t'^2 + 43.249t' - 1.8282 \tag{8}$$

the formula (8) is valid in interval $t_p < t < t_b$; where, $t' = (t-t_p)/(t_b-t_p)$.

$$\frac{Q}{Q_p} = 1 \tag{9}$$

formula (9) applies at $t = t_p$

Substituting the parameterized time in each case the factors in Table 4 are obtained.

Table 4: Factors (Q/Q_p) GP and Lagrange for the desing hydrograph

t, days	GP	Lagrange
1	0.2448	0.2220
2	0.2567	0.2915
3	0.2809	0.2821
4	0.3209	0.2859
5	0.3803	0.4322
6	0.4625	0.4723
7	0.5711	0.4657
8	1.0000	1.0000
9	0.8669	0.9283
10	0.6741	0.7543
11	0.4968	0.3893
12	0.3524	0.2882
13	0.2584	0.2627
14	0.2323	0.2593
15	0.2917	0.2738

3.2 Mean square error and nonlinear determination coefficient

In the Table 5 are set the mean square errors obtained with GP and Lagrange methods for the ascending and descending branch (AB and DB).

Table 5: Mean square error obtained in ascending and descending branches (AB and BD)

GP AB	GP DB	Lagrange AB	Lagrange DB
0.0028	0.0038	0.0008	0.0038

In Figure 4, the measured and calculated points of the ascending and descending branch (AB and DB) were drawn against the perfect fit and the linear R^2 obtained in an Excel© worksheet is given too. Tables 6 and 7 show the variance of parameterized Q/Q_p and the error obtained with both GP and Lagrange models in the ascending and descending branches. Finally in the Table 8 the nonlinear determination and correlation coefficients are shown.
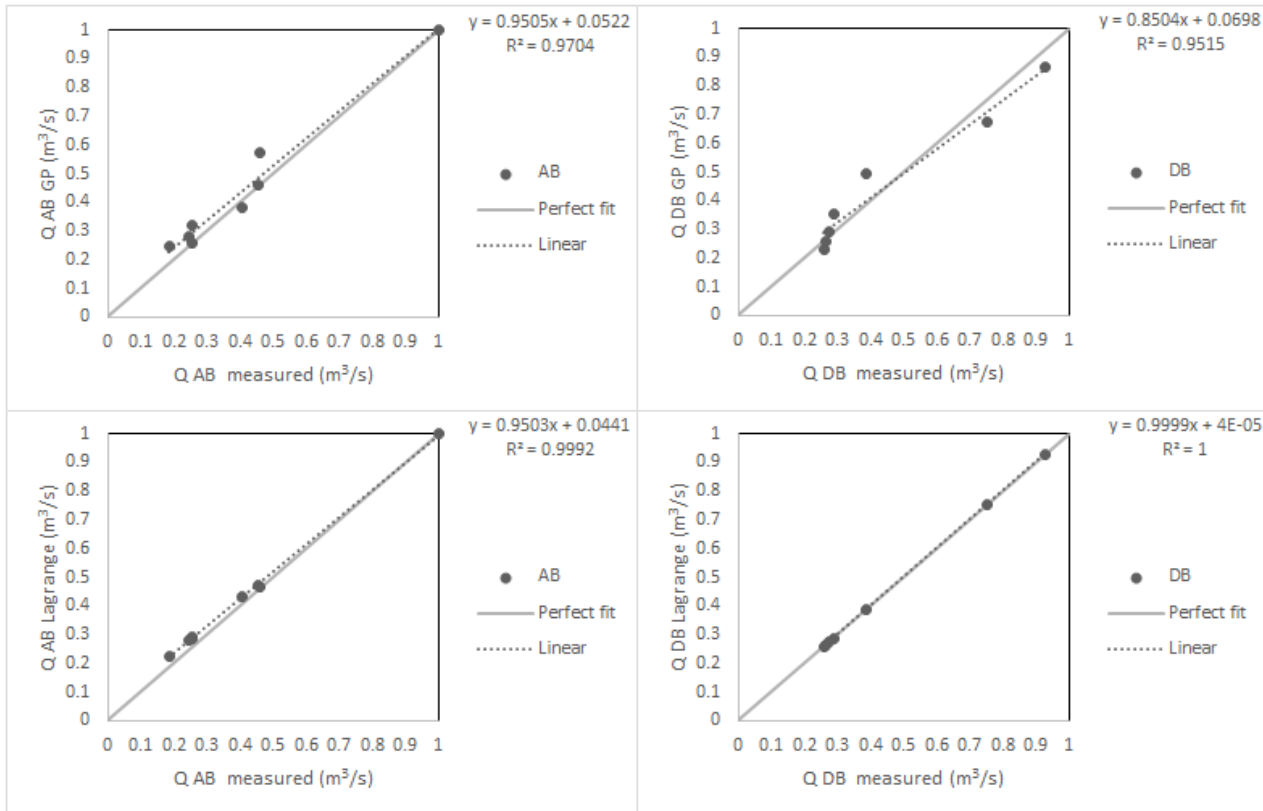
Fig. 4. Measured and calculated data with GP and Lagrange models in ascending and descending branches (AB and DB, respectively) against the perfect fit.

Table 6: Variances for ascending branch (AB)

Parameter	GP AB / Var Q	Var e_Q	Lagrange AB/ Var e_Q
	0.0684	0.0021	0.0002
R^2 nonlinear	0.9700		0.9968
r	0.9849		0.9984

Table 7: Variances for descending branch (DB)

Parameter	GP DB /Var Q	Var e_Q	Lagrange DB/ Var e_Q
	0.0756	0.0045	0.0045
R^2 nonlinear	0.9407		0.9408
r	0.9699		0.9699

Table 8: Nonlinear determination and correlation coefficient (R^2 and r)

Parametre	GP AB	GP DB	Lagrange AB	Lagrange DB
R^2	0.9700	0.9407	0.9968	0.9408
r	0.9849	0.9699	0.9984	0.9699

By multiplying the peak flow Q_p by design factors the hydrographs with the two methods are obtained and this are shown in the column 2 and 3 in the Table 3. The obtained floods were compared with both IINGEN Method and the increase of the historical maximum flood envelope, see the Table 9 and the Figure 4.

Table 9: Comparison of design hydrographs the annual maximum historical floods envelope

t, days	GP Q, m^3/s	Lagrange Q, m^3/s	Max envelope Q, m^3/s	IINGEN Q, m^3/s
1	9116.92	8269.82	6878.38	4990.87
2	9561.37	10857.98	9447.35	10140.71
3	10462.95	10505.14	9156.75	8589.49
4	11953.24	10649.75	9458.49	8616.84
5	14163.82	16098.97	15164.83	9005.45
6	17226.28	17590.45	16995.35	17885.25
7	21272.22	17344.29	17106.79	31500
8	37245.02	37245.02	37245.02	37245.02
9	32289.57	34575.85	34576.16	34754.98
10	25108.41	28094.25	28094.35	25700
11	18502.68	14500.24	14500.10	10636.63
12	13123.90	10734.99	10734.54	5701.63
13	9623.58	9784.81	9783.98	9379.9
14	8653.24	9657.94	9656.69	6456.25
15	10864.40	10197.69	10196.02	6776.73
16	21528.08	21263.66	20649.15	19645.61
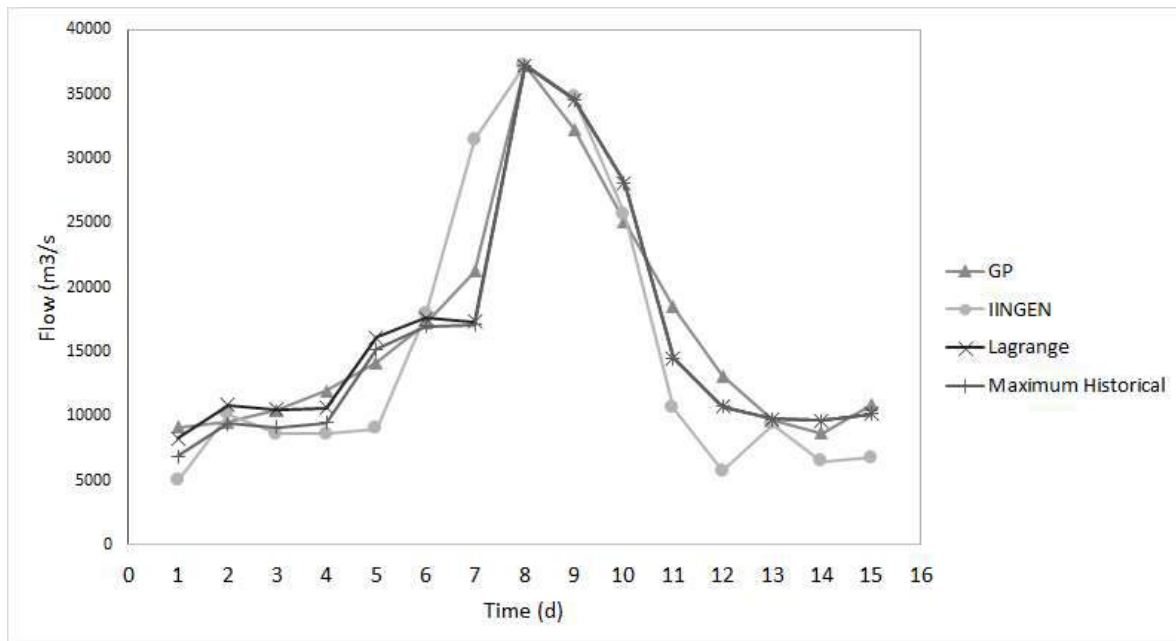
Fig. 5. Comparison of design hydrographs. Tr = 10 000 years. "El Infiernillo" dam.

In the Table 3 and Figure 5 shows that the method GP reports a volume slightly greater than those obtained with Lagrange polynomials respect to the design hydrograph calculated with the historical maximums envelope whereas the method of the Instituto de Ingeniería reported a lower volume.

Using the Solver tool © Excel © and the generalized reduced gradient method (GRG nonlinear), a factor to affect the calculated GP hydrograph was obtained to preserve the volume of the flood equal to that of the IINGEN method but preserving the peak flow; the new hydrograph is shown in Figure 6. The factor multiplies all hydrograph ordinates except the peak flow and was of 0.8972.
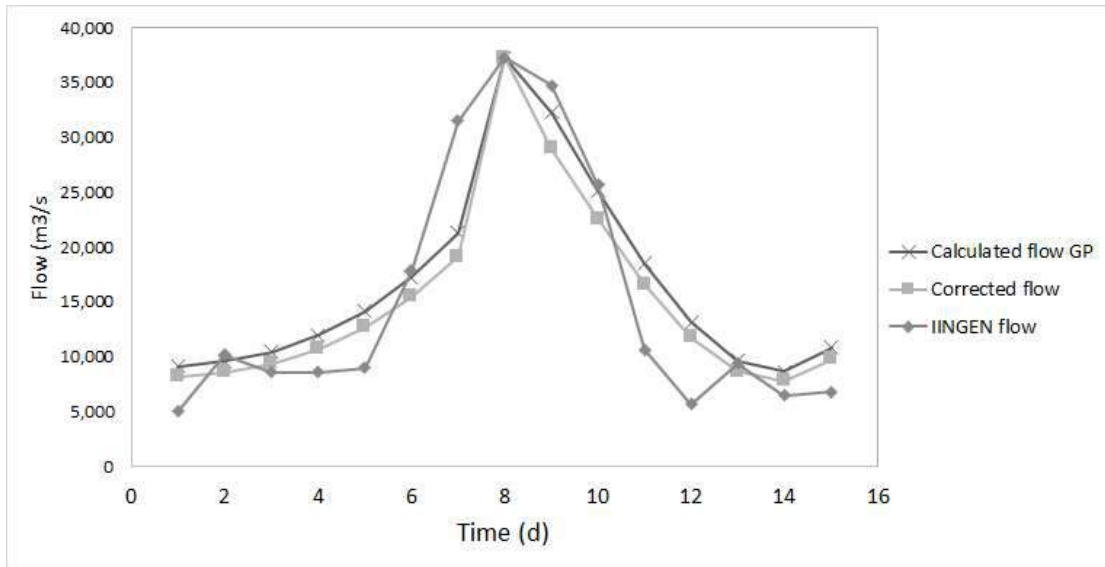
Fig. 6. GP corrected hydrograph to preserve the volume of the flood of IINGEN Method

Finally, the data of a design peak flow $Q_p=19\ 900\ m^3/s$ and a design volume $V=6\ 835.94$ millions of cubic metres obtained with a bivariate method for a return period of 10 000 years, considering different time base in the historic floods (Arganis *et al.* 2015), and the factors of GP see the Table 2 in column two were used to shape the design flood (Table 2), in the column two, then a factor of *0.5230* was obtained and applied in all ordinates except at the peak flow to adjust the volume of the flood (Figure 7). This resulted in a less robust hydrograph shape.
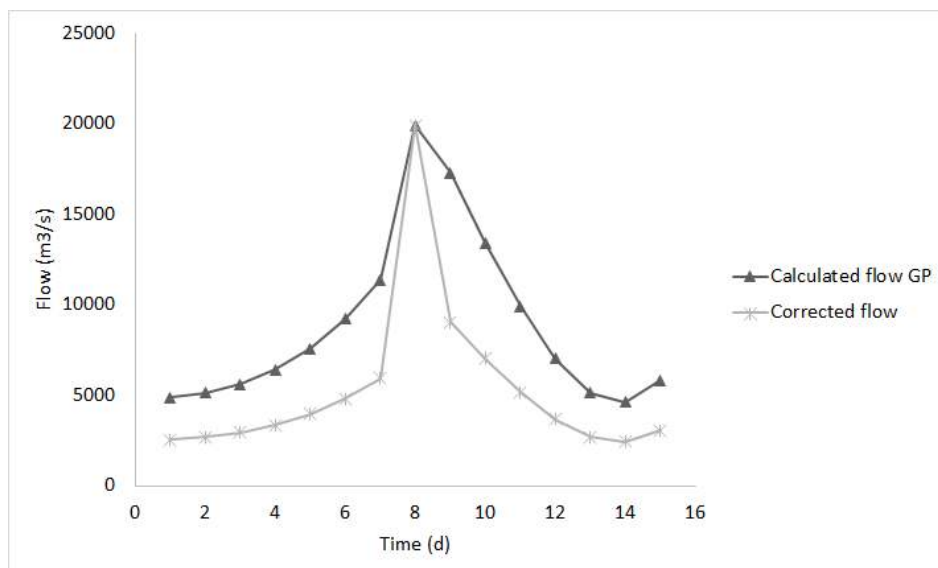
Fig. 7. Design hydrograph obtained for Tr = 10 000 years Q_p = 19 900 cubic metres per second, V = 6 835.94 millions of cubic metres (Bivariate). GP calculated and corrected volume

In the present journal, we show that with the bivariate method we can conserve the volume design and the peak flow; as well the hydrograph shapes, that present the historical behavior of any flood, are maintained. The last, is the contribution of our study. The historical shape is lost in other methods such as the Hermitian hydrographs and the Pearson hydrographs type. In both the base

time is given under a triangular hydrograph, therefore the shapes always correspond to a single peak flow; meanwhile, with the genetic program method we consider the annual maximum historical floods envelope, from which is possible to get diversified shape hydrographs. Finally, with the procedure presented herein the results are nearer to the real flood's behavior "flood"*,* so we can create design flood which simulate in a better way the profile of a analyzed dam, channels or any other hydraulic work. In an extraordinary event scenario this kind of simulation will help to transit more efficiently the flood.

4. Conclusions

A method based on applying genetic programming (GP) in the ascending and descending branch of a parameterized hydrograph was proposed in order to get a design hydrograph. Parameterization was done by considering peak flow, the peak time and the approximate time base estimated from the behavior of the maximum historical floods envelope measured in the study site.

The method of determining the shape of the ascending and descending branches of the maximum historic parameterized floods using polynomial functions obtained with GP is useful to shape the design flood similar to the historical behavior. This method has a correspondence rule which approximates the behavior of the flood and this represents the advantage respect to the increase of the annual maximum historical floods envelope. Additionally, it was possible to obtain a factor with allows corrections in the flood volume, keeping the peak flow and the time base proposed, which was useful when design peak flow and volume were obtained with bivariate methods. The method is an alternative to the IINGEN Method with the advantage that only requires analysis of maximum annual flow with one day duration and an assumed time base, reducing time calculations to shape the design flood.

References

[1] Aldama, Á. A., Ramirez, A. I. "Dam design flood estimation based on bivariate extreme-value distributions", *The extremes of the extremes: extraordinary floods: IAHS, 2002,Wallingford UK,* (271), pp. 257–262;

[2] Arganis M. L., Domínguez M. R., Rodríguez V. K. M., Preciado J., Ocón A. G., "Estimation of the bivariate distribution function of maximun historic floods", 21(2), Valencia, España, 2013, Memorias de las III Jornadas de Ingeniería del Agua, pp. 1-8;

[3] Chapra S. C., Canale R. P. "Numerical methods for engineers". Mc Graw Hill (ed.) 5 th edn, México, 2000;

[4] CONAGUA ftp://ftp.conagua.gob.mx/Bandas/Bases_Datos_Bandas (accessed 26 August 2016);

[5] Danandeh M. A., Kahya E., Olyaie E. "Streamflow prediction using linear genetic programming in comparison with a neuro-wavelet technique". 505(10), 2013,Journal of Hydrology, pp. 240-249;

[6] Domínguez M R., Arganis J. M. L. "Validation of methods to estimate flow rates for design discharge dam spillways with large regulating capacity". Hydrological Sciences Journal, 2012, 57(3), pp. 1-19;

[7] Domínguez M. R., Arganis J. M. L., Carrizosa E. E., Ramírez M. R., Gómez G. F. "Hydrologic study and determination of the operating policies of the vessels storage dams cascading over the Balsas River Balsas: El Caracol (CH Carlos Ramírez Ulloa), Adolfo Lopez Mateos (CH Infiernillo) and Jose Ma. Morelos y Pavon (CH La Villita))", Report CFE, Federal Electricity Commission, Mexico;

[8] Dorado J., Rabuñal J. R., Pazos A., Rivero D., Santos A., Puertas J. "Prediction and modeling of the rainfall-runoff transformation of a typical urban basin using ANN and GP". Applied Artificial Intelligence, 17(4), 2003, pp. 329-343;

[9] Fuentes M. O. A., Domínguez M. R., Arganis J. M. L., Herrera A. J. L., Carrizosa E. E., Sánchez C. J. A. "Estimate of design Hydrographs for the Angostura dam, Sonora, using statistical and spectral methods". Water Resources Management. Water Resour Manage, 2015, 29(11), p.p. 4021-4043;

[10] Goldberg D. E., Holland J. H. "Genetic Algorithms and Machine Learning. Kluwer Academic Publishers", 3(2), 1988, pp. 95-99;

[11] Goldberg D. E. "Genetic algorithms in search, optimization and machine learning". Addison-Wesley (ed.), 1a edn, New York, 1989;

[12] Gómez G. F. "Update the desing floods of the spillway of the dam "El Infiernillo"". Master's thesis, Universidad Nacional Autónoma de México, Mexico, 2015;

[13] Hiemstra L. A. V., Francis D. M. "The run hydrograph. In Theory and application for flood predictions", 107(6), 1979, Pretoria: Water Research Commission, pp. 759-775.

[14] Jiménez E.M. "Integral design of weirs. Ph.D thesis, Universidad Nacional Autónoma de México, México, 2000;

[15] Koza J. R. "Genetic programming, On the Programming of Computers by Means of Natural Selection". In: A Bradford Book (ed.), 1st. edn. London, England, 1992;

[16] Luthe R .A., Olivera S. F. "Métodos numéricos", Limusa Noriega (ed.), Mexico, 1994;

[17] Meshgi A., Schmitter P., Chui-Fong T. M., Babovic V. "Development of a modular model to quantify streamflow runoff from different land use Contributions in tropical urban environments using Genetic Programming". 525, 2015, Journal of Hydrology, pp. 711-723;

[18] Nourani V., Komasi M. & Alami M. "Hybrid Wavelet-Genetic Programming Approach to Optimize ANN Modeling of Rainfall-Runoff Process". Journal of Hydrologic Engineering 17(6), 2012, pp. 724-741;

[19] Pegram G. G. S., Deacon M. P. "Extreme flood Hydrographs of Chosen probability. International Symposium on Dams and Extreme Floods". International Symposium on Dams and Extreme Floods, ICOLD. Granada, Spain 16 September 1992, 17(6);

[20] Rabuñal J. R., Puertas J., Suárez J., Rivero D. "Determination of the unit hydrograph of a typical urban basin using genetic programming and artificial neural networks". Hydrological Processes, 21(4), 2007, pp. 476-485;

[21] Ramírez A. I., Aldama A. "Frequency joint analysis for the estimation of design floods", , IMTA, Serie Avances en Hidráulica, México, 2000;

[22] Savic D. A., Walters G., Davidson J. W. "A genetic programming approach to rainfall-runoff modeling. Water Resources Management", 13(3), 1999, pp. 219-231;

[23] http://www.sc.ehu.es/sbweb/energias-renovables/index.html], (accessed 26 August 2016);

[24] Whigham P. A., Crapper P. F. "Modelling rainfall-runoff using genetic programming". 33(7), 2001, Mathematical and Computer Modelling, pp. 707-721.

Comparative Study of the AWJ Cutting Geometry using the 3D Point Measuring Method versus 3D Scanning of the Surfaces

PhD. Stud. Eng. **Adrian Paul BASARMAN**[1] **,** PhD. Eng. **Nicolae MEDAN**[1]

[1]Technical University of Cluj-Napoca – North University Center at Baia Mare, Faculty of Engineering,
Victor Babeş str., No. 62A, 430083, Baia Mare, Romania
adrian.basarman@cunbm.utcluj.ro / nicolae.medan@cunbm.utcluj.ro

Abstract: The abrasive waterjet cutting (AWJ) method is a modern and very a useful technology cause it uses a different technique of cutting the material, more different than the classic way of cuting in which a tool takes contact with the part that needs to be cut. In order to asses the surface resulted after cutting, the kerf width, the surface has to be analysed on both sides of the cut, both on the part and the counterpart. In this paper it is presented a comparative study on a C45 part cutted using AWJ and, the surface resulted is first measured using a 3D measuring arm that measured the surface in points per surface and, second, using a more modern technology, the 3D scanning device. The same surface has been measured with this two different technologies and the results are compared and presented in this paper.

Keywords: Abrasive water jet (AWJ), kerf width, geometry of cut, 3D measuring of surface, 3D scan.

1. Introduction

The abrasive waterjet (AWJ) cutting method is, as mentioned in the abstract, a modern method for cutting different types of materials, from glass, rocks, steel to, even, titanium. The way of cutting the material is one aspect of the situation, the other one is the way of analysing and measuring the resulted surface. In order to have more accurate results, the techonology used for analysing the surface, the kerf width, is of vital importance. The geometry of cut is one of the most important factors in analysing and determining the quality and precision of cut when using AWJ technology.
In this paper it is presented a comparative study on a C45 part cutted using AWJ and, the surface resulted is first measured using a 3D measuring arm that measured the surface in points per surface and, second, using a more modern technology, the 3D scanning device. The same surface has been measured with this two different technologies and the results are compared and presented in this paper.
Studies regarding the field of waterjet cutting have been made by authors like Srivastava et.al. [1], Marcu et. al.[2], Filip et.al. [3], Hereghelegiu et.al [4], and also Hreha et.al. [5].

2. Work method and experimental setup

2.1 Abrasive Water Jet (AWJ) Machine

The experiments were conducted using an abrasive waterjet (AWJ) cutting machine - *Bystronic ByJet Pro L* - presented in Figure 1.

Fig. 1. Bystronic ByJet Pro L water jet cutting machine;

2.2 Part cutting

First of all, the part that was cuted was a 50x50x20 mm part made from a C45 plate, as presented in figure 2. The parameters for the cutting regime used for cutting the C45 part are presented in table 1.
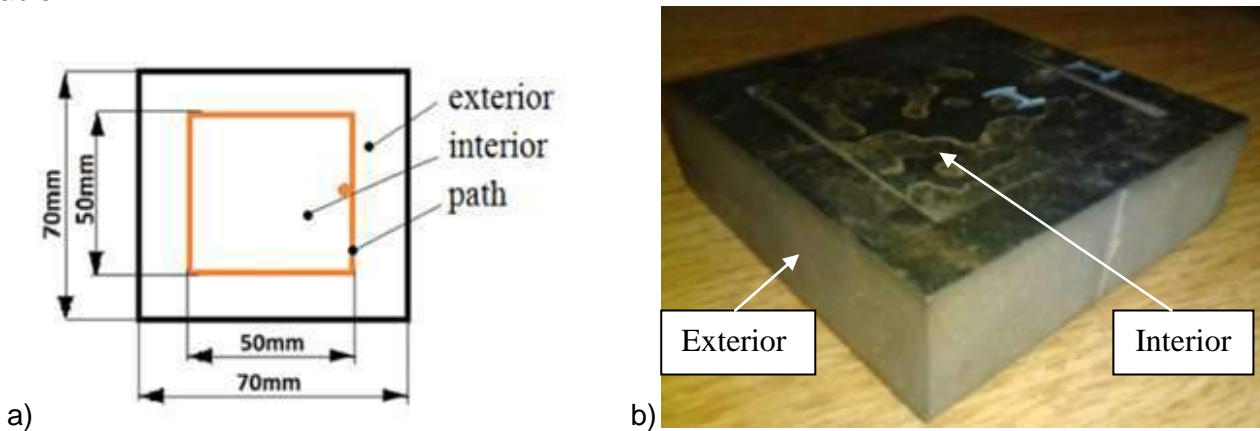
Fig. 2. a) Design for cutting, b)The cutted C45 part

In order to take notice of how the surface has modified after cutting, we had to analyse, in parallel, both the interior and the exterior of the kerf, as presented in figure 2.

Table 1: The selected cutting regime parameters

Parameters	Value selected
Breakthrough time	13 s
Breakthrough pressure	3600 bar
Abrasive material used	GMA Garnet 80 Mesh (300-150 micron)
Quantity of abrasive material	342 g/min
Cutting pressure	3600 bar
Cutting speed	45 mm/min
Interior sapphire nozzle	0,28 mm
Exterior nozzle	0,8 mm

2.3 Method of measuring

After cutting the steel part, both the interior and the exterior, as presented in figure 3, were analysed, in order to determine the exact geometry of the surfaces. For analysing, two different methods were selected:
- measuring the surfaces in points per surface to describe the surface, using a 3D measuring arm
- scaning the surfaces to get a 3D version of the part, using a 3D scanner
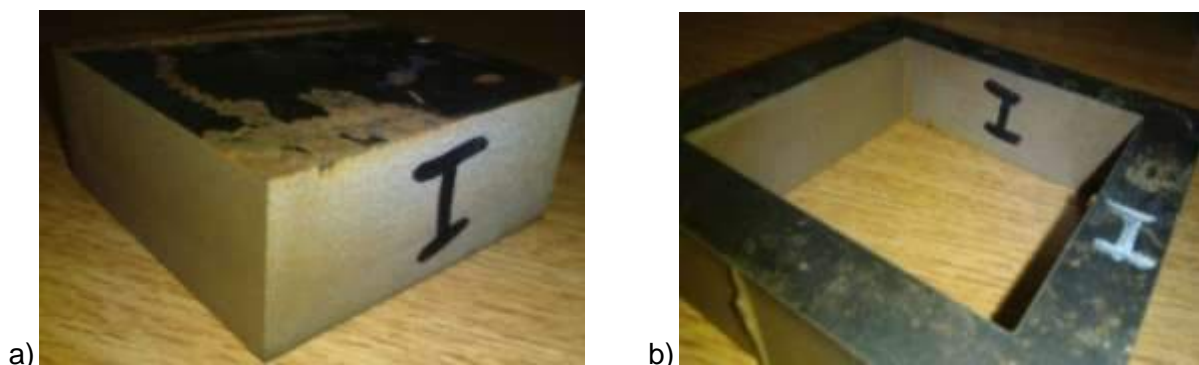
Fig. 3. a) Interior of the cutted part, b) Exterior of the cutted part

The way of numbering, measuring and analysing the surfaces is presented in figure 4. The way of analysing is in this position and the interior (I1-4) with the exterior (E1-4).

Fig. 4. The way of numbering and analysing the surfaces on the C45 part

2.3.1 Using the 3D measuring arm

After cutting the steel part, for both the interior and the exterior, as presented in figure 3, in order to determine the exact geometry of the surface, there were measured a total of 30 points on each surface, using a 3D measuring arm, as presented in figure 5a and b. The 30 measurements were divided on 3 rows, 10 measurements on each row, as presented in figure 5c.

a)

b)

c)
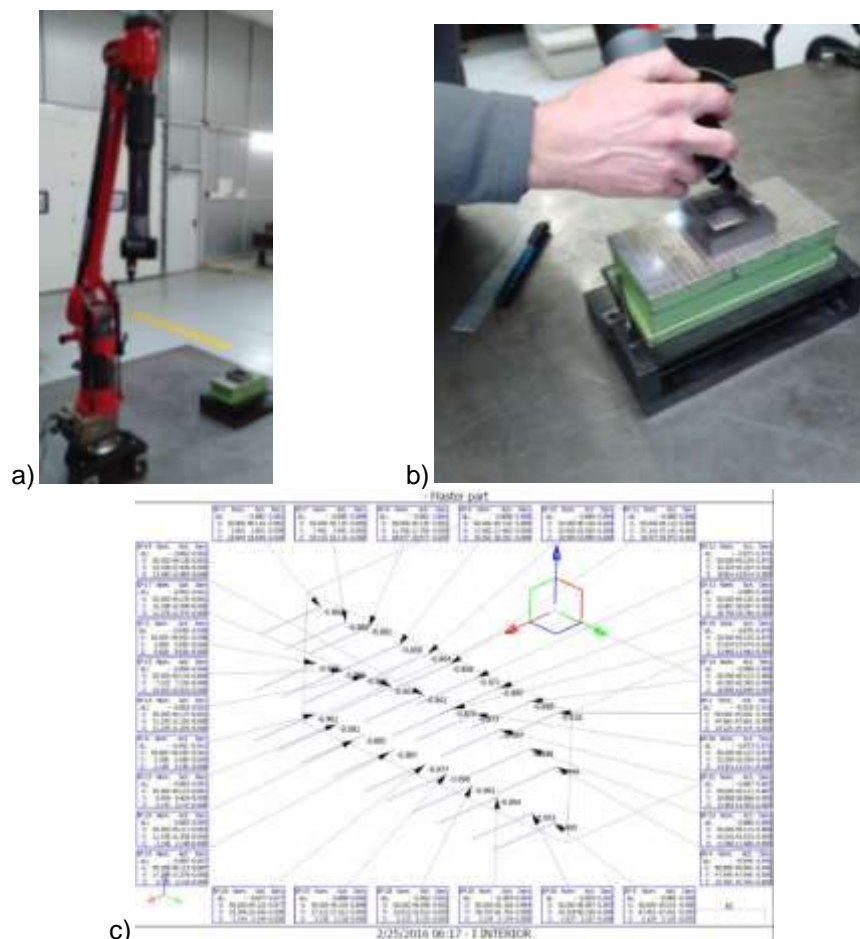
Fig. 5. a) Cimcore Infinite 3D measuring arm, b) Measuring the part, c) The way of measuring the part

2.3.2 Using the 3D scanner

The 3D scanning is a state-of-the-art technology that, by recording the images and matching them to build a virtual image of the scanned object, succeeds in copying the look and feel of the scanned object and transposing it into the virtual environment. The scanner used for this research is presented in figure 6a.

In order to make the part visible for the scanner, a layer of white titanium based spray had to be applied, making it of a lusterless white, which doesn't reflect the light anymore. The process of spraying can be seen in figure 6b.

Also, after spraying, the part is set on the machines rotative board and the automatic scanner does it's job and scans the part, as presented in figure 6c, and the part is beeing then transfered to computer to be processed and analysed.

a)   b)

c)
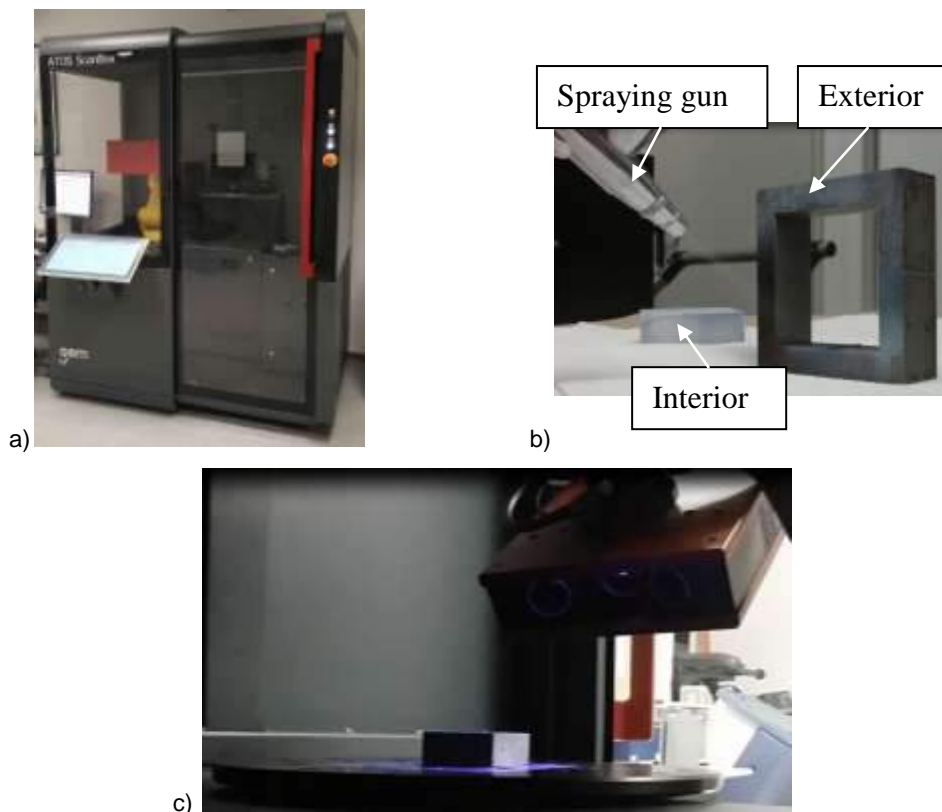
Fig. 6. a) *GOM ATOS ScanBox 4105*, b) Spraying the parts with titanium based spray paint,   c) Scanning the parts

The result after scanning the surfaces of the C45 part, both interior and exterior, made as an assembly, can be observed in figure 7.
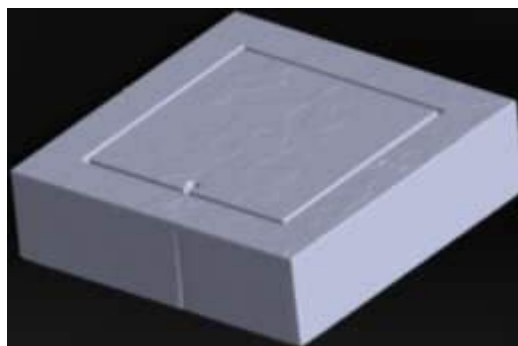
Fig. 7. The C45 3D scanned assembly (interior + exterior)

3. Results after measuring and analysing the surfaces

After measuring and scanning every surfaces, as mentioned before, the values were obtained, centralised and analysed. In both cases, the opposite surfaces were analysed one with another, exterior with interior, generating some results that presented two different values: the minimum kerf width and the maximum kerf width.

3.1 Results after measuring the surface using the 3D measuring arm

Regarding the measures that were made using the 3D measuring arm, after finishing the measurements and analysing the results, the minimum and the maximum kerf width are presented for all surfaces, as one can observe, in table 2.

Table 2: Results after measuring the surfaces using the 3D measuring arm

Surfaces	Kerf width	
	min [mm]	max [mm]
S1	0.733	0.988
S2	0.752	0.989
S3	0.731	0.971
S4	0.733	1.031

3.2 Results after measuring the surface using the 3D scanner

Regarding the analysing made after scanning the surfaces using the 3D scanner, a table similar with the one made with the results for the other method of measuring the surface was made. The table with the results can be observed in table 3.

Table 3: Results after measuring the surfaces using the 3D scanner

Surfaces	Kerf width	
	min [mm]	max [mm]
S1	0.61	1.16
S2	0.63	1.59
S3	0.60	1.15
S4	0.69	1.15

After obtaining the results from both of the methods of measuring and analysing the C45 part cutted using AWJ, two graphics have been made to describe the differences in the measured values, both for the minimum value of the kerf width and also for the maximum value of the kerf width, as one can observe in figure 8 a and b.
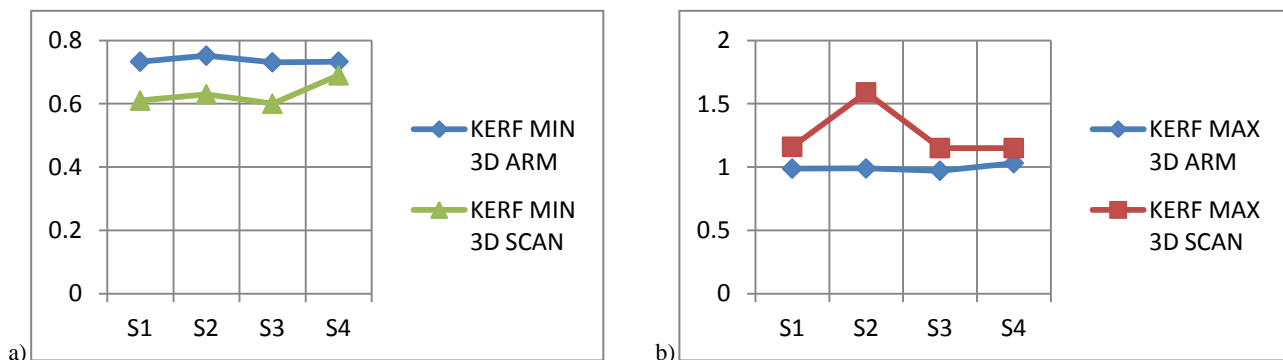
Fig. 8. Analysing the kerf width in both of the analysed cases (using the 3D measuring arm and also using the 3D scaner): a) Kerf width minimum values, b) Kerf width maximum values.

4. Conclusions

After analysing all the results of the described experiments, realised for a part cutted from a specified material (C45), the following conclusions can be highlighted:

a) The results for both measurements are aproximatelly close, but a slight difference can be observed in both the minimum and maximum values, for both measurements;

b) Using the 3D measuring arm is a less precise method because it uses a ball tipe tip for taking the measurements on surfaces, and the tip sometimes can be bigger and doesn't take the measurements corectlly;

c) The 3D measuring arm takes points on surface, and the process is random, possibly missing the bigges or the smalles kerf width values;

d) Using the 3D scanning method is the most precise method because it transforms the C45 part into a 3D part that can be viewed very precise;

e) Analysing the measurements made using the 3D measuring arm, as one can observe, the biggest kerf width 1.031 mm and, the smallest kerf width 0.731;

f) Analysing the measurements made using the 3D scanner, as one can observe, the biggest kerf width 1.59 mm and, the smallest kerf width 0.6.

References

[1] M. Srivastava, R. Tripathi, S. Hloch, S. Chattopadhyaya et al., "Potential of using water jet peening as a surface treatment process for welded joints",Vol.149. Procedia Engineering, pp. 472-480, 2016;

[2] I.L. Marcu, and C. Ciupan, "Alternating Flow Hydraulic Generator for Water Jet Cutting Systems", "Hidraulica" (No. 1/2016) Magazine of Hydraulics, Pneumatics, Tribology, Ecology, Sensorics, Mechatronics, ISSN 1453 - 7303, pp. 61-66;

[3] A. C. Filip, M. A. Vasiloni, L. A. Mihail, "Experimental research on the machinability of Hardox steel by abrasive waterjet cutting",Vol.94. In *MATEC Web of Conferences.* EDP Sciences, pp. 03003, 2017;

[4] E. Herghelegiu, M. C. Radu, C. Schnakovszky and C. N. Tampu, "Considerations on material thickness influence on the AWJ processing quality of an aluminium alloy", Vol.94. In *MATEC Web of Conferences.* EDP Sciences, pp. 03007, 2017;

[5] P. Hreha, A. Radvanska, L. Knapcikova, G. M. Królczyk et al., "Roughness Parameters Calculation By Means Of On-Line Vibration Monitoring Emerging From AWJ Interaction With Material", Vol.2.(22) Metrology and Measurement Systems, pp. 315-326, 2015.

Examining the Characteristics of Pedrollo_CP130 Centrifugal Pump in Simulated Service Conditions

Assist. Prof. PhD. Student Eng. **Nikolett FECSER**[1]

[1] Széchenyi István University, H-9026 Győr Egyetem Square 1, Hungary; fecser.nikolett@sze.hu

Abstract: *In my study I examine the characteristics of a Pedrollo_CP130 centrifugal pump during operation. My choice of topic is justified by the facts that Pedrollo pumps have widely been applied, they are reliable and can be operated highly efficiently. Since their improper usage can cause problems, I decided to study the parameters of Pedrollo_CP130 pumps during operation to be able to avoid these problems. The fundamental characteristics of these pumps are flow rate, elevation head, power demand and efficiency. The monitoring of the pump's characteristics is undertaken in the fluid dynamics laboratory in Széchenyi István University. The measuring device available in the laboratory is suitable for measuring the parameters of pumps. The whole measurement process is traceable on the screen belonging to the measuring device and the measurement parameters can be determined and the results can be recorded by computer software. In my study I describe the measuring device used in the hydrodynamics laboratory at Széchenyi István University. I give a description about the types of measurements available in the laboratory and show the measurement results carried out by a Pedrollo_CP130 pump, the correlations determined from them and the conclusions taken from the measurement. The outcomes of my study can be beneficial when we operate pumps of similar types.*

Keywords: *Elevation head, flow rate, power demand, efficiency, pump*

1. Introduction

Pumps determine all aspects of our lives and influence them directly or indirectly. Some areas, including but not limited to water supply, water-related activities, crisis and disaster management, firefighting, health care, agriculture, industry, producing electricity, household technology and food industry, where pumps play an important role. Pumps are one of the most well-known and widespread type of a machine. Their task is to move fluid from one place to another, generally from a lower place to a higher one in a certain distance. The most important technical parameters of a pump are fluid volume moved per unit time, elevation head, NPSH and efficiency [1]. The operational characteristics of a pump are the data and the correlations which reflect the characteristics of the pump during operation. Pumps always carry various types of fluids integrated with some type of motor, pipes and packers. These are called outer characteristics. The hydraulic system, the construction materials and the structure of the pump belong to its internal characteristics [2].

2. The description of the laboratory of fluid mechanics at Széchenyi István University

2.1 The construction of the measuring device in the Laboratrory of Fluid Mechanics at Széchenyi István University

Certain measurements in a pump start-up required for "The Machinery in Thermotechnics and Fluid Mechanics" are carried out in the laboratory of the Széchenyi István University (Fig. 1). The Pedrollo CP_130 and Nocchi_CB80_38T hydraulic pumps move water from a lower tank into a upper tank through a symmetric pipe system. Due to the design of the pipe system, ball valves allow different ways for water to be moved between the two tanks. This makes it possible to examine their operation in line or in parallel and the parallel operation of the pipes. The elevation head of the pumps can be determined by the manometers installed into the suction and the discharge lines. Primarily the control fittings installed into the section placed after the connection of the two lines control the flow rate of the pumps. The flow meters installed into the discharge pipes are used to measure the flow rate of the water carried by the pumps [3].

From the discharge pipe of the pump a bypass branches and returns to the suction tank which allows to carry out measurements relative to the so-called bypass control. Control fittings and flow rate gauge can be found int the bypass. Both the lower and the upper tank bear hose fittings. Overpressure and vacuum can be created in the tanks with modifying the position of the fitting installed into the pipe for the returning water. By means of the frequency inverter on the pumps' motors, revolution can be controlled within certain limits. Water control is performed with Programmable Logic Controllers placed into the switch cabinet next to the apparatus. Opening the ball valve, water can be returned from the upper tank into the lower tank. Stopping and restarting the pumps, the power absorbed by the engine, the modification of revolution, the modification of mains frequency and its instantaneous value together with recording the pressures and flow rates in the software running in the portable computer can be carried out with connecting the measuring device and the computer with a USB. The measuring device is demonstrated on the graphic user interface, on which the position of the pins and control fittings can be illustrated. The different measured values can be read. The software opens the measured values and the applied settings can be opened with MS Excel program [3].

Fig. 1. Laboratory of Fluid Mechanics at Széchenyi István University [3]

Table 1: Technical Specifications of Measuring Equipment [4]

	Technical Specifications	
Pump Type	Pedrolló CP130	Nocchi CB80/38
Amount of Delivered Water	Q_{max}=100 l/min	Q_{max}=80 l/min
Delivery Height	H_{max}=20 metre (2 bar)	H_{max}=30 metre (3 bar)
Number of Impeller Vanes	N=1pc	N=2 pcs
Electric Motor	P=0,37 kW, 3x400 V AC	P=1,1 kW, 3x400 V AC
Speed of Electric Motor	n= 2800 rpm	n= 2800 rpm
Range Regulated by Frequency changer	f=30-60Hz	f=30-60Hz

2.2 The measurements that can be carried out in the Fluid Mechanincs Laboratory at Széchenyi István University

Current measurements related to the subject of "Machinery in Fluid Mechanics and Thermotechnics" are the realization of the Affinity Laws, the Affinity Laws on the Best Efficiency Point of the characteristic curve, joint operation of pipes in parallel, joint operation of pumps in parallel and joint operation of pumps in-line

3. Measurements carried out in the Fluid Mechanics laboratory at Széchenyi István University

3.1 Taking the characteristic curve of the pump

As the first step in my examination, I selected the pipeline track, which can be seen in Fig.2.
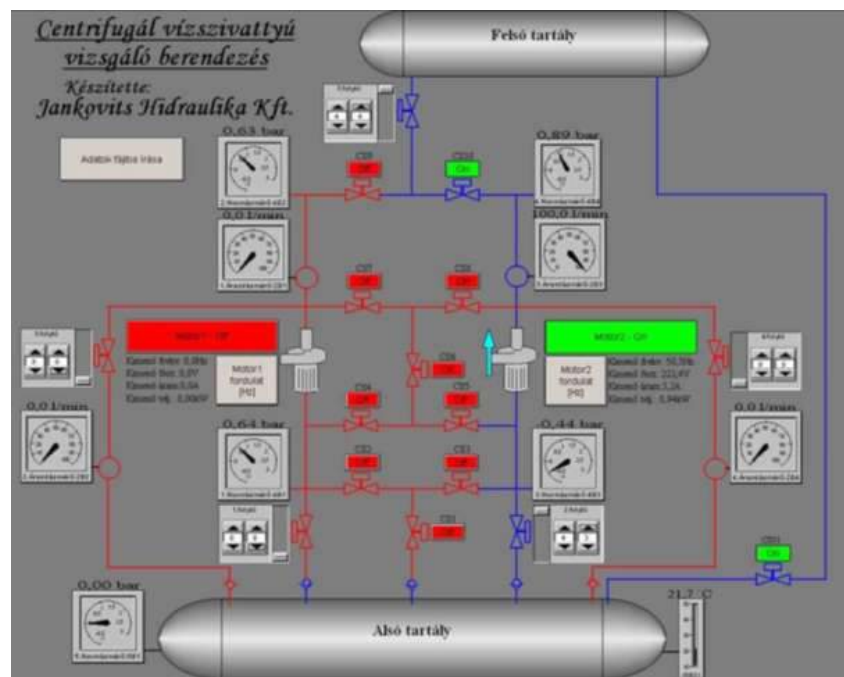
Fig. 2. Graphic User Interface of the software [3]

In Figure 2 fluid can flow in the blue lines. Green fittings are in an open stage, red pipes do not let fluid flow because the red fittings are in closed stage. These settings were carried out on the test bench and digitally on the evaluating software interface as well. The collected data were documented by the software of the computer. At the end of the measurement phase, I saved the data as a csv file and processed them with MS-Excel. The current status of the measured values was monitored on the LCD screen see Figure 1. At the constant speed of the pump (3000 rpm) I increased the flow rate from zero to the maximum possible with gradually opening the control fitting installed into the discharge pipe. At each measuring point, I recorded the values both in front of the inlet and after the outlet of the pump and the power absorbed of the electric motor. To achieve higher accuracy, three measurements were taken with 2-3 seconds difference at each measuring point and their arithmetical mean was used for further calculations. The measured values served as a basis for calculating the elevation head in the following formula (1).

$$H = \frac{(p_2 - p_1) \cdot 10^5}{\rho \cdot g} \tag{1}$$

Table 2: The measured and calculated data of Pedrollo pump [Author compilation]

Motor frequency [Hz]	Pump revolution [rpm/min]	Motor performance [kW]	Flow rate [l/min]	Pressure [bar]	Elevation head [m]
50	3000	0,21	0,00	2,13	21,71
		0,22	7,00	2,01	20,49
		0,23	16,00	1,93	19,67
		0,25	23,00	1,85	18,86
		0,26	31,00	1,78	18,14
		0,27	40,00	1,67	17,02
		0,28	48,00	1,57	16,00
		0,29	56,00	1,47	14,98
		0,30	64,00	1,33	13,56
		0,31	79,00	1,07	10,91
		0,31	82,00	1,02	10,40

Using the measured values, after carrying out the necessary calculations, I drew a series of points illustrating how the elevation head changes in the function of flow rate.
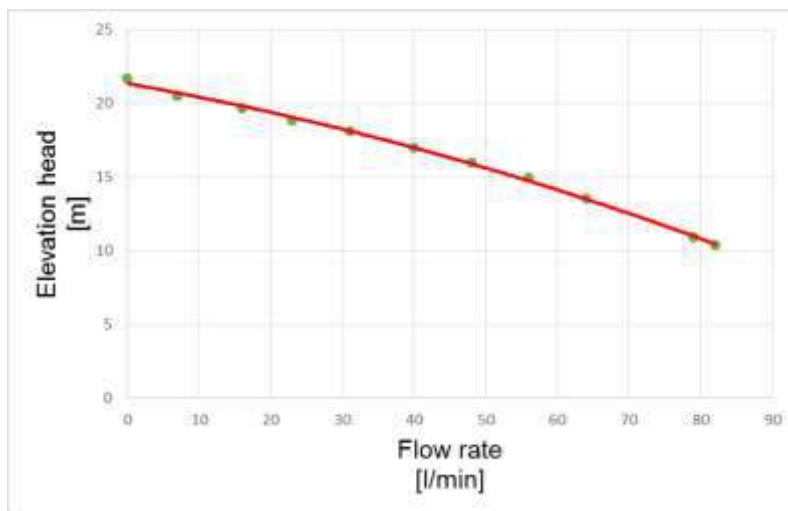
Fig. 3. Characteristic curve of Pedrollo pump [Author compilation]

Table 3 shows the flow rate and the elevation head of the Pedrollo CP_130 pump given by the manufacturer.

Table 3: The measured and calculated data of Pedrollo pump [4]

Motor frequency [Hz]	Flow rate [l/min]	Elevation head [m]
50	0,00	23,00
	10,00	22,00
	20,00	21,00
	30,00	20,00
	40,00	19,00
	50,00	18,00
	60,00	17,00
	70,00	15,50
	80,00	14,00

Figure 4 shows the characteristic curves of various Pedrollo pumps given by the manufacturer. I

used the CP_130 type for testing.
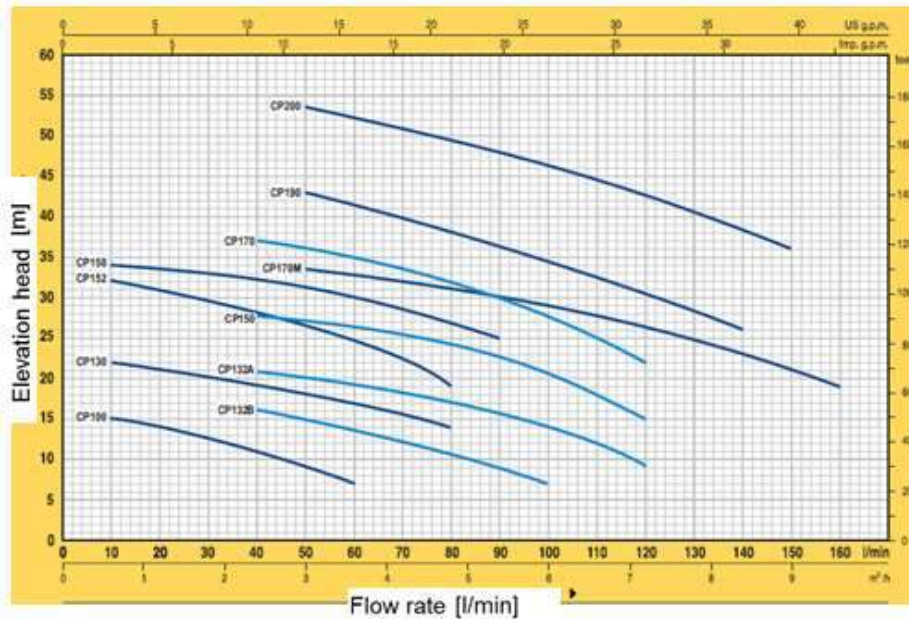
Fig. 4. Characteristic curves of various Pedrollo pumps

From fig. 4 and the data in the instruction manual, it can be concluded that the data I measured and my calculated results show a 5%-difference on average. It can be justified with with the fact that my measurements were carried out under non-standard circumstances. Due to local conditions there can be significant differences as well.

3.2 Defining the flow rate – performance curve of the pump

Table 4 shows the results of my measurements on flow rate-performance.

Table 4: Pedrollo pump flow rate performance [Author compilation]

Motor frequency [Hz]	Pump revolution [rpm/min]	Motor performance [kW]	Flow rate [l/min]
		0,210	0,00
		0,220	7,00
		0,230	16,00
		0,250	23,00
		0,260	31,00
50	3000	0,270	40,00
		0,280	48,00
		0,290	56,00
		0,300	64,00
		0,310	79,00
		0,310	82,00

I designed the flow rate-performance curve on the basis of the measured data.
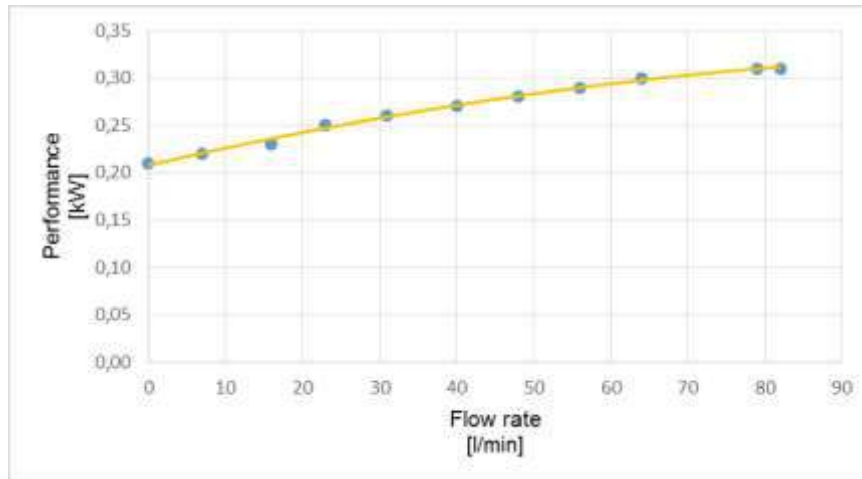
Fig. 5. Pedrollo pumps flow rate – performance curve [Author compilation]

3.3 Examining the Affinity Laws on the Best Efficiency Point of the curve

The purpose of the measurement is to examine the realization of the Affinity Laws on the Best Efficiency Points of the characteristic curves with different revolutions. The Affinity Laws states that the characteristic curves' corresponding points at different revolution values lay on the same central quadratic parabola. It means that the elevation head is proportional to the square of revolution and flow rate is directly proportional to revolution [5].

$$\frac{\dot{V}_1}{\dot{V}_2} = \frac{n_1}{n_2} \tag{2}$$

$$\frac{H_1}{H_2} = \left(\frac{n_1}{n_2}\right)^2 \tag{3}$$

$$\dot{V}_2 = \frac{n_2}{n_1} \cdot \dot{V}_1 \tag{4}$$

$$H_2 = \left(\frac{n_2}{n_1}\right)^2 \cdot H_1 \tag{5}$$

$$\left(\frac{\dot{V}_2}{\dot{V}_1}\right)^2 = \left(\frac{H_2}{H_1}\right) \tag{6}$$

$$H_2 = \frac{H_1}{\dot{V}_1^{\,2}} \cdot \dot{V}_2^{\,2} \tag{7}$$

$$H_2 = K \cdot \dot{V}_2^{\,2} \tag{8}$$

To examine the Affinity Laws on the Best Point Efficiency it is needed to create the pump's characteristic and flow-efficiency fitting curve taken at various revolution values. Based on the measuring method introduced in 3.1, I drew the pump's characteristic curve on rated speed (at 50 Hz power frequency), a smaller than rated speed (at 30Hz power frequency) and a higher than

rated speed (at 60Hz power frequency). Flow rate and the density of the transport medium served as a base for my calculations to determine the theoretically appropriate efficiency and the one on the basis of the motor performance [6].

$$\eta = \frac{H \cdot \rho \cdot g \cdot \dot{V}}{P} \qquad (9)$$

Tables 5-6-7 show the measured and calculated values at different revolutions.

Table 5: Measurement results of the motor operated at 30 Hz frequency [Author compilation]

Motor frequency [Hz]	Pump revolution [rpm/min]	Motor performance [kW]	Flow rate [l/min]	Pressure [bar]	Elevation head [m]	Efficiency [%]
30	1800 ford/min	0,07	0,00	0,82	8,36	0,00
		0,07	8,00	0,77	7,85	14,67
		0,08	16,00	0,74	7,54	24,67
		0,08	24,00	0,69	7,03	34,50
		0,09	31,00	0,65	6,63	37,31
		0,10	39,00	0,58	5,91	37,70
		0,10	48,00	0,50	5,10	40,00

Table 6: Measurement results of the motor operated at 50 Hz frequency [Author compilation]

Motor frequency [Hz]	Pump revolution [rpm/min]	Motor performance [kW]	Flow rate [l/min]	Pressure [bar]	Elevation head [m]	Efficiency [%]
50	3000	0,21	0,00	2,13	21,71	0,00
		0,22	7,00	2,01	20,49	10,66
		0,23	16,00	1,93	19,67	22,38
		0,25	23,00	1,85	18,86	28,37
		0,26	31,00	1,78	18,14	35,37
		0,27	40,00	1,67	17,02	41,23
		0,28	48,00	1,57	16,00	44,86
		0,29	56,00	1,47	14,98	47,31
		0,30	64,00	1,33	13,56	47,29
		0,31	79,00	1,07	10,91	45,45
		0,31	82,00	1,02	10,40	44,97

Table 7: Measurement results of the motor operated at 60 Hz frequency [Author compilation]

Motor frequency [Hz]	Pump revolution [rpm/min]	Motor performance [kW]	Flow rate [l/min]	Pressure [bar]	Elevation head [m]	Efficiency [%]
60	3600 ford/min	0,29	0,00	2,70	27,52	0,00
		0,30	7,00	2,53	25,79	9,84
		0,33	16,00	2,35	23,96	18,99
		0,35	23,00	2,26	23,04	24,75
		0,36	31,00	2,14	21,81	30,71
		0,39	39,00	2,01	20,49	33,50
		0,40	48,00	1,86	18,96	37,20
		0,41	55,00	1,71	17,43	38,23
		0,42	63,00	1,56	15,90	39,00
		0,43	71,00	1,40	14,27	38,53
		0,44	80,00	1,22	12,44	36,97
		0,44	85,00	1,09	11,11	35,09

To be able to determine the flow rate at Best Efficiency Point, I illustrated the relevant efficiency curve belonging to each revolution value separately. Then I drew all the curves in one diagram. (Fig. 6) The values are summarised in Table 8.
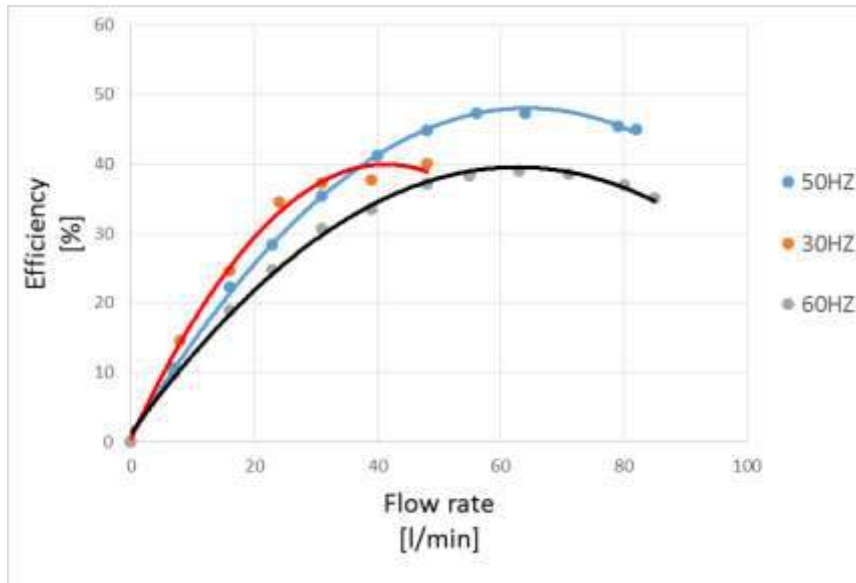
Fig. 6. Efficiency curves of a Pedrollo pump [Author compilation]

Table 8: Measurement results of the motor operated at 60 Hz frequency [Author compilation]

Motor frequency [Hz]	Maximum efficiency/Best Efficiency Point [%]	Flow rate [l/min]
30	40,00	48,00
50	47,31	56,00
60	39,00	63,00

The characteristic curve shown in Figure 7 presents the values recorded as the result of the measurements in one coordinate-system.
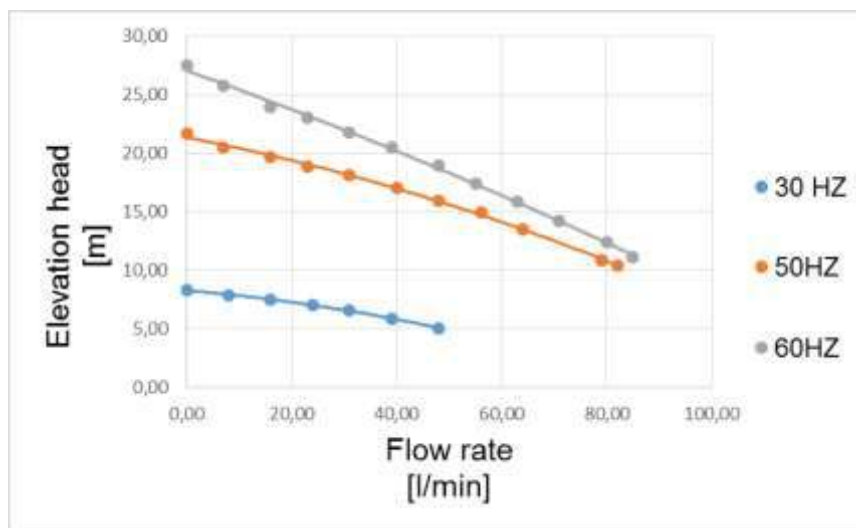
Fig. 7. Characteristic curves of a Pedrollo pump [Author compilation]

In the coordinate-system of the characteristic curves I drew the affinity parabola, which intersects the characteristic curve of rated speed at the Best Efficiency Point (also known as normal operating point of a pump). This is shown in Fig.8.

Table 9: Best efficiency Point at rated speed/revolution [Author compilation]

Motor frequency [Hz]	Maximum efficiency/Best Efficiency Point [%]	Flow rate [l/min]	Elevation head [m]
50	47,31	56,00	14,98
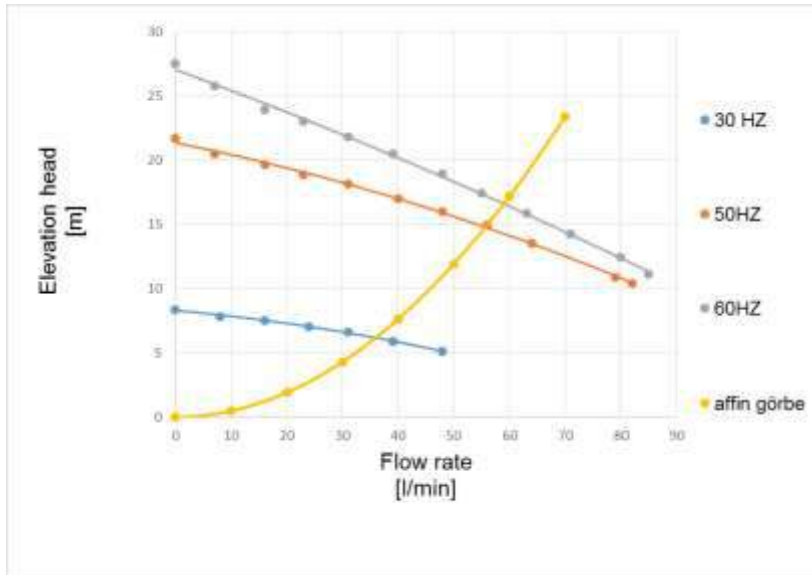
Fig. 8. Characteristic curves of Pedrollo pumps, affinity parabola [Author compilation]

I read the coordinates of the intersection of affinity parabola and the characteristic curve taken at 30 Hz and 60 Hz and summarised them in Table 10.

Table 10: Best efficiency Point at rated speed/revolution [Author compilation]

Revolution [rpm/min]	Flow rate [l/min]	Elevation head [m]
1800	36,00	6,15
3000	56,00	14,98
3600	59,00	16,85

I calculated the Affinity Laws' realization degree:

$$\frac{\dfrac{\left|\dfrac{Q_2}{Q_1}-\dfrac{n_2}{n_1}\right|}{\dfrac{n_2}{n_1}}+\dfrac{\left|\dfrac{Q_2}{Q_3}-\dfrac{n_2}{n_3}\right|}{\dfrac{n_2}{n_3}}}{2} \qquad (10)$$

With the first method the Affinity Laws' realization degree is: 10,275 % The Affinity Laws are realized at the Best Efficiency Point in the characteristic curve since it is within 9%. On the basis of the given results it can be stated that the Affinity Laws came to realization. The differences may be caused by the volumetric and hydraulic losses [7]. The accuracy of measurement and evaluation must be added to the consideration of the given results. During the measurement process the set frequency fluctuated influencing the characteristic curve and the values among the measuring points [8].

4. Conclusions

In my study I presented the measuring device in the Fluid Mechanics laboratory at Széchenyi István University. I explained the types of measurements available in the laboratory and described the measurement results carried out by a Nocchi_CB80_38T pump. I stated the relations and made conclusions from the results. It is important to note that measurements during operation are generally carried out under non-standard conditions. Due to the local conditions, usually you must accept the sometimes significant differences as well. The results clearly show that if the revolution decreases, the flow changes and the efficiency is highly reduced. Increasing revolution may cause stiffness related problems on the one hand, or the appearance of cavitation resulting in "broken down" characteristic curves on the other hand. The experience and results recorded in my study are suitable to make the operation of pumps more effective. A more detailed studying of cavitation and processing its measurement results are likely to improve the efficiency and the safety of the system.

References

[1] R. Kuti, "Advantages of Water Fog Use as a Fire Extinguisher", ACADEMIC AND APPLIED RESEARCH IN PUBLIC MANAGEMENT SCIENCE 14:(2) pp. 259-264, 2015;

[2] Cs. Fáy, Á. Troskolanski, J. Varga, "Szivattyúüzemi kézikönyv", Műszaki Könyvkiadó, Budapest, 1966, pp. 11-45;

[3] B. Író, "A hő- és áramlástan gépei tárgyhoz kapcsolódó szivattyúüzemi mérések lebonyolításához mérési útmutató", Győr, Széchenyi István Egyetem, 2015, pp. 3-19;

[4] NOCCHI_CB80_38T and PEDROLLO CP 130 Pump Catalogue;

[5] S. Török, Áramlástani gépek. 2011 Downloaded from: http://www.tankonyvtar.hu/hu/tartalom/tamop412A/20100019_aramlastani_gepek/ch05s02.html on 2nd January 2017;

[6] I. Józsa, "Örvényszivattyúk a gyakorlatban"; INVEST-MARKETING Bt., Budapest, 2013. pp. 108-196;

[7] R. Kuti, "A víz tűzoltói felhasználhatóságának lehetőségei, korlátai", VÉDELEM ONLINE: TŰZ- ÉS KATASZTRÓFAVÉDELMI SZAKKÖNYVTÁR 2015:(tanulmány 536) pp. 1-8. (2015);

[8] F. Szlivka, Vízgazdálkodás gépei. 2002 pp. 63-75. Downloaded from: http://www.ontozesmuzeum.hu/1.%20ViZGAZD%20aramlastani%20alapok%20tartalomjegyzekkel.pdf.

Assessing the Hydro Power Potential of Bistrita River

Prof. PhD.Eng. **Mariana PANAITESCU**[1], Prof. PhD.Eng. **Fanel-Viorel PANAITESCU**[2]

[1] Constanta Maritime University, e-mail address: marianapan@yahoo.com

[2] Constanta Maritime University, e-mail address: viopanaitescu@yahoo.ro

Abstract: *The aim of the paper is the study of the Bistrita River from the point of view of water. It proposes a linear representation of the specific synoptic potential and graphical representation of water cadastre. The calculation is done on each sector and it follows the steps: sector fall, average flow per sector, theoretical power sector, theoretical energy sector, sector length, specific theoretical linear potential of the k sector and the specific power. Using specific software for the representation of the theoretical linear synoptic potential and analyzing the water cadastre representation, one can notice that the maximum amount of hydro power potential is achieved on one specific sector. Therefore, it is most suitable for hydropower facilities.*

Keywords: *River, potential, energy, evaluation, flow, cadastre, power*

1. Introduction

Use of water energy purposes is known for thousands of years. An approach to investment in the field of renewable resources, selecting locations favourable energy applications is done taking into account certain criteria that include technical, economic and environmental conditions and restrictions.

The main selection criteria are as follows [1]:

- renewable energy potential of the energy source in the area of interest;
- concrete conditions of the terrain: morphology, roughness, obstacles, the nature of the terrain;
- proximity to human settlements;
- nature reserves, historical areas, archaeological tourism;
- special highlights: prohibited areas, civil/military airport, goals of special telecommunications;
- the existence and condition of access roads;
- conditions of use of the land: the legal regime, the concession/purchase;
- connection possibilities to the power grid: power distance, etc.
- potential investors in the area
- potential auto-manufacturers in the area
- the possibility of a public/private partnership
- technical-economic indicators performance in selected location.

The aim of the paper is the study of the Bistrita River from the point of view of water.
It proposes a linear representation of the potential specific synoptic and graphical representation of water cadastre.
Theoretical linear potential of water courses represent the maximum energy that can be obtained on the river Bistrita (or on a particular sector), without taking into account the losses which arise from transformation of hydraulic energy into electricity.
Considering the great lengths of water courses for the interests of potential values, dozens or even hundreds of kilometres, the calculation is done on the sectors [2].
Evaluation of linear potential joins two graphics:
-synoptic representation of linear theoretical potential, p,
-land-or water-power profile, where on the same graph are depending on length [3].

2. Method and research

For study it was selected the River Siret, Bistrita [4]
This river springs from Rodna Mountains in Maramures County, flows through the Eastern Carpathians, then passes through the towns of Bicaz, Neamt, Stone Roznov, Buhuşi and Bacău to spill in the Siret River near the town.

- *Geographical data*

The Iezerul Mare river mouth area: Bistrita, Rodna Mountains
From its source elevation: 1649 M.A.S.L. (metres above the sea)
Emissary: Crafty
Elevation: 134 M.A.S.L.
Coordinates: 49 ° elevation 29 ' 28 "N 26 ° 59 ' 13" E
Point of bloodshed: Gălbeni
Difference in elevation: 1515 m

- *Hydrological data*

Reception basin: 6400 km

- *General data*

Traversed counties: Maramureş, Suceava, Neamţ, Bacău
Location: Romania
Isometric view of the river requires four sizes:
- profile of the river in long-odds corresponding to the characteristic sections, Z;
- flow characteristic in sections, Q;
- linear theoretical potential, p;
- theoretical power limits for each sector-specific basis, as the sum of the powers of the sectors between that limit and the upper limit of the river.

Bistriţa River is considered to be in respect of which there are 7 sections:
- flow-module Q,
- Z shares black sea level and
- the lengths it toward the downstream section located at the end of the river.

For the calculations shall be attached to the current sector index k, the same as that of the upstream which confines, where: k = 1, n − 1.

The calculation is done on each sector and it follows the steps below:
1) sector fall, ΔZ_k

$$\Delta Z_k = Z_k - Z_{k+1}[m] \tag{1}$$

2) average flow per sector k,

$$Q_k^- = \frac{Q_k + Q_{k+1}}{2};[m^3/s] \tag{2}$$

3) theoretical power sector k,

$$\Delta P_k = 9.81 \cdot Q_k \cdot \Delta Z_k;[kW] \tag{3}$$

4) theoretical energy sector k,

$$\Delta E_k = 8760 \cdot \Delta P_k;[kWh] \tag{4}$$

5) sector length, k

$$\Delta L_k = L_k - L_{k+1}; [km] \tag{5}$$

6) specific theoretical linear potential of the k sector ,

$$p_k = \frac{\Delta P_k}{\Delta L_k}; [kW/km] \tag{6}$$

Finally, there is calculated the specific power:

$$e_k = \frac{\Delta E_k}{\Delta L_k}; [kWh/km] \tag{7}.$$

3. Results and interpretations

3.1 Data of river sections

Bistriţa River is considered from Fig. 1. Share course through 7 sections in the sectors.
Its boundaries are numbered as follows:

1-section upstream; 7-section downstream, 2 ... 6-intermediate sections that divide the river into sectors.
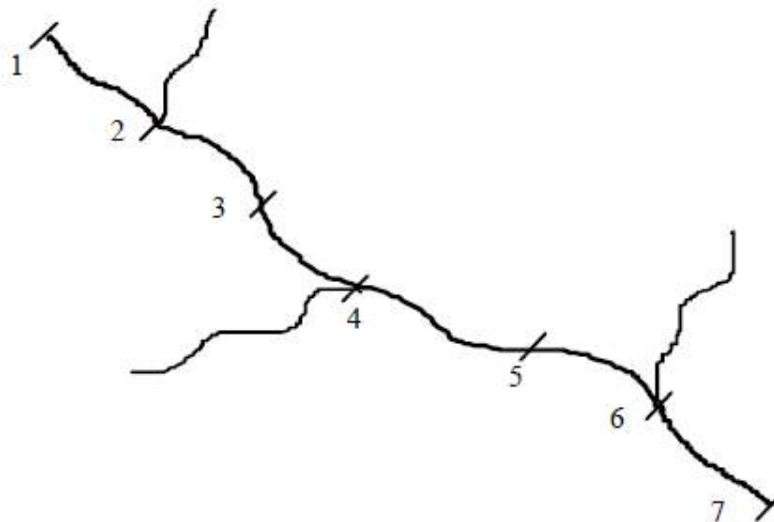
Fig. 1. River sector scheme

For each section: 1, 2, ... 7, the following features are known:
- the multiannual average flow rates, Q,
- the odds against black sea level Z, and
- lengths against section 7 (downstream), L.

These values are presented in Table 1.

Table 1: Data on the characteristic section

Section	Value:		
	Q [m³/s]	Z [M.A.S.L.]*	L [km]
Section 1	35.37	1623	63
Section 2	39.58	1612	56
Section 3	42.94	1603	46
Section 4	46.26	1621	37
Section 5	50.19	1626	28
Section 6	52.46	1593	26
Section 7	61.01	1586	23

MASL= metres above sea level.

Tipical sector sizes for the studied river are presented in Table 2.

Table 2: Sizes for each sector of the river

Size/sector/unit		1-2	2-3	3-4	4-5	5-6	6-7
ΔZ	[m]	45	90	95	60	30	40
Q	[m³/s]	37.47	41.26	44.62	48.22	51.32	56.73
ΔP	[kW]	16541	36428	41583	28382	15103	22260
ΔE	[GWh]	144.89	319.10	364.26	248.62	132.62	194.69
ΔL	[km]	7	10	9	9	2	3
P	[kW/km]	2363	3642.8	4620.33	3153.55	7551.5	7420
E	[GWh/km]	20.69	31.91	40.47	27.62	66.31	64.89
ΣΔp	[kW]	16541	52969	94552	122934	138037	160297

3.2 The representation of theoretical linear specific synoptic potential

Figure 2 contains the representation of the theoretical linear specific synoptic potential p [3], by following the steps below:
-   choose an appropriate scale for lengths and is the route of the river;
-   inspection of corresponding line of p in the Table 2 and is chosen for its convenient scale representation;
-   on a sector that is part p lane width proportional to it, the chosen, the symmetric part of the river and it marks the lines perpendicular to the route of the river.
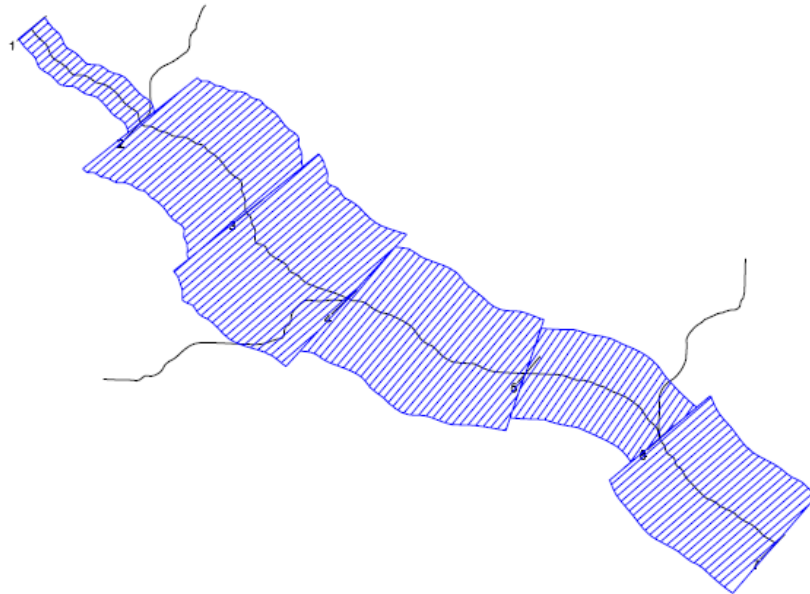
Fig. 2. The representation of the theoretical linear specific synoptic potential

3.3 The representation of hydro power profile

Figure 3 contains the representation of the water cadastre for Bistrita River:
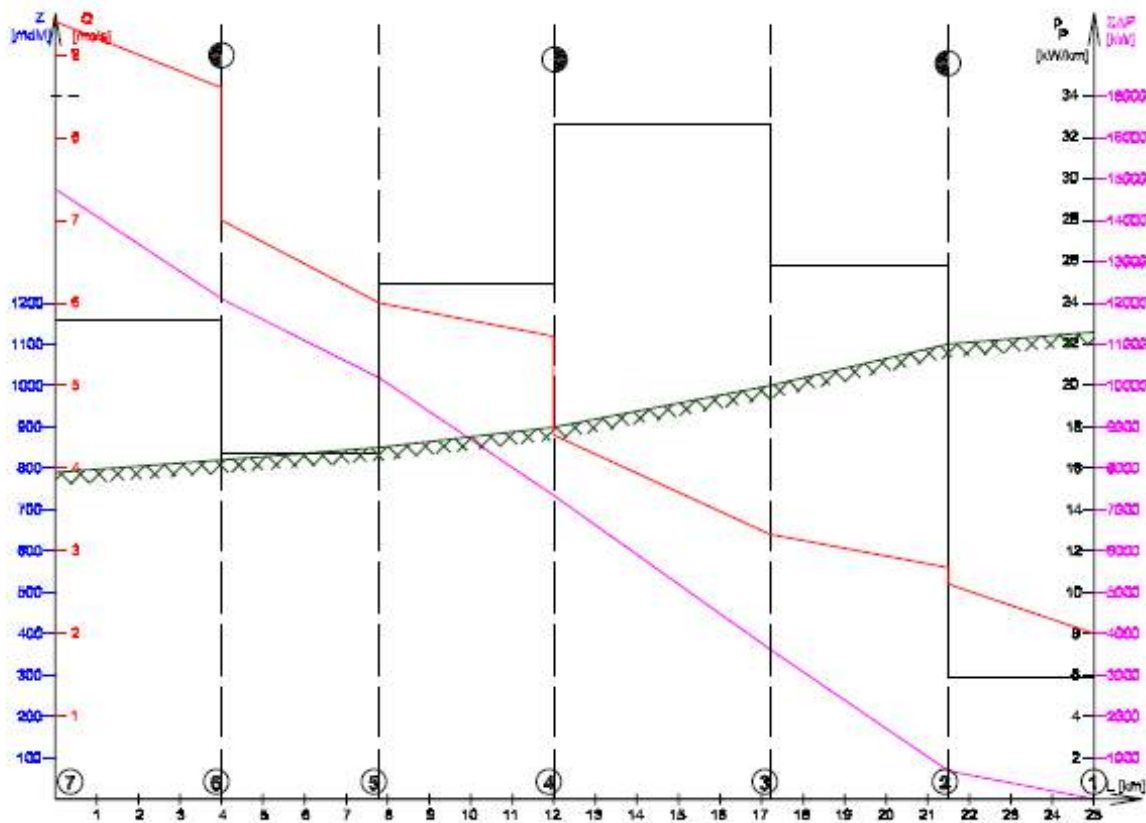
Fig. 3. The representation of the hydro power profile for Bistrita River

As one can see, the section 3-4 presented the maximum hydro power potential.

4. Conclusions

Analyzing the figures, we can conclude that:
- the maximum amount of hydropower potential is achieved on specific sector 3-4;
- therefore, it is most suitable for hydropower facilities;
- for the river is advantageous to carry out a dam in section 4, section characterized by share the thalweg: Z_0 = 900 M.A.S.L. and the multiannual average flow, Q_m = 62.5 m^3/s.

References

[1] *** UPB, ENERO, Hidroelectrica, 2006;
[2] R. Popa, "Elements of rivers hydrodinamics" ("Elemente de hidrodinamica raurilor"), Didactic and Pedagogic Publishing House, R.A. Bucharest, 1997;
[3] R. Popa, "Modeling water quality from rivers" ("Modelarea calitatii apei din rauri"), *H*G*A* Publishing House, Bucharest, 1998;
[4] http://cadastru.8k.com/catalog.html;
[5] http://PSpice-manuals-SCHMURGD.pdf.

Optimizing the Equation of Impact Forces Produced by Water Jets Used in Sewer Cleaning

PhD. Eng. **Nicolae MEDAN**[1], PhD. Student Eng. **Adrian Paul BASARMAN**[1]

[1] Technical University of Cluj-Napoca, North University Center Baia Mare

Nicolae.Medan@cunbm.utcluj.ro / adrian.basarman@cunbm.utcluj.ro

Abstract: The purpose of this paper is to optimize the equation of the impact forces produced by water jets used in sewer cleaning. The functioning of the cleaning sewer is dependent on certain process parameters, which can vary, causing variations of the impact forces. The research method used is Taguchi design of experiment. To be able to make the experiments there was used a stand to generate the water jets and a device to measure the impact forces. In the first part of paper was determined the percentage of influence of parameters involved in the process and then there was developed a multiple linear regression model in three different ways to optimize the prediction of the proposed equation.

Keywords: Impact force, water jet, Taguchi method, multiple linear regression model

1. Introduction

Industry water jet technology is frequently used in a lot of areas such as: concrete hydro demolition, jet cutting for different type of materials, mechanical processing of minerals, medical applications, rock fragmentation, and surface preparation for protective coatings [1].

Industrial cleaning is a classic application of water jets technology. In the late 1950s, when reliable high pressure pumps were built, the usage of water jets spread widely in the field of pipes and sewerage cleaning.

Phenomena that occur in the cleaning water jets are complex. Adler [2] describes mechanisms occurring at the impact of a jet with a surface. Leach et al [3], Leu et al [4] and Guha et al [5] analyzed pressure distribution along centreline of the water jet. Several papers have studied the influence of nozzle geometry on water jet [6, 7].

The regular cleaning of the materials deposed in sewer networks is realized, especially with equipment that uses high pressure water jets. The functioning of this equipment is dependent on certain process parameters [1] that can vary, causing variations of the impact forces. The impact forces directly affect the cleaning of sewer systems.

To determine an equation who described the values of impact forces in concordance with the process parameters is necessary to realised practical experiments to determine the values of impact forces for different set-up values of process parameters [8].

Using the data obtained there can be determined linear regression model to describe the process studied. In some cases, it is indicated to optimise the regression [9].

In this paper, the research method used is Taguchi design of experiments [10]. After determining impact forces, in concordance with the experimental domain set-up, was determined a linear regression model and this regression model was optimised to increase the degree of prediction for this model.

2. Apparatus used and methodology of the measurements

To measure the impact forces produced by water jet, were used and built a stand for generating pressure jets, as well as a device to measure the impact force [8].

2.1 Stand to generate pressure water jets

Schematic diagram of the stand to generate pressure jet is shown in figure 1.
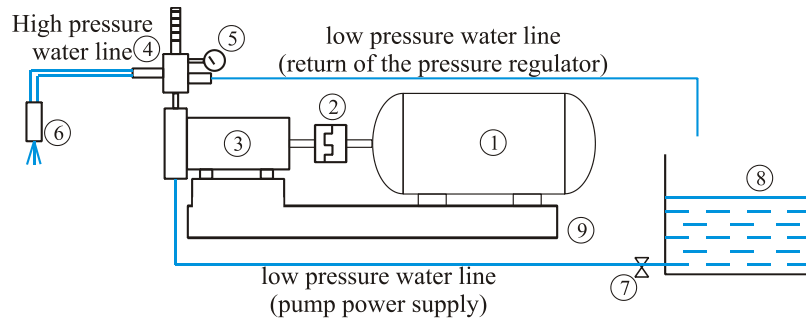
Fig. 1. Schematic diagram of the stand to generate pressure jet

Component parts of stand: (1) electric motor (2) flexible coupling; (3) high pressure pump, 4) pressure regulator, 5) pressure gauge, 6) nozzle, 7) tap water, 8) water tank, 9) chassis.

Water coming out of the high-pressure pump (3) goes into the pressure regulator (4). Through it adjusts the pressure and flow of water in the path of the high-pressure water. This pressure corresponds to the one at the outlet of nozzle.

2.2 Device for measurement the impact forces

In figure 2 is represented the principle diagram of the device for measurement the impact force of the water jet produced when the water jet hit a flat and rigid surface.
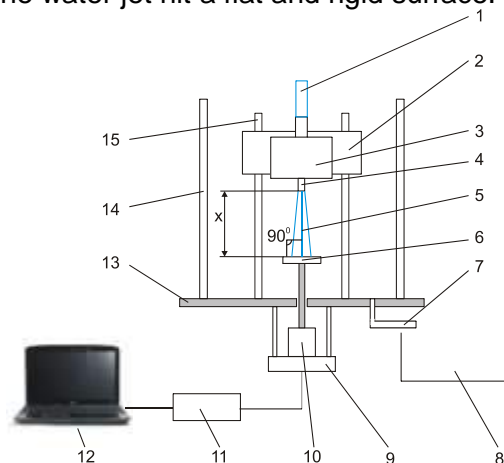
Fig. 2. Diagram of the device for measuring the impact force of the water jet

Main component parts of the device are: 1) high-pressure water hose, 2) support nozzle, 3) nozzle block, 4) nozzle, 5) water jet, 6) flat and rigid target plate, 7) collection path water, 8) scaled container for measurement of the flow of water jet, 9) piezoelectric sensor mounting, 10) piezoelectric sensor, 11) data acquisition Personal Daq/3000, 12) computer for the processing of data; 13) support plate, 14) acrylic tube, 15) rods for adjusting distance x.

From high pressure water hose (1) there comes water at a certain pressure p desired. At the outlet of nozzle is generated a water jet (5) that striking target plate (6), who is located at a certain distance x in front of the nozzle. The jet (5) generates an impact force at a time when he meets target plate (6). This force produces axial movement of target plate. This movement is converted into an electric signal by the piezoelectric sensor (10). Electrical signal is collected by data acquisition Personal Daq/3000 (11), which forward data to a computer (12) using DaqView soft processes data actually obtained.

2.3 Methodology of the measurements

The research method of this study is the experiment. To determine the values of impact forces produced by water jets is used the Taguchi method. To determine the impact forces, it is necessary to set up the experimental domain.

In the water jet cleaning process a series of parameters are involved [1]. These parameters can be divided into two major groups, namely: 1) target parameters which shall be defined according to

the contact area between the water jet and the surface to be cleaned and 2) process parameters. In the measurement of the impact forces of a stationary water jet and flat and rigid surface the process parameters are involved (figure 3).
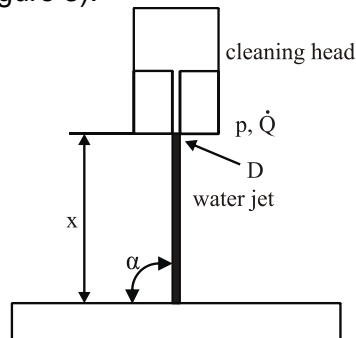
Fig. 3. Process parameters

Setting up the experimental domain:
The process parameters that influence the impact force are: 1) D nozzle diameter, [mm]; 2) P water pressure, [bars]; 3) x distance between the nozzle and impact surface, [mm]; 4) α impact angle (angle formed by the jet and impact surface), [^{0}].
The value of diameter of nozzle are D=1mm, 1.5mm and 2mm. These are common values used in equipment to maintenance and cleaning of sewers.
The pressures used to perform the measurements have the values p=100 bars, 120bars, 140bars, 160bars, 180bars and 200bars. For the maintenance sewers, are used high pressure water pumps which generate a maximum pressure of 200 bars.
To perform the measurements distance x has been fixed at the values x=25 mm, 50 mm, 75 mm, 100 mm, 125 mm, 150 mm, 175 mm and 200 mm.
The impact angle α has values 60^0, 75^0 and 90^0. For cleaning heads, usual value of the angle of impact α is 75^0. If impact angle α decrease below 60^0 lead to a drop in of the impact forces.
In table 1 are presented the process parameters and levels values according with Taguchi method.

Table 1: Process parameters and level values

Abbreviation	Parameter	Name	Value 1 minimum Notation (1)	Value 2 maximum Notation (2)
A	Parameter 1	Nozzle diameter	1mm	2mm
B	Parameter 2	Pressure	100bars	200bars
C	Parameter 3	Distance x	25mm	200mm
D	Parameter 4	Angle α	60^0	90^0

Corresponding to the 4 parameters and second degree interactions of the parameters, for Taguchi method result an orthogonal array L16 (2^4). In conclusion, it is necessary to make a plan of experiments which contains 16 experiments.

3. Results

For each of the 16 experiments (determined according to the Taguchi design of experiments) three sets of measurements of the impact force were performed. For each experiment there was determined the average force (F_{med}). The data are summarized in table 2.

Table 2: The measured force F according to the parameters set

No. of exp.	Parameters				Impact force F [N]			
	A	B	C	D	1	2	3	F_{med}
1	1	100	25	60	8.08	7.69	7.94	7.46
2	1	100	25	90	10.49	10.48	10.36	9.95
3	1	200	200	60	14.79	14.92	14.55	13.69

4	1	200	200	90	19.32	18.70	19.08	18.25
5	1	100	200	60	6.39	6.15	6.40	6.83
6	1	100	200	90	7.84	7.83	8.03	9.10
7	1	200	25	60	17.12	16.98	16.69	15.87
8	1	200	25	90	21.67	21.72	21.83	21.16
9	2	100	200	60	29.06	29.94	29.46	26.01
10	2	100	200	90	36.97	36.71	36.21	34.68
11	2	200	25	60	65.37	65.10	64.80	64.99
12	2	200	25	90	86.00	85.98	86.24	86.65
13	2	100	25	60	30.82	31.31	30.72	30.19
14	2	100	25	90	40.44	40.30	40.18	40.26
15	2	200	200	60	59.95	59.47	60.14	57.78
16	2	200	200	90	76.32	76.30	76.35	77.04

3.1 Determining the contributions of the parameters and their interactions

To calculate the contributions of parameters and their interactions we have used the data in table 2. Using the method Taguchi we have conducted an analysis of the variance to determine the influence of each parameter and their interactions on the impact force. In table 3 is presented the analysis of the variance, using Minitab 17.

Table 3: Analysis of Variance (Minitab 17)

Source	DF (degree of freedom)	SS (sum of square)	Contribution
Regression	10	10008.3	99.80%
Diameter	1	6213.7	61.96%
Pressure	1	2279.1	22.73%
Distance	1	68.8	0.69%
Angle	1	344.8	3.44%
Diameter*Pressure	1	895.0	8.93%
Diameter*Distance	1	25.0	0.25%
Diameter*Angle	1	126.8	1.26%
Pressure*Distance	1	7.1	0.07%
Pressure*Angle	1	46.5	0.46%
Distance*Angle	1	1.4	0.01%
Error	5	19.7	0.20%
Total	15	10027.9	100.00%

From table 3 can be seen only 3 parameters and 2 interactions have a significant contribution to the values of impact forces for experimental domain established: diameter D, pressure p, angle α, interaction between diameter D and pressure p and interaction between diameter D and angle α.

3.2 Determining the regression equation of impact forces

According to the results obtain in table 3, the next step is to determine the equation of the impact forces using only the parameters and interactions previously set.
Using Minitab 17, the multiple linear regression model of impact forces for Taguchi method was determined (equation 1):

$$F_{med} = 23.9 - 33.6 \cdot A - 0.2101 \cdot B - 0.254 \cdot D + 0.2992 \cdot A \cdot B + 0.375 \cdot A \cdot D \qquad (1)$$

This multiple linear regression model was obtaining without Box-Cox transformation.
In table 4 is presented the analysis of variance of equation (1).

Table 4: Analysis of Variance for equation 1

Source	DF (degree of freedom)	SS (sum of square)	Contribution
Regression	5	9859.4	98.32%
Diameter	1	6213.7	61.96%

Pressure	1	2279.1	22.73%
Angle	1	344.8	3.44%
Diameter*Pressure	1	895.0	8.93%
Diameter*Angle	1	126.8	1.26%
Error	10	168.5	1.68%
Total	15	10027.9	100.00%

The regression statistics of equation (1) are: R squared: 98.32%, R squared adjusted: 97.48% and R squared predicted: 95.70%.

To optimise the equation (1), the next step is to be made a regression using Box-Cox transformation with rounded λ. Result the equation (2):

$$ln(F_{med}) = -0.646 + 1.311 \cdot A + 0.00668 \cdot B + 0.00958 \cdot D \tag{2}$$

In table 5 is presented the analysis of variance of equation (2).

Table 5: Analysis of Variance for equation 2

Source	DF (degree of freedom)	SS (sum of square)	Contribution
Regression	5	10.40	99.73%
Diameter	1	7.79	74.47%
Pressure	1	2.27	21.71%
Angle	1	0.33	3.16%
Diameter*Pressure	1	0.003	0.03%
Diameter*Angle	1	0.000	0.00%
Error	10	0.066	0.63%
Total	15	10.47	100.00%

The regression statistics of equation (2) are: R squared: 99.37%, R squared adjusted: 99.06% and R squared predicted: 98.39%.

Another possible optimisation of equation (1) is realised made a regression using Box-Cox transformation with λ=0.5. There results the equation (3):

$$(F_{med})^{0.5} = 0.28 + 0.08 \cdot A - 0.00209 \cdot B - 0.0003 \cdot D + 0.01469 \cdot A \cdot B + 0.01706 \cdot A \cdot D \tag{3}$$

In table 6 is presented the analysis of variance of equation (3).

Table 6: Analysis of Variance for equation 3

Source	DF (degree of freedom)	SS (sum of square)	Contribution
Regression	5	71.44	99.12%
Diameter	1	50.78	70.47%
Pressure	1	15.92	22.09%
Angle	1	2.30	3.20%
Diameter*Pressure	1	2.15	3.00%
Diameter*Angle	1	0.26	0.36%
Error	10	0.63	0.88%
Total	15	72.07	100.00%

The regression statistics of equation (3) are: R squared: 99.12%, R squared adjusted: 98.68% and R squared predicted: 97,75%.

In table 7 are presented the regression statistics for all of three equation determined.

Table 7: Regression statistics for all 3 equations

Type of regression	Equation no.	R squared	R squared adjusted	R squared predicted
without transformation	(1)	98.32%	97.48%	95.70%

rounded λ transformation	(2)	99.37%	99.06%	98.39%
λ=0.5 transformation	(3)	99.12%	98.68%	97.75%

4. Conclusions

1) In this work, it is presented a methodology to determine the impact forces produced by water jets used in sewer cleaning. The impact forces dependent on certain process parameters.

2) The research method used is Taguchi design of experiment. After applying Taguchi itinerary for calculating the percentage of influence of parameters and their interactions of the impact forces, it is found:

- nozzle diameter D is the largest influence, with a percentage of 61.96%;
- in the second place is pressure P with a value of 22.73%;
- interaction between nozzle diameter D and pressure p with a value of 8.93%;
- the impact angle α with a value of 3.44%;
- interaction between nozzle diameter D and impact angle α with a value of 1.26%.

3) For the experimental domain, the parameter distance x has a percentage of influence of only 0.69% for impact forces, virtually insignificant.

4) According with the influence of parameters and their interactions, was realised a multiple linear regression model in three different ways to optimise the prediction of the proposed equation:

- first type regression without transformation with R squared predicted 95.70%;
- second type regression using rounded λ transformation with R squared predicted 98.39%;
- third type regression using λ=0.5 transformation with R squared predicted 97.75%.

5) The best prediction is given by the regression using rounded λ transformation, followed by the regression using λ=0.5 transformation. The lowest degree of prediction is given by the regression without transformation.

6) It can be observed that it is possible to improve the prediction of the equation who describe the impact forces only using different type of regression and using the same measured values of the impact forces.

References

[1] A. W. Momber, "Hydroblasting and Coating of Stell structures", Oxford: Elsevier Ltd, 2003;

[2] W. F. Adler, "The Mechanics of Liquid Impact. Treatise on Materials Science and Technology", 1979. pp. 127-183;

[3] S. J. Leach, G. L. Walker, "Some Aspects of Rock cutting by High Speed Water Jets", Philosophical Transactions of the Royal Society of London, Series A, Vol. 260, pp. 295-308, July 1966;

[4] M. C. Leu, P. Meng, E. S. Geskin, L.Tismeneskiy, "Mathematical modelling and experimental verification of stationary waterjet cleaning process", Journal of Manufacturing Science and Engineering, 120(3), 1998, 571-579;

[5] A. Guha, R. M. Barron, R. Balachandar, "An Experimental and Numerical Study of Water Jet Cleaning Process", Journal of Materials Processing Technology, pp. 610-618, 2011;

[6] M. Annoni, L. Cristaldi, M. Faifer, M. Norgia, "Orifice Coefficients Evaluation for Water Jet Application", Sept. 22-24, 2008, Florence, Italy, 16th IMECO TC4 Symposium, "Exploring New Frontiers of Instrumentation and Method for Electrical and Electronic Measurement", pp. 761-766;

[7] S. Dimitrov, S. Simeonov, S. Cvetkov, "Static Characteristics of the Orifices in a Pilot Operated Pressure Relief Valve", "Hidraulica" (No. 2/2015) Magazine of Hydraulics, Pneumatics, Tribology, Ecology, Sensorics, Mechatronics, ISSN 1453 – 7303, pp.35-39;

[8] N. Medan, S. Ravai Nagy, " Determining the Equation of the Impact Forces Produced by Water Jets Used in Sewer Cleaning", Innovative Manufacturing Engineering & Energy International Conference 2015 (IMANEE 2015), Applied Mechanics and Materials Vol. 809-810 (2015), pp. 1579-1584;

[9] M. Rusănescu, A. Purcărea, " Validation of a Multiple Linear Regression Model", "Hidraulica" (No. 4/2015) Magazine of Hydraulics, Pneumatics, Tribology, Ecology, Sensorics, Mechatronics, ISSN 1453 – 7303, pp. 66-70;

[10] D.C. Montgomery, "Design and analysis of experiments", 8th edition, Wiley, 2013.

Maintaining Position of Servo Cylinders by Means of Digital Hydraulics

Tech. **Ioan PAVEL**[1], Dipl. Eng. **Bogdan TUDOR**[1],
Dipl. Eng. **Mihai Alexandru HRISTEA**[1], Res. Assist. **Ana-Maria POPESCU**[1]

[1] Hydraulics and Pneumatics Research Institute INOE 2000-IHP, Bucharest; pavel.ihp@fluidas.ro

Abstract: Replacing hydraulic proportional equipment and servovalves by simple-design systems in the area of digital hydraulics within positioning applications that use hydraulic cylinders is a solution that can lower the production price and can bring important energy savings in operation.

Keywords: Servo cylinder, digital hydraulics, on / off electrovalves, digital valves, positioning applications

1. Introduction

The structure of classic hydraulic positioning servo systems comprises: devices for generating, conditioning, adjusting and distributing the working fluid, and also linear hydraulic servomotors, as hydraulic actuators, which, in fact, perform transformation / conversion of hydrostatic energy of the system into mechanical energy, in order to carry out the mechanical work required by the system / work equipment [1]. The linear hydraulic servomotors, which are hydraulic actuators within positioning equipment, perform a linear motion controlled with a certain force on the working mechanism, and they are characterized by controlled rectilinear motion. They are commonly known and currently referred to as 'servo cylinders' (Fig. 1) or 'hydraulic actuators' [2].
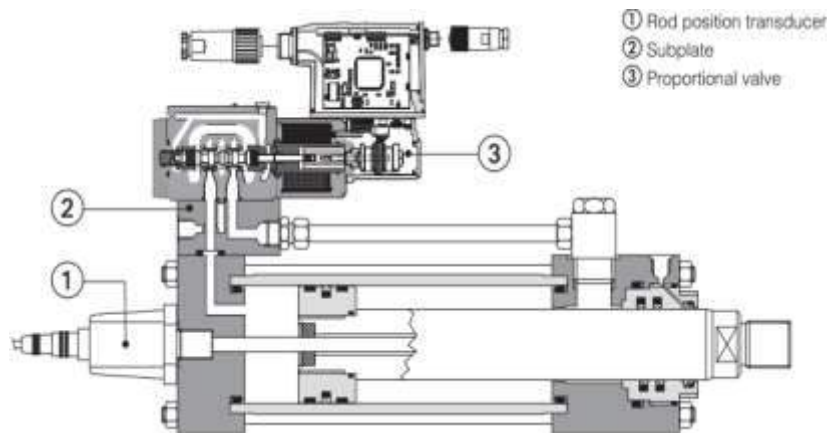
Fig. 1. Positioning servo cylinder [1]

Hydraulic proportional directional valves and servovalves (Fig. 2, left) are part of the linear hydraulic servomotors. They are expensive and demanding in operation, require very good oil filtration, cooling systems and pumps with increased flow. A good functioning of the system requires continuous operation of pumps to ensure the working flow and current flow and pressure losses which are not to be neglected. Each type of hydraulic proportional directional valve and servovalve is designed for specific conditions, so there are a very large number of types of such equipment. In the event of a failure in the operation of the proportional device, the functioning of the equipment is totally compromised.

In digital hydraulic systems (Fig. 2, right), with a combination of simple, robust and cheap on / off electrovalves or with directional switching valve, one can replace a proportional valve. The control module has the role of controlling the on / off position of the electrovalves to accurately ensure the flow and pressure required in the system, at lower production and operating costs compared to the classic solution.
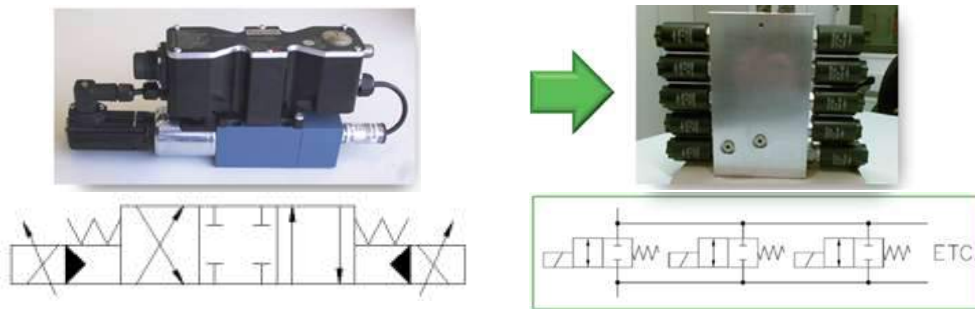
Fig. 2. Hydraulic proportional directional valve and servovalve (left); group of digital electrovalves (right) [3]

2. Solutions involving digital hydraulic devices

In the following we will present two solutions that can be applied. The first one is a solution which involves a digital hydraulic cylinder and classic on / off directional control valves, and it has been successfully applied in the specialized laboratory of INOE 2000-IHP. The second is the solution presented by Professor Matti Linjama in Finland, and it uses digital hydraulic directional valves.

2.1 The solution with digital hydraulic cylinder

A group of specialists within INOE 2000-IHP has developed a patent application [4] for a multiple area hydraulic actuator meeting the requirements of a digital linear motor.

The hydraulic actuator [4] (Fig. 3) with multiple active areas, divided, in compact structure, has the active surface of the piston made up of three concentric surfaces, with binary multiplied areas, which can be fed separately but also cumulatively, according to well-established binary rules, to achieve combinations of powered areas with which one can obtain relatively linear controlled movement, with variable speeds or loads, thus meeting the force and speed requirements of a hydraulic system.
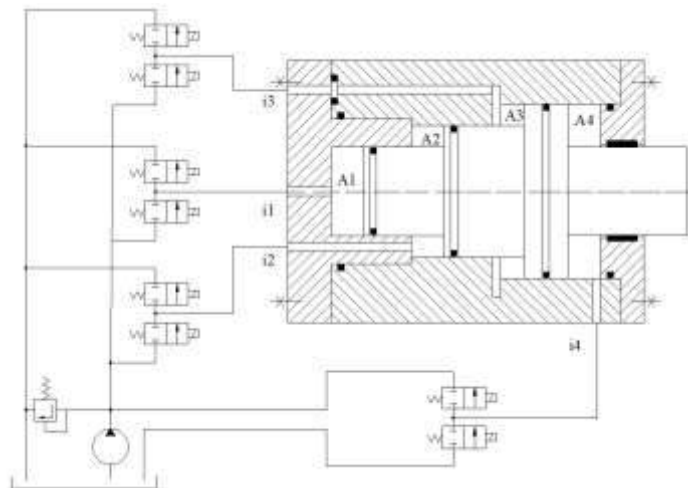
Fig. 3. Drive solution for a linear digital hydraulic motor [5]

The multiple area hydraulic actuator consists of a piston with four concentric diameters, a cylinder liner with three concentric diameters, a centering and feeding cap, a guiding cap and guiding and sealing systems. The small number of parts and their simplicity make the above mentioned patent application a technically and technologically feasible solution.

The piston has three binary multiplied concentric areas. Thus, $A2=2A1$ and $A3=2A2$. The solution enables, by selecting combinations of areas fed with constant flow and pressure, a relatively linear adjustable speed or force to be achieved:

$F= f(Ai)$, when $P = ct$

$V=f(Ai)$, when $Q = ct$

Where:
F= force
Ai= active area
P= pressure
V= speed
Q= flow

Supply control at the 4 ports i1, i2, i3, i4 by means of on/off directional control valves turns the multiple area actuator into a linear, digital hydraulic motor, feasible, which may be the subject of study for the implementation of digital hydraulics.

There are intense concerns about introducing the concept of digital hydraulics and intensifying research on the topic. In INOE 2000-IHP a specialized laboratory in Digital Hydraulics has been set up, for the two branches of this field, namely switching technology and parallel distribution technology. In the near future, two digital servo cylinders will be developed and tested. Testing the solution will be conducted on a specialized test bench (Fig. 4), with controlled hydraulic load, equipped with a force transducer, for active control of the adjusted force and for data acquisition, and with displacement transducer, also for active control of the adjusted force and for data acquisition. The results of this research will be the subject of several papers that will appear in specialized publications.
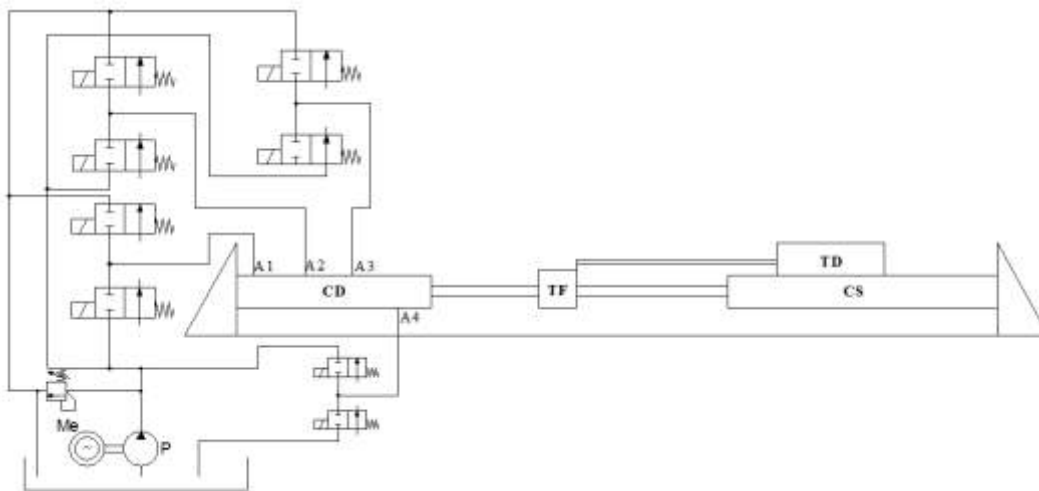
Fig. 4. Test bench for a linear digital hydraulic motor

Servomotors with digital hydraulic cylinders are controlled by a group of simple, cheap and very resistant electrovalves, individually actuated by a control unit which ensures their operation according to an optimal algorithm [6,7], enabling the functioning of systems with the same performance as in the case of actuation with proportional drive equipment, but at lower construction and operation costs. They are two-way normally closed directional valves which can maintain position of servomechanism when the electromagnet is disengaged, and when powering it enable flow transiting to adjust its position. Electrovalves do not lose oil in normal operation, and for this reason, when maintaining the position of a servomechanism there is no need for the pump to work continuously, and the working flow can be provided by a battery located near it, thus shortening the connection lines and eliminating the ΔP parameter, which is the loss along the connection lines. This solution can significantly reduce energy consumption because the pump may be smaller and will only work for charging the battery.

Digital electrovalves (Fig. 2 right) are smaller, cheaper, more reliable, and they are produced in large series, compared to proportional devices (Fig. 2 left) which have more complicated, expensive, and less reliable controls (torque motors or proportional electromagnets), and require higher initial, maintenance and operation costs.

In the event that a digital valve fails, (Fig. 5) the control unit automatically reconfigures the other valves in order to maintain the position of the servomechanism and mitigate negative effects on system performance. Compare this with the situation when the proportional device would fail; in

this event the equipment can no longer work or even worse, parts of it may degrade by fatal loss of position control.

Even the locking of an electrovalve on the open position can be compensated by the rest of the group's electrovalves by way of reconfiguring the digital controls. In this situation, flow consumption will unnecessarily increase, but the system will operate until the next scheduled stop. If a load peak accidentally occurs in the system, the digital system will react more quickly compared to the classic system, due to the multiple opening of the electrovalves.

Fig. 5. Digital control reconfiguration in case of failure of a digital electrovalve [3]

Digital electrovalves are very quick (Fig. 6), with the performance of switching open / closed mode within a few milliseconds, and by programming a PLC in a binary system one can get very good performance for a positioning system [8, 9].
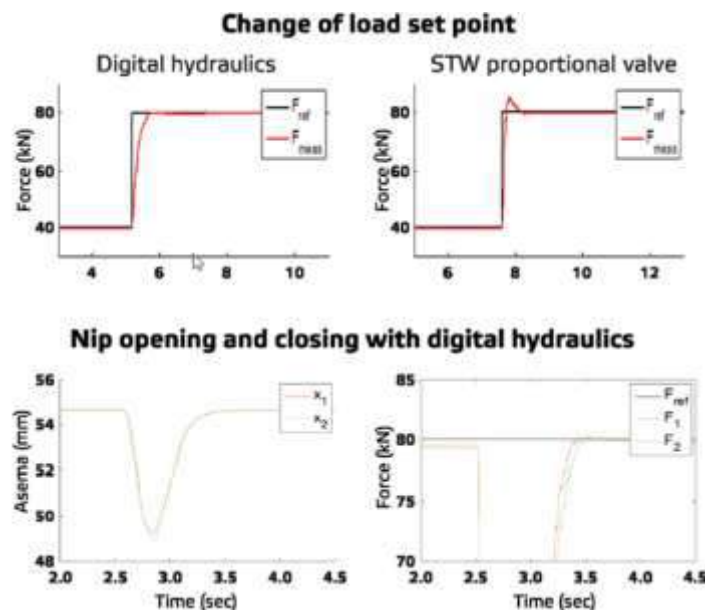
Fig. 6. Response time of digital electrovalves compared to classic servovalves [3]

2.2 The solution with digital hydraulic directional valves

An example of the use of digital electrovalves to obtain a variable flow rate [8] is shown in Figure 7.
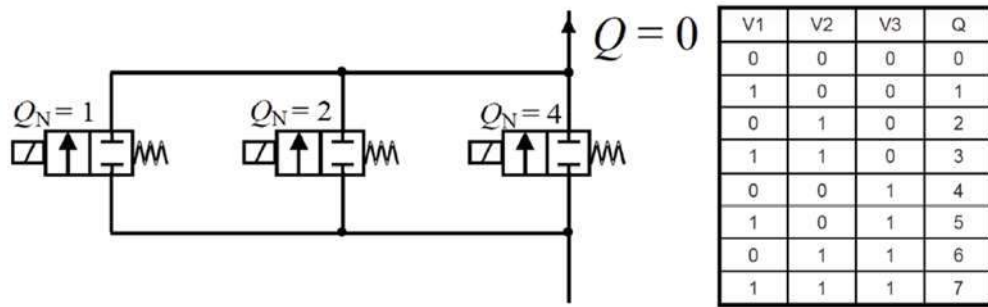
Fig. 7. Flow control unit diagram (left); table of binary combinations for 7 flow stages (right) [3]

Electrovalves individually allow transit of a flow rate of dimensional size of 1, 2 and 4 measurement units (m.u.), and by combinations of controlled electrovalves variable flow rates are obtained within the range 0 - 7 m.u. (table in Fig. 7). If there is necessary a more accurate flow adjustment another electrovalve of dimensional size of 8 m.u. can be added, thus obtaining flow rates stages from 0 to 15 m.u., which can be equated with the performance of a proportional valve. The performance of a servovalve can be met by a group of 6 electrovalves (of 1, 2, 4, 8, 16, 32 m.u), obtaining a continuous flow adjustment in the range 0 - 63 m.u. Adding an electrovalve to the group of electrovalves doubles flow rate value and increases resolution.

In figure 8 one can notice the shape of the flow control chart in the three variants: with proportional device (left), with 4 digital electrovalves (middle), and with 6 digital electrovalves (right).
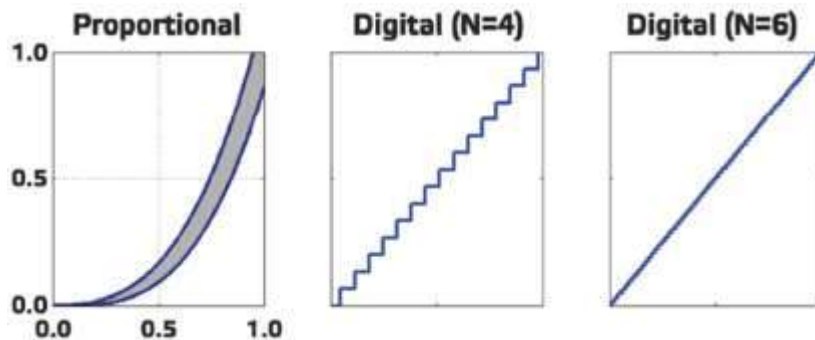
Fig. 8. Flow control by using proportional device (left), a group of 4 digital electrovalves (middle) and a group of 6 digital electrovalves (right) [3]

Using digital hydraulic drive equipment for hydraulic positioning systems shows a number of advantages. The first and most important is reliability. Classic proportional devices have small tolerances and sensitive electronic components located right on the device, in a not really friendly environment, as they are exposed to vibrations and temperature variations, which shortens significantly their normal operating time. In the event that the proportional hydraulic device fails, in the best case scenario the process stops and the valve must be replaced, which means costs for a new proportional device and losses in the working process during the repairing. In the worst case scenario, failure of the proportional device can lead to failure of the parts along the production line, or even worse, failure of the positioning system, which means high repair costs and significant looses in the working process.

Proportional devices (directional valves and servo valves) control the flow by moving the spool in both directions and, though the tolerances are very small, on high pressure flow leaks occur to the drainage port of approx. 0.40-0.65 l/min. Also small tolerances require very good filtration of the working oil.

In case of digital electrovalves no flow leaks to the drainage occur, because by construction they have a sealing face. They allow a contamination of the working oil up to 30 times higher comparative with proportional valves and can work correctly up to a oil temperature of 75° C, in many cases not requiring the cooling of the oil. Due to their simple and robust construction digital

electrovalves are very reliable and can work very well even in the range of 300 millions – 1 billion working cycles, thus avoiding unscheduled stops. The lack of oil losses at the drainage allows the utilization of the hydraulic accumulator for maintaining the position, and in steady situations the servo system stays on the position, under pressure, for long periods of time, solution which can bring energy savings of up to 90%. In any situation, the control unit chooses the optimal combination of opened electrovalves, with minim energy consumption, according to an algorithm with high speed switching, to meet the system requirements. Digital electrovalves are on/off, and combining them enables the development of any proportional device diagram; they have a small response time because do not require tray position control and have linear behavior, without hysteresis or uncontrolled command peaks (Fig. 4).

Each flow direction (P-A, P-B, A-T, B-T) is independently and firmly controlled with an electrovalve, and their parallel opening results in small response time, high accuracy and working speeds, and finally productivity is increased and energy consumption is lowered.

3. Conclusions

The main benefits of digital hydraulic system, comparative with conventional proportional hydraulic devices are reduction of energy consumption and reliability. Digital hydraulic systems offer additional benefits relative to higher productivity, smaller procurement price, cheaper spare parts, space savings, fewer connecting pipes, resistance to higher temperature, higher accuracy and control.

Technologic development of digital hydraulic motors could reform the industries which use hydraulic systems and could transform them into the fastest and most efficient form of power transmission. Energy savings resulting from the implementation of digital hydraulic motors can improve the technical and economic performance of the technological lines where they are used, and they are reflected in the end in the manufacturing price of the products placed on the market. At the same time, by energy savings and efficient use of resources, they contribute to the foundations of sustainable development.

References

[1] D. Prodan, C. Cristescu, D. Popescu, "Machine tools and presses. Hydrostatic elements" ("Maşini-unelte şi prese. Elemente hidrostatice"), Printech Publishing House, Bucharest, 2001;
[2] V. Marin, Al. Marin, "Automatic hydraulic systems. Construction, adjustment and operation" ("Sisteme hidraulice automate. Construcţie, reglare, exploatare"), Technical Publishing House, Bucharest, 1987;
[3] http://www.valmet.com/globalassets/media/downloads/white-papers/process-improvements-and-parts/wpp_digihydraulics.pdf;
[4] Patent application no. A/00779 on 01.11.2016;
[5] P. Drumea, I. Pavel, G. Matache, "Digital hydraulic motors", Hervex 2016, November 9-11, Baile Govora, Romania*, Proc. of 2016 International Conference on Hydraulics and Pneumatics – Hervex*, ISSN 1454 – 8003, pp. 50-55*;*
[6] A. Oprean, C. Ispas, E. Ciobanu, Al. Dorin, S. Medar, A. Olaru, D. Prodan, "Hydraulic drive and automation. Modeling, simulation, testing" ("Acţionări şi automatizări hidraulice. Modelare, simulare, încercare"), Technical Publishing House, Bucharest, 1989;
[7] C. Călinoiu, "Sensors and transducers" ("Senzori şi traductoare"), vol. I, Technical Publishing House, Bucharest, 2009;
[8] M. Linjama, "Digital Fluid Power - State of the Art", *Proc. of the 12th Scandinavian International Conference on Fluid Power*, 18-20 May, 2011, Tampere, Finland;
[9] E. Bishop, "Digital Hydraulics" on http://www.digitalhydraulic.com/technology.html.

Possibilities for Agricultural Farms of Adopting and Applying Optimal Energy Recovery Solutions from Nearby Water Flows

Assistant professor **Fănel Dorel ȘCHEAUA[1]**

[1]"Dunărea de Jos" University of Galați, MECMET Research Center, fanel.scheaua@ugal.ro

Abstract: *Today, must be highlighted the increase of energy needs according to continues population growths worldwide. That is why it should be increasingly used the possibilities of energy obtaining by optimizing the resources at hand. These clean resources that do not have a major impact on the environment, are represented by water falls and flows. These resources are among the most advantageous in terms of obtaining the electrical energy by converting the mechanical energy obtained by the flowing water from a river. A method of obtaining electric energy based on the water flow power is presented in this paper. It is about a mini-hydroelectric power system that can be achieved and mounted on a water body with a lower water flow rate, with the ability to supply power for a nearby agricultural farm. Based on the continuous water stream flow a rotational motion is carried out at the helicoidally rotor shaft which is connected to a power generator thereby achieving the mechanical energy conversion into electrical energy with optimal results for producing continuous electric energy. The water intake assembly system consisting of water channel and the helicoidally rotor it has been modelled as a three-dimensional model, on which an flow analysis has been made in order to highlight the distribution of fluid flow from the inlet to the outlet of the supply channel of the hydroelectric plant model. The obtained results are presented in terms of fluid velocity across regions and specific pressures appearing on the fluid region in which the helicoidally rotor of the system is immersed.*

Keywords: *Hydro power, hydraulic energy, water resource, agricultural farm, rotor model, fluid flow, 3D modelling, computational fluid dynamics (CFD)*

1. Introduction

It can be observed today worldwide that the population living standard is steadily increasing. In order to support this growth, it is necessary for the production of goods and services to be supplied continuously with the necessary resources. The primary resource is the energy, without which the proposed activities can not be performed. This can highlight the major role of energy in the development of human communities over time.

If initially for power generation fossil fuels were used mainly, now it needs to be implemented more and more the handy solutions for power production that implies a minimum impact on the environment.

These solutions are represented by the power recovery from the water flows in rivers, seas and oceans waves force, wind force or capture energy from the sun. Throughout the world, these power generation processes are being used, and are being constantly developed.

For a lower water flow, a mini hydropower solution is available that can be built relatively easily and used on an agricultural farm to produce the electricity needed in order to meet internal needs.

The proposed solution consists in the construction of a special channel with a certain inclination degree, inside which is mounted a helical rotor which is driven in rotational motion based on the water flow force.

For the construction of this mini hydroelectric power model, a river near the farm can be used, thus enabling the generation of electricity through a generator mounted on the rotor shaft.

Such mini hydropower solutions can be the optimal solution for obtaining electricity for farms that have nearby flowing water, where the collector channel and the rotor can be easily mounted.

2. General aspects regarding the hydro power plants

The operation of a hydro power unit can be described based on the available water stream flow rate. Depending on this key parameter the total power can be calculated referring on the hydraulic

head, expressed as the energy amount on the water weight unit, for the static head or water stream velocity for the dynamic head.

For a water stream can be calculated the available power that can be obtained if we know the rotor efficiency and the water flow rate. In the equation enter also the water density, gravitational acceleration and the total head. The relation can be written as follows: [5]

$$P = \rho \cdot g \cdot h \cdot \eta \cdot Q$$

(1)

Based on the power relation presented can be aproximated the potential power values for a small water stream.

Table 1: The power diagrams based on water volumetric flow rate and rotor yield

a) case I - Water flow rate between 0.4 an 0.6 m3/s	b) case II - Water flow rate between 0.7 and 0.85 m3/s
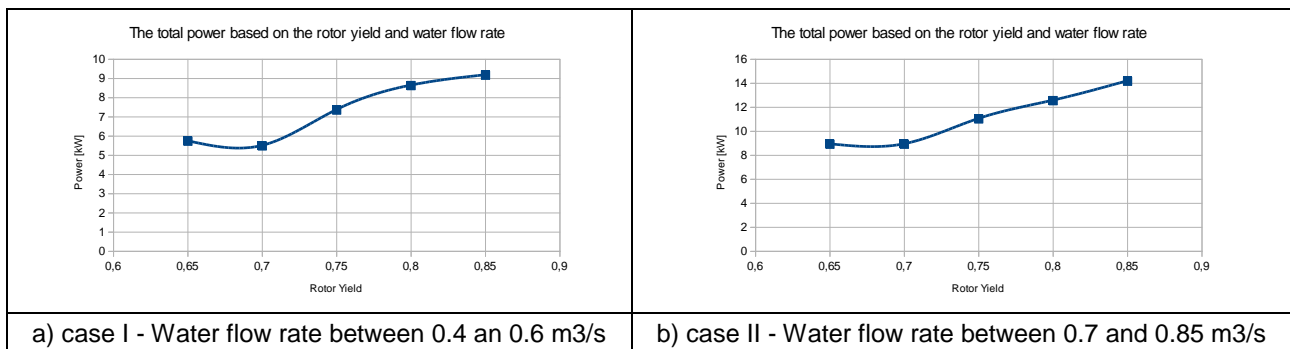
It is possible to estimate the total energy amount that can be obtained by means of a hydropower plant model at which the difference level is relatively low (2 m) and the water flow is considered between 0.4 and 0.85 cubic meters per second. Thus, it can be seen that the total values of the obtained energy amount is from about 6 kW to over 9 kW for the first case and between 9 kW and 14 kW per hour of operation of the hydropower plant for the second case.

3. CFD analysis for the Hydro Power Flow System

In order to illustrate the working process of a micro hydro power plant, an overall model of the adduction system has been built, which is in fact a three-dimensional model that includes the channel and helical rotor. For this model a computational fluid dynamics (CFD) analysis was carried out that can achieve the water trajectory calculation across the channel, describing the water flow from the upstream inlet region to the downstream exit region. The overall model of the adduction channel is shown in Figure 1a, along with the triangular shape mesh network with 39072 nodes and 173354 elements, Figure 1b.

a) Overall adduction channel model   b) Mesh network
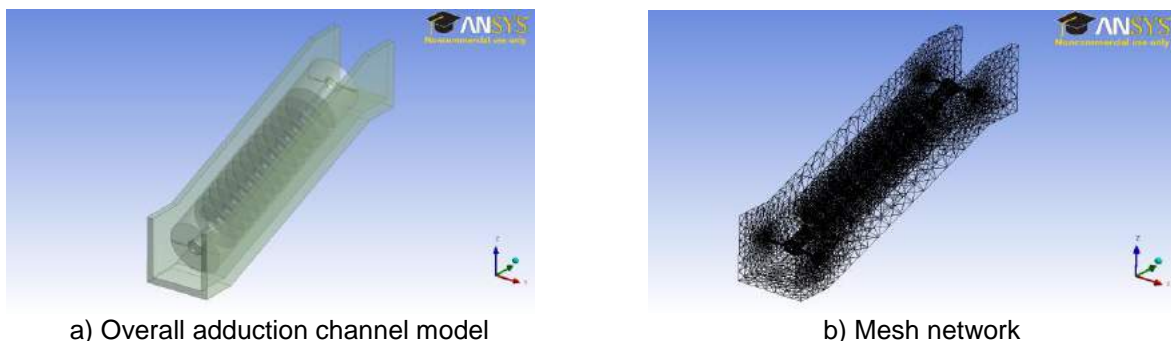
Fig. 1. Mini-hydropower water supply channel assembly

For the fluid region, the chosen fluid was water at the reference pressure of 1 atm, having a temperature of 25 degrees Celsius. An entry fluid velocity of 1 m / s was adopted. The helical rotor is considered as solid, being firmly immersed in the fluid, having a rotation movement of 60 rpm.
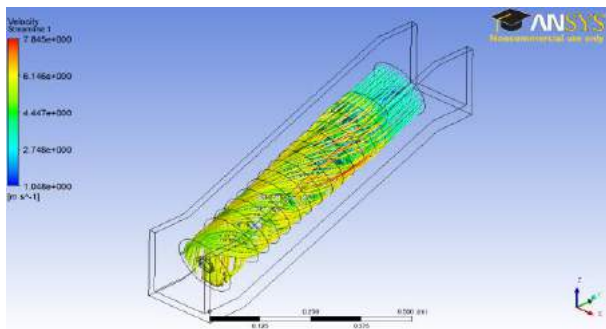
a) water velocity streamlines
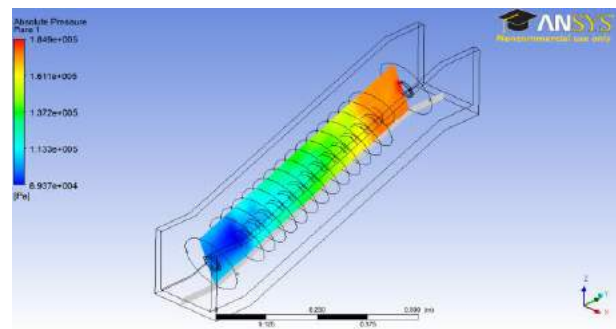
b) absolute pressure values
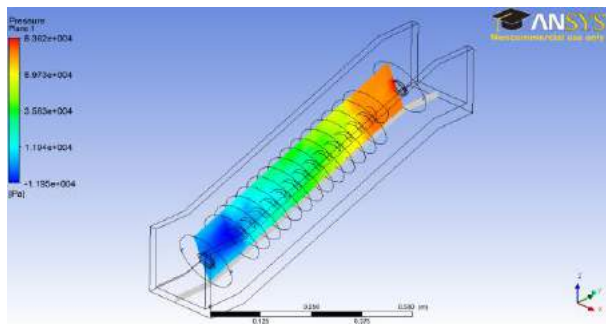
c) static pressure values
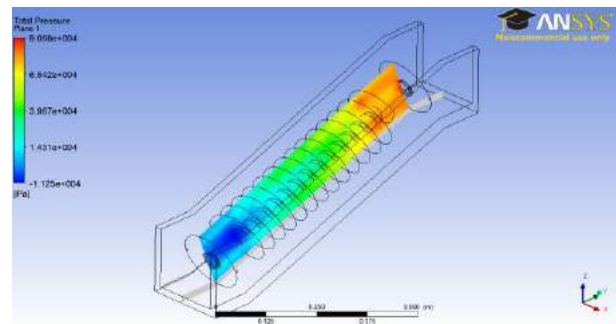
d) total pressure values
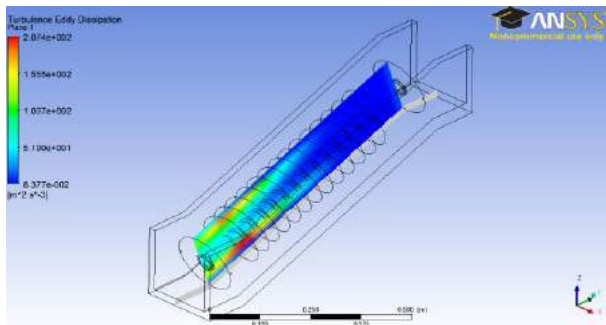
e) turbulence eddy dissipation values
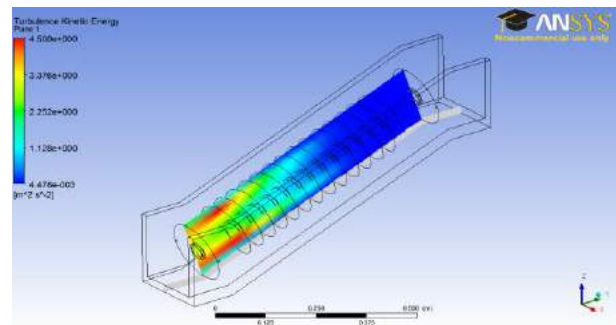
f) turbulence kinetic energy values
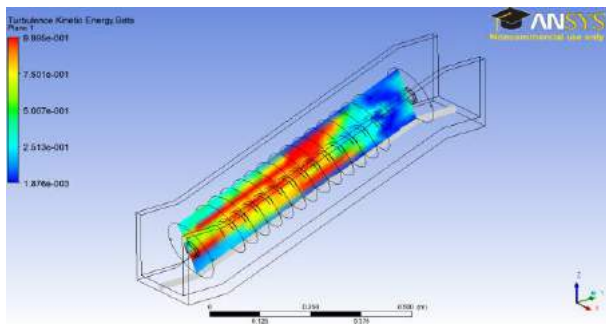
g) turbulence kinetic energy beta
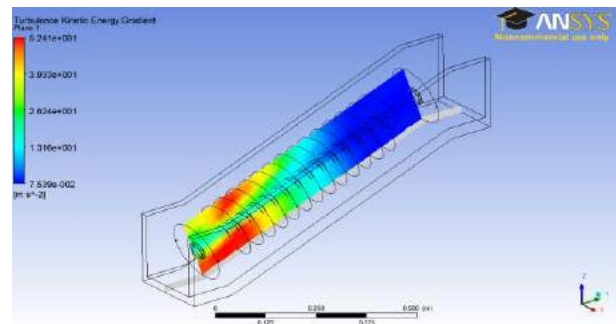
h) turbulence kinetic energy gradient

Fig. 2. The result obtained from the flow analysis

The results are shown in Figure 2, illustrating the main flow parameters such as fluid velocity, static pressure, total and absolute pressure, turbulence kinetic energy and turbulence eddy dissipation rates. Also, the values for the created turbulences as a result of the kinetic energy dissipation on the fluid mass unit engaged in the turbulent flow, the energy dissipation rate or the energy amount loses of the fluid during the flow between the inlet and the outlet region are also highlighted.

Table 2: The diagrams for fluid velocity and absolute pressure values in time
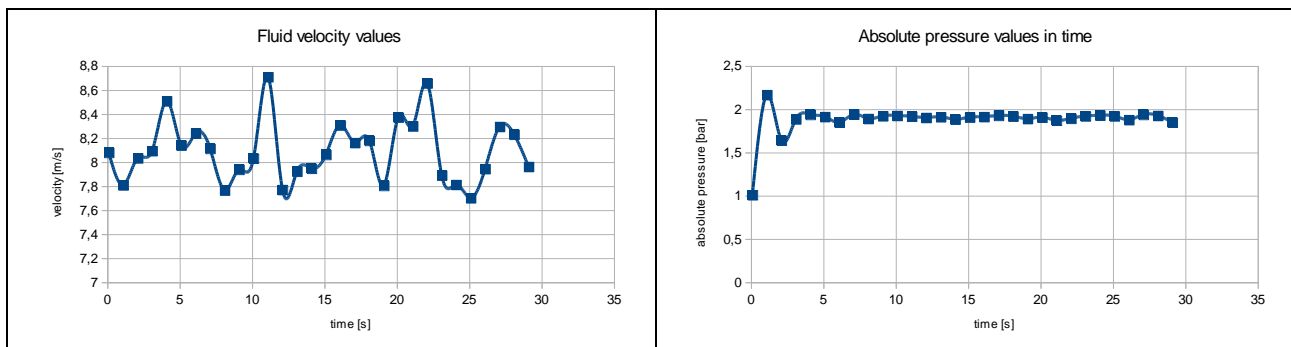
In Table 1 are presented the results diagrams for the fluid velocity values and absolute pressure values in time.

The flow pattern is that of turbulent flow (Re> 2300), as can be seen from the fluctuations of the pressure and velocity values of the fluid over the analyzed region over time due to the ratio of the inertia forces to the viscous friction forces between the fluid particles.

Energia potențială acumulată a apei din amonte determină formarea energiei cinetice la curgerea prin canalul de aducțiune a apei care antrenează în mișcare rotorul elicoidal al centralei.

Acest proces este de fapt o conversie a energiei hidraulice a fluidului în mișcare în energie mecanică de mișcare a rotorului, conectat cu un generator care produce energie electrică.

The accumulated potential energy of upstream water determines the formation of kinetic energy when flowing through the water intake channel that drives the helical rotor of the plant in motion.

This process is in fact a conversion of the hydraulic energy of the moving fluid into mechanical rotational motion energy of the helical rotor shaft, connected to a generator that produces electrical energy.

4. Conclusions

This paper presents a mini-hydroelectric model designed for the production of electricity based on the water flow.

This model can be adopted for electric power production within an agricultural farm located in the vicinity of a flowing stream that meets the conditions of construction and operation of such hydropower plant.

Once built, such a hydropower plant unit can provide the farm's electricity demand, with medium and long-term economic benefits.

An adduction channel assembly pattern has been built and analyzed in terms of fluid flow in order to highlight the velocity and pressure values that occur in the analyzed fluid region.

Fluctuating values of absolute pressure and velocity of the fluid in the turbulent flow motion, as well as values obtained for energy dissipation rate or turbulence kinetic energy were presented.

All results show the particulars of the water flow through the fluid region of the adduction channel according to the input data originally considered.

References

[1] G. Axinti, A.S. Axinti, "Acționări hidraulice și pneumatice", Editura Tehnica-Info, Chișinău, 2009;
[2] A.S. Axinti, F.D. Șcheaua, "Introducere în hidraulica industrială", Editura Galați University Press, 2015;
[3] Al.A. Vasilescu, "Mecanica fluidelor", Ministerul Educatiei și Învățământului, Universitatea din Galați, Galați, 1979;
[4] F.D. Scheaua, "Aspects Regarding the Special Hydraulic Distributors Operation", Hidraulica Magazine, ISSN 1453-7303, no.4, 2016;
[5] https://en.wikipedia.org/wiki/Hydropower.